DOCTOR OF PHILOSOPHY

# Bifurcation contrasts between plane Poiseuille flow and plane Magnetohydrodynamic flow

Benjamin Tocher

2013

Aston University

Aston University

**Some pages of this thesis may have been removed for copyright restrictions.**

If you have discovered material in AURA which is unlawful e.g. breaches copyright, (either yours or that of a third party) or any other law, including but not limited to those relating to patent, trademark, confidentiality, data protection, obscenity, defamation, libel, then please read our Takedown Policy and contact the service immediately

# Bifurcation Contrasts Between Plane Poiseuille Flow and Plane Magnetohydrodynamic Flow

BENJAMIN MICHAEL TOCHER

Doctor Of Philosophy


ASTON UNIVERSITY

*October 2011*

This copy of the thesis has been supplied on condition that anyone who consults it is understood to recognise that its copyright rests with its author and that no quotation from the thesis and no information derived from it may be published without proper acknowledgement.

ASTON UNIVERSITY

# Bifurcation Contrasts Between Plane Poiseuille Flow and Plane Magnetohydrodynamic Flow

BENJAMIN MICHAEL TOCHER

Doctor Of Philosophy, 2011

**Thesis Summary**

The stability characteristics of an incompressible viscous pressure-driven flow of an electrically conducting fluid between two parallel boundaries in the presence of a transverse magnetic field are compared and contrasted with those of Plane Poiseuille flow (PPF). Assuming that the outer regions adjacent to the fluid layer are perfectly electrically insulating, the appropriate boundary conditions are applied. The eigenvalue problems are then solved numerically to obtain the critical Reynolds number $Re_c$ and the critical wave number $\alpha_c$ in the limit of small Hartmann number (M) range to produce the curves of marginal stability. The non-linear two-dimensional travelling waves that bifurcate by way of a Hopf bifurcation from the neutral curves are approximated by a truncated Fourier series in the streamwise direction. Two and three dimensional secondary disturbances are applied to both the constant pressure and constant flux equilibrium solutions using Floquet theory as this is believed to be the generic mechanism of instability in shear flows. The change in shape of the undisturbed velocity profile caused by the magnetic field is found to be the dominant factor. Consequently the critical Reynolds number is found to increase rapidly with increasing M so the transverse magnetic field has a powerful stabilising effect on this type of flow.

**Keywords:** plane Poiseuille flow, Reynolds number, Hartmann number, travelling waves, secondary solutions, Fourier series, Chebyshev series, Floquet theory

# Contents

# List of Figures

*To*

*Dad.*

# Acknowledgements

First and foremost I am grateful to my supervisor Dr Sotos Generalis for the support, encouragement and much needed guidance offered to me during my studies at Aston.
Special thanks to my friends and colleagues James Bowley, Harry Goldingay, Jan Duracz, Diar Nasiev, Richard Jones and Ryszard Maciol who helped me tremendously and made my time in Birmingham enjoyable.
I would like to thank my family who's support made it possible to complete my studies.
Finally I would like to thank Albert Mantiziba who's inspirational teaching enthused me to study physics in the first place.

# Nomenclature

- $\alpha$ - Streamwise wavenumber
- $\mathbf{B}$ - Magnetic flux density
- $\hat{\mathbf{b}}$ - Magnetic field deviations
- $\beta$ - Spanwise wavenumber
- $c$ - speed of light
- $\mathbf{D}$ - Electric displacement
- $\mathbf{E}$ - Electric field
- $\varepsilon$ - Electrical permittivity
- $\mathbf{H}$ - Magnetic field strength
- $h$ - Half channel width
- $\mathbf{J}$ - Current density
- $L_2 - norm$ - Vector normal
- $\hat{i}, \hat{j}, \hat{k}$ - Unit normals
- $M = Bh\sqrt{(\sigma/\rho\nu)}$ - Hartmann number
- $\mathbf{P}$ - Pressure
- $\rho$ - Fluid density
- $\rho_c$ - Electric charge density
- $\sigma$ - Electrical conductivity

- $P_m$ - Magnetic Prandtl number
- $Re = (uh/\nu)$ - Reynolds number
- $Re_m = (uh/\sigma\mu)$ - Magnetic Reynolds number
- $\mathbf{u}$ - Velocity
- $\hat{\mathbf{u}}$ - Velocity deviations
- $\nu$ - Kinematic viscosity
- $\mu$ - Magnetic permeability
- $\phi$ - Streamwise streamfunction
- $\psi$ - Spanwise streamfunction

# 1 Introduction

*CONTENTS*

The aim of this project is to investigate the effect that an externally applied transverse magnetic field has on plane Poiseuille flow (PPF). To do this the Navier-Stokes equations are used as they describe the motion of fluids. They are derived by applying Newtons seconds law of motion $F = ma$ to a small fluid element in conjunction with the assumption that the fluid stress is the sum of a diffusing viscous term and a pressure term. The Navier-Stokes equations are coupled with Maxwells equations to study the magnetohydrodynamic side of the problem. The reason the Navier-Stokes equations are so useful is because their solutions are velocity fields which describes the velocity at any given point in space and time. To model the fluid motion more accurately appropriate boundary conditions must be applied along with certain assumptions such as the conservation of mass and the fluid is a continuum, incompressible and is Newtonian, for a good introduction to the subject see Elementary Fluid Dynamics by D. J. Acheson [1].

In the context of this thesis the transition or evolution of the steady regular laminar flow

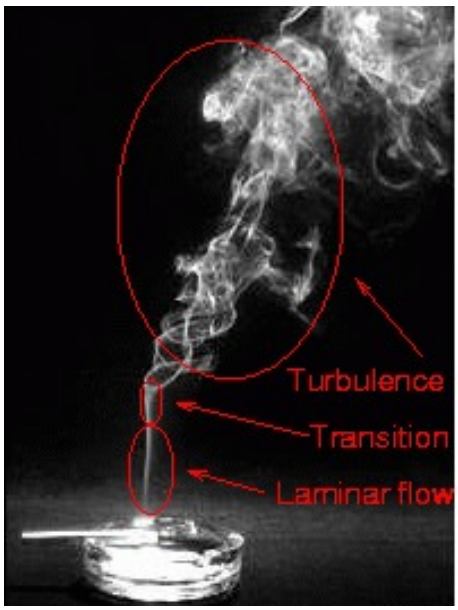


Figure 1.1: Cigarette smoke bifurcation diagram.

regime into the chaotic turbulent flow regime is of main concern. Fig1.1 visualises this process in the case of cigarette smoke in air rather nicely. A point of transition is known as a bifurcation and is caused when the flow becomes unstable with regards to a given disturbance or oscillation. The whole transition process can be made up of any number of individual bifurcations depending on the flow and the geometry of the system. Fig1.2 demonstrate the different cases of stability. A physical system is defined as stable if, after

a disturbance has been applied, it returns to its original state (case (a)), unstable if it never returns back to the original state (case (b)), neutrally stable if the system is not sensitive to any perturbation (case (c)) and stable for small disturbances if it returns to the original state only if the perturbation applied is small, whereas it never returns if the perturbation is larger than a certain threshold (case (d)). It should be clear also that the stability is always referred to a certain original state, called basic state. In fluid dynamics the basic state is called the basic flow and it is usually laminar (for instance, the air on a wing or car surface, the water on a submarine surface, etc.). The laminar flow can be stable or stable for small disturbances if it returns to its original state respectively after any disturbance or a small disturbance has been applied. On the contrary, the laminar flow is unstable if any disturbance does not die out but grows changing the laminar state to another. This other state is usually and commonly the turbulent flow but it could be also a more complicated laminar one. Referring back to the example of the cigarette , the original state (the laminar flow just at the end of the cigarette) undergoes an instability process that leads to the turbulent flow state. This particular laminar flow is thus unstable.

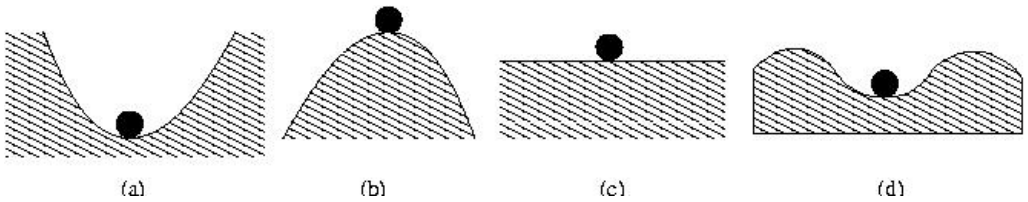


Figure 1.2: (a) stable, (b) unstable, (c) neutrally stable, (d) stable to small disturbances.

This work is supported by an EPSRC Case studentship in conjunction with Maxsys Ltd to elucidate the mechanism at work in the Maxsys Fuel system (MFS). Maxsys claim the MFS can increase the efficiency of a boiler by upto 5% by applying a relatively weak external transverse magnetic field to the gas intake of the burner. By modelling PPF and PPF with an externally applied transverse magnetic field, which shall be called plane pressure-driven magnetohydrodynamic flow (PPMF), and comparing the two, the effect that the magnetic field has on the flow and how it alters the stability characteristics will become apparent. Fig 1.3 shows a simple schematic representation of the MFS, with its two parallel channels it is clear to see why PPF is the basis of the model. The reason this work was commissioned is because the magnetic field in the MFS is too weak to ionise the natural gas flowing through it, so it was considered that the magnetic field may alter the flow

leading to the efficiency savings. Unfortunately natural gas has a low electrical conductivity and magnetic permeability (comparable to air), which means the MFS operates at a negligibly low Hartmann number $(M < 1 \times 10^{-5})$ and therefore does not have any significant affect on the flow which has lead many scientists and customers alike to dismiss the technology. The velocity of the gas flow is typically $u \approx 20ms^{-1}$ and the magnetic field strength in the MFS is $B < 1T$. From this it must be concluded that flow alterations are not responsible for the MFS efficiency savings and another mechanism is responsible. None the less this is an interesting problem in its own right and because it was initially commissioned for the MFS this study concentrates on a range of low Hartmann numbers, the Hartmann number being a dimensionless parameter that is the approximate ratio of the electromagnetic body force to the viscous force $M = Bh\sqrt{(\sigma/\rho\upsilon)}$. PPF is the viscous incompressible flow between two parallel boundaries, driven by a streamwise pressure gradient. It is an exact solution to the Navier-Stokes equation, has a finite critical Reynolds number and is a useful prototype to illustrate the fundamentals of stability theory in shear flows. This is because it has a simple solution structure so streamwise periodicity can be assumed and the complications of streamwise growth of the laminar boundary layer are avoided. The Reynolds number is also a dimensionless quantity and is the approximate ratio between the inertial forces and the viscous forces $Re = U_0 h/\upsilon$. The interactions between conducting shear flows and transverse magnetic fields have many practical applications such as designing magnetohydrodynamic (HMD) flow meters, HDM power generators, HDM pumps, HDM accelerator and nuclear fusion devices [80], [37]. There are also many theoretical astrophysical and geophysical problems such as accretion disks around black holes or neutron stars and how the Earth's magnetic field is influenced by the presence of hydrodynamic shear motions in the liquid core.

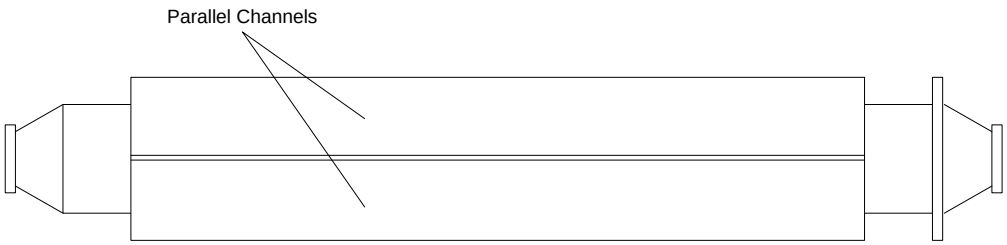


Figure 1.3: Schematic diagram of MFS.

The superimposition of a transverse magnetic field on PPF has two physical effects on

the fluid. Firstly a weak electromagnetic damping force known as the Lorentz force is produced and secondly it causes the basic velocity profile to become flat in the core or center of the flow due to the electromagnetic braking effect. The braking is caused by the interaction between the induced current and the applied magnetic field this in turn causes an electric current to flow down the boundary layers. This causes the boundary layers to become compressed against the boundary and has the aforementioned affect on the velocity profile. They were theoretically predicted and experimentally investigated in the seminal work of Hartmann and Lazarus [24] [25] and are consequently known as Hartmann layers. The Hartmann layer thickness $\delta$ is of the order $\delta = \frac{1}{B}\sqrt{\frac{\rho\nu}{\sigma}}$. To calculate these forces the fact that an electric current density $\mathbf{J}$ flows through the fluid in the presence of a magnetic field $\mathbf{B}$ was used, which in turn produces a force per unit volume of $\mathbf{J} \times \mathbf{B}$. This term in conjunction with the quasi steady state approximations of Maxwell's equations are used to formulate the Lorentz force term in the modified Navier-Stokes equation. The quasi steady state approximations of Maxwell's equations neglect the displacement current from Maxwell's version of Amperes law Eq 2.4. The steady state form of the modified Navier-Stokes equation is then solved using the boundary conditions to give the new parabolic velocity profile of PPMF.

Magnetohydrodynamics is a branch of continuum mechanics which deals with the motion of an electrically conducting fluid in the presence of a magnetic field. The motion of the conducting fluid across the magnetic field lines creates a potential difference which in general causes an electric current to flow. The magnetic fields generated by the current then alters the original magnetic field thereby changing the electromagnetic state of the system. Conversely the flow of electric current across a magnetic field is associated with a body force, called the Lorentz force which influences the fluid flow. These two effects together create an extremely complex feedback system. The magnetic Reynolds number is the ratio of the induced magnetic field relative to the inducing magnetic field and is found to be negligible at laboratory scales [88] and therefore the magnetic field is treated as homogeneous.

To study the effect that applying a transverse magnetic field has on the fluid flow from the view point of stability theory a global numerical bifurcation analysis of PPF and PPMF will be undertaken in the following three essential stages:

1. primary (linear) instability of the basic flow;
2. non-linear saturation of the primary instability and the formation of secondary flows;
3. secondary instability (Floquet theory).

The process by which PPF undergoes transition from smooth laminar flow to chaotic turbulent flow has been extensively studied both theoretically and experimentally. Thanks to its basic geometry and the relatively simple apparatus required it makes it an ideal candidate to demonstrate the fundamentals of stability theory in shear flows. PPF and PPMF are both examples of canonical flows and as previously mentioned are exact solutions of the Navier-Stokes equation. The early stages of turbulence however are still not theoretically fully understood but the basic understanding is as follows. PPF with its parabolic profile is stable up to $Re \approx 5800$ to infinitesimal disturbances, where upon a single mode at the boundary layer known as a wall mode becomes unstable, this mode will be looked at in some detail in chapter 3. This instability is known as a *Tollmien-Schlichting wave* and was experimentally verified by the experiments of Schubauer and Skramstad [95] for Blasius boundary layer flows and later confirmed for PPF. A Blasius boundary layer describes the steady two-dimensional boundary layer that forms on a semi-infinite plate which is parallel to a constant flow with a free top surface. Note that Blasius flow transitions evolve in space and are periodic in time and are said to exhibit spatial instability similar to PPF and PPMF. When no care is taken to exclude finite disturbances from the flow, turbulent streaks are observed at $Re \approx 500$ with the onset of fully turbulent flow at $Re \approx 1000$. This is far below the value predicted by linear theory. The transition to turbulence is abrupt in the sense that the laminar state becomes highly chaotic with no obvious intermediate bifurcations and is known as a *bypass transition* or the *jump phenomenon*. To try and reconcile this disparity non-linear disturbances are considered which give rise to vortical states, of which two-dimensional travelling wave type disturbances are the simplest type and for a long time had the lowest known limit point [11]. The term 'vortical states' was coined by Saffman [92] and refers to the various types of equilibrium solutions that exist, which are numerical solutions to the Navier-Stokes equation. The two-dimensional travelling wave equilibrium solutions persist to $Re \approx 2900$ and are highly unstable to three-dimensional secondary infinitesimal disturbances which explains the *jump phenomena*. There is much debate about how to reduce the critical Reynolds

number into the experimentally observed transition region and will be discussed later. This qualitatively relates to some point well below the linear critical Reynolds number where a finite disturbance is introduced, possibly by an irregularity on the wall or some external factor and provided this perturbation is not too small will grow rapidly with a sinusoidal motion producing the travelling wave solutions. The travelling waves themselves are highly unstable to infinitesimal three-dimensional secondary disturbances so much so that the onset of turbulence can appear instantaneous. At high Reynolds numbers turbulence ensues at once and the flow becomes random and strongly non-linear everywhere. From experiments it is not possible to observe the travelling waves directly as they are so unstable to three-dimensional secondary disturbances and therefore it is impossible to determine if they are two or three dimensional. So although the onset of turbulence appears to be a three-dimensional phenomenon because of the secondary instabilities this may not be the case, after all linear theory predicts that two-dimensional disturbances are the first to grow.

By contrast not such a large body of work has been conducted in the area of PPMF, possibly due to the difficulties analysing PPF it has been felt that an extra layer of complexity is undesirable. More likely though, PPF is a simple flow and a good prototype for more complex flows whereas PPMF is rather specialized and is only studied in its own right. Another draw back in the study of PPMF are the practical difficulties of laboratory magnetohydrodynamics. The major problem is that at the laboratory scales it is impractical to generate induced magnetic fields of comparable magnitude to those of the inducing fields. This makes it only possible to demonstrate one side of the magnetohydrodynamic relationship, fortunately it is comparatively easy to demonstrate the effect that a magnetic field has on fluid motion provided the Hartmann number value is high enough. It also explains why historically this side of the magnetohydrodynamic effect was discovered first and why the full understanding of magnetohydrodynamics came from the disciplines of astrophysics and geophysics.

To demonstrate the practical difficulties of magnetohydrodynamics the simple example of a *homopolar dynamo* is considered. A *homopolar dynamo* consists of a solid conducting disk mounted on an axle which is rotated with a constant torque in the presence of a

perpendicular uniform magnetic field with the fluid velocity in the direction of rotation. This experiment as with most others is limited by a dimensionless parameter known as the magnetic Reynolds number $Re_m = \mu\sigma uL$ which can be considered a rough measure of the induced field relative to that of the inducing field. The Magnetic Reynolds number has four variables the electrical conductivity and the magnetic permeability of the fluid, its velocity and the characteristic length scale of the experiment. To maximise the conductivity a liquid metal such as mercury (Hg) or liquid sodium (Na) is used. The conductivity of mercury (Hg) at $20^{\circ}C$ has a conductivity of $\sigma \approx 1.05 \times 10^6 Sm^{-1}$ and permeability of $\mu \approx 4\pi \times 10^{-7} Hm^{-1}$, giving $Re_m = 1.32uhm^2s^{-1}$, with H being the SI unit Henry and S being a Siemens. This leaves L and u, it is impractical to make L large because if you had a sphere with a radius of only r=1m this would contain 55 tons of Hg which would cost well over half a million pounds at today's market rate, making the experiment far too expensive. So to achieve an $Re_m$ of unity you require a fluid velocity of $u \approx 3/4ms^{-1}$. To make matters worse the magnetic Prandtl number $P_m = \frac{Re_m}{Re} = \nu\mu\sigma$ which is the approximate ratio of the viscous diffusivity to the magnetic diffusivity, where $\upsilon$ is the kinematic viscosity, is small for Hg $P_m = 1.57 \times 10^{-7}$. So the corresponding $Re \approx 6.7 \times 10^6$. This value of Re would cause the flow to be extremely turbulent making the results almost impossible to interpret with precision.

The work in this thesis carries on from the linear analysis of Lock [51] which itself is a continuation of the studies of Hartmann and Lazarus [24] [25]. Hartmann and Lazarus were the real pioneers of PPMF, they demonstrated that in the case of laminar flow the hydraulic resistance of a considered channel is in good agreement with the theoretical prediction obtained from the PPMF velocity profile. Moreover they showed that the transition between laminar and turbulent flow is governed by the dimensionless parameter $R = \frac{Re}{M} = \frac{U\delta}{\nu}$. They also found that the transition occurs in the range $150 < R < 250$. Lock showed that by comparing his results with those of Stuart [102]. He found that the principle effect of the transverse magnetic field is to modify the velocity distribution of the flow. Stuarts work considered a similar system but with a perpendicular magnetic field rather than a transverse one which has the same basic flow profile as PPF. So the only effect of the magnetic field was the direct electromagnetic damping of the linear disturbances from the Lorentz force term. This also has a stabilizing effect but to a much lesser degree. He also showed that as the Hartmann number M increased the shorter wavelength

perturbations experience a greater damping effect than the longer ones leading to a corresponding decrease in critical wavenumber $\alpha_c$. For the flow between two rotating cylinders with a magnetic field parallel to the axis of rotation it also experiences a similar dampening [10]. This is in contrast to Locks findings for a transverse magnetic field which despite an initial decrease in $\alpha_c$ the general trend is for $\alpha_c$ to increase with M, for large values of M (greater than about 20) they become directly proportional at $Re_c = 50000M$. The fact that $Re_c$ eventually becomes proportional to M had been conjectured on physical ground by Lundquist [52]. The wavenumber increases due to the thinning of the Hartmann layer, which at large values of M $(M > 5)$ becomes of the order $\alpha$ /M and will be of the same order of magnitude as the critical wavelength. The Hartmann layer can be treated as such because for $M > 5$ the velocity distribution is equivalent to an exponential boundary layer with a core of almost uniform velocity in the center. In addition Lock showed that Squire's theorem [98] is applicable for PPMF for fixed values of M and therefore only two-dimensional disturbances are considered for linear analysis. To the best of the authors knowledge this work is the first attempt at studying the non-linear aspects of PPMF. From the understanding obtained from the work on PPF it may seem that the linear stage can be dispensed with altogether, but mathematically it is the intermediate step before non-linearity is considered. Additionally, when comparing the two types of flow the linear stage is an important consideration because it shows to what degree the magnetic field's dampens the linear perturbations with respect to the non-linear disturbances. It is logical to expect the magnetic field to have a stabilising effect as energy is required to force the conducting fluid across the magnetic flux lines. This manifests itself by flattening out the velocity profile and squashing the boundary layers against the channel walls see Fig (3.1). It should be noted that although a magnetic field usually has a stabilizing effect in a rotating systems it has a destabilizing effect.

Turbulence is a ubiquitous phenomenon and is nature's way of restoring entropy to a system. What is surprising is that despite the diversity of the onset of chaos and the many different turbulent patterns which are observed for given systems is that in the last twenty years a certain universality of the routes to chaos has been observed in physical systems. It should been noted that a given system can exhibit several different types of transition for different ranges of parameter values. Mathematically, only a few solutions to non-linear differential equations are known and each of these had to be developed individually for

the case at hand. So one might reasonably imagine as no general solution method exists there is no general character to the solution. This explains the two schools of thought, the first that each system is different with the transition to chaos very sensitive to the initial conditions and therefore unique, and it certainly appears this way from the perspective of individual trajectories or Lyapunov exponents. The second being that as turbulence is ubiquitous and demonstrates large scale coherent patterns the mechanisms that cause its onset can be grouped into just a few broad categories as follows.

1. Via Local Bifurcations
    - Period-doubling:
    - Quasi-periodicity:
    - Intermittency:
        - Type 1 (tangent bifurcation intermittency)
        - Type 2 (Hopf bifurcation intermittency)
        - Type 3 (period-doubling intermittency)
        - On-off intermittency
2. Via Global Bifurcations
    - Chaotic transients
    - Crises

In the case of local bifurcations, which refers to linear disturbances, a limit cycle occurs for a range of parameter values until a transition occurs and the behaviour becomes chaotic by one of the methods outlined above. For global bifurcations the long term behaviour is influenced by unstable fixed points or cycles as well as attractors. As a parameter is changed, the transient trajectories become increasingly more complicated, producing chaotic transients. A period doubling bifurcation as the name suggests is a bifurcation in which a limit cycle becomes unstable and switches to a new behaviour with twice the period of the original, this process may continue until the period becomes infinite so the trajectory never repeats itself and is therefore chaotic. The quasi-periodic scenario involves the competition between two or more independent frequencies that characterise the behaviour of the system. The frequencies compete with one another and if the frequency ratio is irrational or incommensurate the behaviour is known as quasi-periodic

because the system never exactly repeats itself. This route to chaos is similar to that of period doubling in that one would observe a long sequence of different frequencies to occur as the control parameter is changed. The Intermittency route to chaos is characterized by dynamics with irregularly occurring bursts of turbulence interspersed with intervals of periodic behaviour. As some control parameter is changed the chaotic bursts become longer and occur more frequently until the entire time record is chaotic. A tangent bifurcation is when an attractor becomes a saddle node as a parameter passes through a certain value, then as the parameter is increased further it becomes a repellor, it is also called a saddle-node bifurcation or a fold bifurcation. A Hopf bifurcation is simply the birth of a limit cycle. In a chaotic transient, the system's trajectory wanders through state space, in an apparently chaotic manner until it approaches a regular periodic attractor. As the control parameter is changed this chaotic transients lasts longer until finally the asymptotic behaviour becomes chaotic. A crisis is a bifurcation event in which a chaotic attractor and its basin of attraction suddenly disappears or reduces in size due to the chaotic attractors interaction with an unstable fixed point or unstable limit cycle, as some control parameter is adjusted. The converse is also true, when the parameter value is changed in the opposite direction the chaotic attractor may suddenly appear or the basin of attraction increases.

The complexities of shear flows is partially to do with the dual role viscosity plays in open flows. Firstly it has the expected stabilising effect, where by it dissipates energy throughout the system thereby dampening any initial disturbance. This can be thought of as analogous to the diffusion of heat. It also has a second more complicated effect of diffusing momentum, which in shear flows has a destabilising effect because if there is strong shear in the boundary layers it can be diffused inwards towards the center of the flow. It also means once an instability does become non-linear some of the energy of the mean flow is diverted into the instability causing the shear layers to mix resulting in a *by-pass transition*. It has been shown that the two-dimensional travelling waves mediate the transfer of energy from the mean flow to the three-dimensional secondary perturbations but does not provide energy directly to the perturbations [73].

The other main problem with modelling shear flows is that using the methods outlined earlier it is not possible to take account of the adverse streamwise pressure gradient along the channel edges which results in boundary layer separation. The study of flow separation from the surface of a solid body, and the determination of global changes in the

flow field that develop as a result of the separation, are among the most fundamental and difficult problems of fluid dynamics. Boundary layer separation occurs when the portion of the boundary layer closest to the wall reverses in flow direction. As a result, the overall boundary layer suddenly thickens and is then forced off the surface by the reversed flow at the boundary edges. Once the fluid flow becomes detached from the surface it takes the forms of eddies and vortices. In aerodynamics, flow separation can often result in increased drag, particularly pressure drag, which is caused by the pressure differential between the front and rear surfaces of the object as it travels through the fluid. But the general magnitudes of the negative velocity gradient required for separation are much greater for turbulent than for laminar flow, the former being able to tolerate nearly an order of magnitude stronger flow deceleration. For this reason much effort and research has gone into the design of aerodynamic and hydrodynamic surfaces, which delay flow separation and keep the local flow attached for as long as possible. Examples of this include the fur on a tennis ball, dimples on a golf ball, turbulators on a glider, which induce an early transition to turbulent flow regime; vortex generators on light aircraft, for controlling the separation pattern amongst other examples. Another effect of boundary layer separation is shedding vortices, known as Karman vortex street. When the vortices begin to shed off the bounded surface they do so at a certain frequency and this results in the all to familiar 'snake like' disturbance pattern in shear flows, albeit with the vortices rotating in the opposite direction to PPF.

Present day transition predictions schemes are very crude and have severe limitations. Engineers still have to rely on a method developed in the 1950s which uses a combination of linear primary stability theory and an $e^N$ correlation scheme [96]. This method essentially equates the disturbance amplitude at transition with the amplitude at the first neutral stability point obtained from experiments. Used with care these semi-empirical prediction methods work fairly well for a wide range of situations of engineering interest. The success the $e^N$ method has in low disturbance environments is attributed to the rapidity of the non-linear process which allows it to be neglected in these situations. For PPF and PPMF where the linear stage is bypassed the $e^N$ method is not so useful unless backed up by extensive experimental data. To provide physical insight and ultimately produce a physically sound transition prediction scheme three-dimensionality and non-linearity must be considered. Despite this the analysis of the primary instability will be

mainly restricted to two-dimensions in accordance with Squire's findings [98]. Linear three-dimensional disturbances will only be considered briefly to show their stabilizing effect. The two-dimensional non-linear primary solutions will be the primary focus because considering three-dimensional states considerably complicates the secondary stability analysis and drastically increases the computational time required. In particular three-dimensional modes do not appear to saturate in order states for PPF [70]. In the PPMF analysis the magnetic term in the toroidal part has an inverse Laplacian operator that is expressed using type two Chebysev polynomials, which do not converge properly and is another reason why two-dimensional waves are the main focus. Chebysev polynomials are a sequence of orthogonal polynomials defined as the solutions to the Chebysev differential equations of which there are two kinds type 1 and type 2. Type 1 Chebysev polynomials are used as an approximation for the least square fit and are closely connected with trigonometric multi-angle formulas. They are used in the approximation of $\phi$ as they minimise the Runge's phenomenon and converge quickly between 1 and -1. It has been shown that three-dimensional primary instabilities do eventually lead to turbulence but not on a convective timescale and therefore bear no resemblance to experimentally observed transitions [73]. Using Keller's pseudo-archlength continuation method Ehrenstein studied pre-chaotic three-dimensional travelling waves in his PhD thesis and showed in their saturated state they do not lead to a reduction of the critical Reynolds number beyond that of the two-dimensional finite amplitude travelling waves [15]. Saying that he did locate bi-critical phase locked three-dimensional travelling waves which reduced the $Re_c \approx 1000$ [15], although not all the spanwise modes are included and therefore may well be an artificial construct. His study was confined to phase locked modes ($\sigma_i = 0$) as it is not possible to globally study quasi-periodic solutions due to their different phase velocity, it is still not clear the physical importance that non-phase locked modes have.

By using a similar method to Ehrenstein the finite amplitude disturbances are examined, by following the different bifurcating solution branches and looking at their basins of attraction and repulsion by performing a stability analysis. The non-linear analysis will concentrate on the two-dimensional non-linear saturated waves because in a moving frame they appear as steady solutions and therefore the time domain can be treated analytically by means of an eigenvalue problem which considerably simplifies their computation. The advantage of this is that unstable solutions can be found and a parameter search can be

performed in the solution space although high resolution numerics are not possible because of the poor convergence. It has been shown that spectral methods calculations made with only a few modes can be sufficient to obtain good qualitative results. Remarkably the *mean-field* approximation showed the sub-critical nature of PPF without taking into account the full effects of non-linearity. The *mean-field* approximation only takes into account the interaction between the first harmonic in the streamwise direction and the mean flow, this in effect modifies the variation in z but neglects the generation of higher harmonics outside the mean field. This follows from the reasoning that the mean flow profile in the presence of a steady wave will be different from the profile of the undisturbed flow due to the action of Reynolds stresses. So if the wave amplitude is not too large its evolution can be approximated by the linearisation about the distorted mean flow profile.

The real merit of global numerical bifurcation analysis comes in when looking at Saffman's hypothesis [92]. This states that during the transition from laminar to turbulent flow there exist unstable intermediate vortical states and that transition is caused by their instability to three-dimensional secondary disturbances and the complex interactions of these states. The intermediate states are not forgotten but manifest them-selves as the large scale coherent structures observed in turbulent flows. Typical examples of these vortical states are temporally periodic solutions with their most basic manifestation being two-dimensional travelling waves [11]. Pugh & Saffman [82] identified two types of of non-linear solution, constant pressure and constant flux. The two types of solution correspond to not having fixed the form of non-dimensionalization for the center line velocity $U_0$. The constant flux center line velocity relates to the flow being normalized in relation to the mass flux $U_0 = U_Q$ and the constant pressure by a mean pressure gradient $U_0 = U_P$. The two forms of center line velocity give rise to two Reynolds numbers $Re_Q$ and $Re_P$, which represent the extremes of a continuous range. With the constant flux condition having no flux perturbations but maximum pressure perturbations, as one travel through the spectrum the flux disturbances increase and the pressure ones decrease until the constant pressure condition remains. The different forms of non-dimensionalization alter the scaling of the problem but the underlying physics is the same. The constant flux condition has the lower limit point of the two.

To reduce the critical Reynolds number from $Re \approx 2900$ into the experimentally observed

range Orsag & Patera [73] proposed the analysis of quasi-equilibrium states which persist to $Re \approx 500$ in good agreement with the experimental result. These quasi-equilibrium states are not exact solutions to the Navier-Stokes equations with the perturbations proportional to the mean flow. It has been shown by direct numerical calculation that they decay far more slowly than the corresponding linear modes which implies that PPF has effectively stationary states down to Reynolds numbers in the experimental transition region. A three-dimensional stability analysis can also be performed on the quasi-equilibrium states on the assumption that their variation can be neglected. It was shown that three-dimensional secondary perturbations grow explosively if the amplitude of the quasi-equilibrium state is sufficiently large and the decay rate sufficiently small [73]. They found that below $Re \approx 1000$ the quasi-equilibrium states decay too fast for the secondary instability to grow, leading to Orsag and Patera to propose that the three-dimensional instability of two-dimensional quasi-equilibrium states are the primary mechanism of early transitions in PPF. Despite this the search for stable equilibria below $Re \approx 2900$ continues, with much work focusing on the previously mentioned bi-critical phase locked three-dimensional travelling waves which reduced the $Re_c \approx 1000$ [15]. More recently Waleffe [113] used homotopy from free slip Poiseuille or Couette solutions to non slip boundaries to find three-dimensional unstable travelling waves at $Re < 500$. These coherent states arise from saddle node bifurcations. Some of these instabilities will correspond to different physical manifestations such as travelling waves, while others will form *cascades* rather than self sustained structures. These solutions may correlate to the wavy streaks flanked by staggered streamwise vortices observed in boundary layer transitions. The most exciting thing about these results is that the self sustained instabilities are independent of the vorticity generated by the viscosity at the boundaries. There remain several other choices for further investigation such as non-phase locked branches which correspond to quasi-periodic solutions. Unfortunately it is not possible to compute these solutions globally as they do not appear steady in any reference frame so time analysis is be required, but this would also be problematic as the states are unstable.

By contrast in closed flow systems such as Taylor-Couette and Rayleigh-Benard problems viscosity only has a stabilising effect due to the slow flow rate. Therefore the secondary equilibrium solutions bifurcate super-critically from the neutral curve. This means the linear stage is not bypassed and therefore exhibit transitions via local bifurcations, usually

in sequential stages. Most research has concentrated on the diverse routes which closed flows take before they become turbulent. In these flows the transition evolution takes place over time and is periodic in space and is said to exhibit temporal instability. What is observed from experiments is that a thermal instability leads from the simple static state to turbulence through a variety of simple geometric structures or intermediate states, such as two-dimensional rolls or hexagonal cell structures [19]. A number of different transition paths have been identified such as after three incommensurate bifurcations [91], infinite period doubling bifurcations [17] or intermittently occurring turbulence [55]. These are by no means the only different types of transition as there are countless more which have not been identified here. The reason for the variety of different paths that the transitions may take in closed flow systems is due to the low Reynolds numbers at which weak turbulence occurs making it sensitive to initial conditions, the geometry of the system and other features of specific flows. Despite this in closed flow systems which undergo transitions via local bifurcations there does seem to be a certain universality in the transition to chaos which is exhibited by the real physical, chemical and biological systems that are modelled by these equations [32].

It is found in laterally heated flow (LHF) that the energy from the streamwise velocity cascades into the turbulent internal energy at the boundary layer via the intermittent behaviour of hairpin (horseshoe) shaped vortices. These vortices also form an integral part of the mechanism that sustains the turbulent state. They can be consider as analogous to the vortical structures in PPF as they facilitate the energy transfer to the near wall turbulence [109]. Further more in the absence of dampening effects the hairpin vortices generate omega-shaped vortices that dissipate up and down stream [89]. Generalis and Itano [18] recently established the existence of these hairpin vortical states in plane Couette flow (PCF) by using a homotopy method between LHF and PCF, similar sorts of structures have also been observed in boundary layer instabilities in Blasius layer flows [43] which has similar transition characteristics to PPF. This shows that even though LHF is inviscidly unstable, PPF is linearly unstable and PCF is linearly stable, the three examples exhibit similar turbulent structures at various bifurcation stages and hint at a certain universality of chaos. In all three cases the hairpin vortical states are three-dimensional structures.

It is generally accepted that turbulence is a three-dimensional phenomenon with vortex

stretching and tilting playing an important role. Squire's theory predicts that linear two-dimensional disturbances are more unstable than three-dimensional ones. In order to explain this apparent contradiction it does seem that the infinitesimal two-dimensional disturbances are the first to grow but as soon as their amplitude becomes finite they become unstable to three-dimensional secondary disturbances [36]. To this end the discovery that two-dimensional travelling wave equilibrium solution branches are linearly unstable to three-dimensional secondary disturbances with amplification rates an order of magnitude greater than those of the primary instability, constituted a major breakthrough in theoretical transition research [30].

## 1.1 Time dependant evolution

A second approach to studying the stability of finite amplitude disturbances is the integration of the initial value problem, which utilizes the numerical time dependence of the disturbance. This method utilizes direct numerical simulation, meaning the numerical solutions of the fully non-linear time dependent Navier-Stokes equations. This provides a complete space-time history of the flow field and permits precisely controlled experiment, but in reality is still dependent on computing resources and algorithmic limitations. This said in the spatial domain the laminar break down is one or two orders of magnitude smaller than that of the *Tollmien-Schlichting wave*. Providing enough grid points to observe all the phenomena is a challenging undertaking, indeed in the spatial domain the simulations have only reached the laminar breakdown stage. For this reason and partially because of the unresolved outflow boundary condition most work of this kind has been performed in the temporal setting. This means the evolution in space resulting from time dependent periodic forcing is replaced by the evolution in time resulting from a spatial periodic initial condition. This is the opposite of global numerical bifurcation analysis used in this thesis so the two methods can be used in conjunction to complement one another. In the main, time dependent numerical simulations have used finite-difference and/or spectral methods for the discretization in space of the Navier-Stokes equations, while a few transition simulations have utilized vortex methods (Leonard 1981, 1985). More recently, spectral domain-decomposition methods have come to the fore. In this approach, the domain is decomposed into a small number of sub-domains, and on each of these a spectral method is utilized.

Time dependant simulations have the advantage of being able to study flows without equilibrium states such as pipe flow, simulate experimentally observable flows and the feasibility of high-resolution numerics. However, the main problem with time dependent simulations is their dependence on the initial conditions which are never precisely known. This means that a large number of calculations must be carried out with different variations of initial conditions or guidance must be taken from physical experimentation. It also has the disadvantage of not being able to calculate unstable solutions. This approach has been used by a number of different authors Orszag and Kells [70], Orszag and Patera [73], Kleiser [44] and Kim [41] to name but a few. For a detailed review of time dependent transitions see Kleiser & Zang [45]

## 1.2 General historical background of shear flows

The pioneers in the theoretical study of hydrodynamic stability include some of the most illustrious names in physics such as Helmholtz [112], Kelvin [40], Rayleigh [84] [83] and Reynolds [86]. It is the first three that are generally credited with the development of classical *linear primary stability theory* for their work on the inertial instability of incompressible fluids of constant density. Although it was Reynolds (1883) experimental work that really stimulated the systematic study of viscous shear flows. Helmholtz most famous hydrodynamic work described the three-dimensional motion of inviscid fluids in the vicinity of vortex filaments and developed three laws which nowadays have applications in understanding things such as the generation of lift on an aerofoil, starting vortices, horseshoe vortices and the wingtip vortices. The first law stated that the strength of a vortex tube does not vary with time, the second declares that any fluid element that is lying on a vortex line at some instant continues to lie on that vortex line, i.e vortex lines move with the fluid. It also states that vortex lines or tubes must be closed loops, extend to infinity or start/end at a solid boundary. Thirdly any fluid element that is initially free of vorticity will remain free of vorticity. It should be noted that Helmholtz's theorems are generally proven with Kelvin's circulation theorem, although Helmholtz's work was published first there was a great deal of communication between the two on vortex lines. Kelvin's circulation theorem states *In an inviscid barotropic with conservative body forces, the circulation around a closed curve (which encloses the same fluid elements) moving with the fluid remains constant with time.* $\frac{D\Gamma}{Dt} = 0$, where $\Gamma$ is the circulation around a material con-

tour $C(t)$ and the condition of barotropicity implies that density is a function of pressure only $\rho = \rho(p)$. Rayleigh is probably most famous for his work on thermal instabilities, in which he modelled Benard's experiments by determining the equations of motion and boundary conditions and then deriving the linear equations for normal modes. From this he discovered the dimensionless number that bears his name, the Rayleigh number which is associated with buoyancy driven flow and is the ratio of the buoyancy forces and the product of the thermal and momentum diffusivity and it is the product of the Grashof and Prandlt numbers. Below a critical Rayleigh number the primary form of heat transfer is conduction and above it is convection. Although his greatest insight was to come in his famous theorem on the role of inflexion points in inviscid flows, known as the Rayleigh criteria.

In Reynolds classic 1883 paper [86] he writes of his experiments where he used three tubes of diameter 1 inch, $\frac{1}{2}$ inch and $\frac{1}{4}$ inch with all three being four feet six inches long submerged in a large glass tank full of water. Water was then drawn through the tubes which were fitted with trumpet mouthpieces, so the water might enter with out disturbance and arrangements made so a streak of dye can enter the tubes with the clear water. He observed at low velocities the streaks would remain in a straight line throughout the tube. If the water in the tank was disturbed before entering the tubes the streaks would move about in the tubes but with no apparent sinuosity i.e. a regular meandering pattern. As the intake velocity was incrementally increased he observed at some point the band of colour would strongly diffuse throughout the water with the distinctive turbulence pattern of curls and eddies, he also found as the intake velocity was increased the point in the tube where the turbulence begins became closer to the trumpet. To quantify these results he formulated the dimensionless parameter known today as the Reynolds number which is the ratio of inertial forces to viscous forces. Reynolds observed there was no critical value of Re below which the flow was stable and above the flow was unstable but rather the critical velocity was sensitive to the disturbance in the water before entering the tube. It was this that led Reynolds to realise that it was a stability problem. The method of normal modes for studying the oscillations and instability of dynamic systems of particles and rigid bodies was already highly developed in Reynolds time. The equations were linearised by neglecting the products of the perturbations and resolved into there independent components. It was then Stokes, Kelvin and Rayleigh that developed the method

of normal modes for inviscid flows in fluid dynamics by essentially using partial rather than ordinary differential equations. It is fair to say that inviscid theory is now reasonably complete, both physically and mathematically.

The equations of motion for a viscous fluid were established in the first half of the 18th century [64], [77], [93], [101] in what is now known as the Navier-Stokes equations although it was not until 1851 that Stokes formally adopted the no-slip boundary condition [100]. Due to the difficulties of integrating the equations of a viscous fluid the viscosity term was neglected until 1905 [79]. In Prandlt's 1905 paper he considered the flow of a fluid with a low viscosity with the clear recognition that the main effect was the shear forces in the boundary layer. His work went largely unrecognised for two decades partly due to the first world war but mainly because his work was so far ahead of its time. Only a few of his students at Göttingen published any work pertaining to boundary layer flows [6], [7], [31], for a detailed review of the history of boundary layer theory see Tani's 1977 paper [107]. The greatest recognised advance of the time in the the context of the linear stability of parallel shear flows was made by Orr [68] and Sommerfeld [97] who independently solved the linearised form of the Navier-Stokes equation for the perturbation velocity field. They both considered a small travelling wave type disturbance of the otherwise steady parallel flow and derive the so called Orr-Sommerfeld equation. Early attempts to solve the Orr-Sommerfeld equation proved far more complicated than had been anticipated due to the partial differential equations and the underdeveloped methods of asymptotic analysis. One of the first to try and solve the Orr-Sommerfeld equation was Taylor for Couette flow he found it to be stable for all Reynolds numbers in apparent disagreement with experiments although with modern apparatus this is known to be correct for infinitesimal disturbances. Undeterred Taylor then went on to carry out both stability calculations and experiments for circular Couette flow or Taylor-Couette flow [108] and found them to be in relatively good agreement considering the complexity of the mathematics at the time. Next he turned his attention to parallel shear flows and found that viscosity plays a dual role. Firstly it has the expected stabilising effect where by it dissipates energy. He adumbrated that viscosity also has a more complicated effect of diffusing momentum, which in shear flows has a destabilising effect. The effects of the diffusion of momentum and the arising boundary layer had been previously explained by Prandtl [79] unbeknown to Taylor.

In an attempt to solve the Orr-Sommerfeld equations analytically Heisenberg [26], Tollmien [111] and Schlichting [94] applied heuristic arguments by using the *method of matching asymptotic expansions* and although the resulting approximations are not uniformly valid they provide valuable insight into the general structure of the problem. The essential elements of the theory of *method of matching asymptotic expansions* include the derivation of first approximations of inner and outer type, the matching of these approximations and finally the combining of them to form composite approximations. The heuristic nature of this approach left some doubts about the theoretical predictions especially as they appeared in conflict with observations. Due to the experimental difficulties of reproducing the conditions of linear stability it was not until the experiments of Schubauer and Skramstad [95] that the predicted *Tollmien-Schlichting waves* were observed in the Blasius boundary layer. A *Tollmien-Schlichting wave* is a streamwise instability which arises in the viscous boundary layer and is slowly amplified as it moves downstream until it becomes large enough to give rise to non-linearity. It was Lin [50] that finally overcame the analytical difficulties of this earlier work although the asymptotic analysis techniques are far more advanced nowadays.

The first attempt to try and compute two-dimensional travelling waves for PPF was by Noether [67], who expanded the disturbance using a Fourier series using the *mean-field approximation*. It was not until 1951 that Meksyn & Stuart [57] obtained approximate solutions for these equations by using asymptotic expansions when again they looked at the interaction of a linear disturbance and the mean flow driven by a pressure gradient. They showed that PPF is linearly stable to $Re \approx 6000$ and despite the *mean-field approximation* being linear in the fact it only considers the first harmonic, they discovered the sub-critical nature of PPF for $Re > 2900$ based upon the maximum value of the mean velocity and the half-width of the channel. Stuart [103] and Watson [114] derived a more rational approach to calculate the linear stability by specifying a method to find the Landau equation for weakly non-linear disturbances at $Re$ close to $Re_c$ Reynolds & Potter [87] and Pekeris & Shkoller [75] subsequently made more accurate calculations and found $\alpha_c$=1.02 and $Re_c$=5772.22 It follows that a time periodic two-dimensional wave bifurcates from the neutral curve and they showed at lower wavenumbers the bifurcation was super-critical. Herbert demonstrated the limited range there weakly non-linear amplitude expansions have for PPF due to its highly non-linear nature, so there main use is to show what type

of bifurcation takes place (sub-critical or super-critical). Despite this the experiments of Klebanoff, Tidstrom & Sargent [43] revived interest in weakly non-linear theory. They demonstrated that longitudinal vortices are associated with three-dimensional non-linear wave motion. They observed in boundary layer instabilities that the actual breakdown of the wave motion into turbulence is a consequence of a new instability which arises from a two-dimensional Tollmein-Schlichting wave which quickly turns into a three-dimensional wave forming aligned *hairpin* eddies similar to the behaviour in *inflexional instabilities* now known as K-type transitions. The Tollmein-Schlichting wave demonstrates an inflexional velocity distribution with intense shear, known as the spike stage due to the 'spikes' in the waveform of the fluctuation. They appear instantaneously for each cycle of the fundamental frequency. This led Craik to introduce his *resonant triad* model [12], which exploits the resonance between two-dimensional Tollmein-Schlichting waves and two sub-harmonic oblique waves. This is an example of an internal resonance where strong coupling occurs between the shear resonating modes because the non-linear modes act as resonance forcing terms [76]. Another type of internal resonance is *direct resonance* that takes place when two linear eigenvalues coincide and the geometric multiplicity is less than the arithmetic multiplicity. None of this type of first order resonance exists on the linear neutral surface of PPF, but several instances are known between Orr-Sommerfeld and Squire modes for weakly damped modes [22], [23]. Stewartson & Stuart [99] considered spatial and temporal development of slightly unstable weakly non-linear modes, Hocking & Stewarton [33] then solved the Landau equation they derived for various cases and found the *bypass transition* described earlier.

## 1.3 Plane Poiseuille flow experimental background

The experiments of Nishioka, Iida & Ichikawa [66] were the first to experimentally verify linear stability theory, in fact they were able to maintain laminar flow upto $Re = 8000$ for PPF, far higher than linear theory predicts. The reason that laminar flow was possible at such high Reynolds numbers was attributed to the fact that the growth rate of unstable spatial disturbances is small. Consequently their channel was too short for the disturbances to grow sufficiently to cause transition. They experimentally determined the amplification rate and plotted it against the angular frequency and concluded the $Re_c \approx 6000$, in agreement with linear theory. The width to depth ratio or aspect ratio they used was 27.4

and the background turbulence was kept down to 0.05%. They found that the linear transition is preceded by intermittent irregular velocity fluctuations similar to the turbulent spots or bursts observed in Blasius flow transition. As a prelude to each burst there was always a sinusoidal velocity fluctuation, with frequencies just outside the upper branch of the linear neutral curve. The similarity between ribbon induced transition in PPF and boundary-layer flow firmly established PPF as an important model problem for the study of wall-bounded shear flows. Later in 1980 Kozlov & Ramazanov [47] were able to obtain similar results to those of Nishioka *et al* albeit with a longer channel. Before the remarkable experiments of Nishioka *et al* the experimental attempts to verify linear theory for PPF had all failed due to the technical difficulties of minimising the background turbulence. A few of these earlier attempts to prove linear theory experimentally but failed due to non-linear breakdown are outlined. The transition to turbulence in rectangular channels was first studied by Davies & White [13] who, using an aspect ratio greater than 37, found the transition to occur at $Re \approx 1080$ which is less than 20 % of the $Re_c$ predicted by linear theory. They disturbed the flow by a right angled corner at the channel inlet which caused flow separation, the wall pressure measurements indicated an inlet disturbance of $Re > 150$. Patel & Head [74] obtained similar results using a wind tunnel with an aspect ratio of 48 with the transition occurring at $Re \approx 1035$. The transitions in these experiments were caused by high intensity disturbances in the inlet flow. Kao & Park [38] used artificial excitement to examine the effects of sinusoidal disturbances to determine the neutral stability curve and found $Re_c \approx 1100$, their aspect ratio was 8. Carlson *et al* [9] performed a set of flow visualisation experiments of the transition in a water channel of aspect ratio 133. They carefully constructed the channel with a smooth contraction in order to achieve a low turbulence background flow, but nevertheless turbulent spots appeared spontaneously, leading to a transition at Re slightly above 1000. These observations suggest that the disturbances that trigger the onset of turbulence need not be as high as the maximum intensity in fully turbulent PPF. A number of experiments have been performed which have found the onset of turbulence to occur at Re=2500-2900 [63],[115],[27] again with the abrupt appearance of turbulent bursts. The experiments of Karnitz, Potter & Smith [39] with the aspect ratio of 70 and with the background turbulence kept down to 0.3 % managed to raise the $Re_c \approx 5000$. They found a sinusoidal disturbance preceded the turbulent burst although they did not examine the periodic disturbances in detail.

## 1.4 Plane pressure-driven magnetohydrodynamic flow experimental background

Hartmann and Lazarus [25] were the first to experimentally examine the global properties of pressure driven HMD flow in ducts. They found that the applied transverse magnetic field caused the velocity profile to flatten in the center of the flow and moreover for two boundary layers to develop at the walls now known as the Hartmann layers. They verified that the thickness $\delta$ of the boundary layers to be of the order of $\delta = \frac{1}{B}\sqrt{\frac{\rho\nu}{\sigma}}$. So the Hartmann layer thickness is independent of the channel width and decreases with magnetic field strength. To give a practical example liquid metal used in industry or in a laboratory setting such a mercury, gallium or steal typically have a $\rho\nu \approx 1 \times 10^{-3} Kgm^{-1}s^{-1}$, $\sigma \approx 1 \times 10^{6}\Omega^{-1}m^{-1}$, $B = 1T$ giving $\delta \approx 30\mu m$. Thus, Hartmann layers are usually very thin. The ratio between the channel width and the Hartmann layer thickness gives the dimensionless parameter known as the Hartmann number $M = \frac{d}{\delta} = Bd\sqrt{\frac{\sigma}{\rho\nu}}$ and is an approximate ratio of the electromagnetic force to the viscous force. They also showed that in the laminar region that the induced change in the velocity profile resulted in an increase of the apparent viscosity leading to a pressure drop along the duct. In the turbulent region this effect was counteracted by a decrease in the vorticity perpendicular to the magnetic field which can of set the effect of the pressure drop. Murgatroyd [59] found that the friction factor is a function of the ratio of the Reynolds number ($Re$) to the Hartmann number ($M$, which is equivalent to $R = \frac{Re}{M} = \frac{U\delta}{\nu}$. His experiments concentrated on the laminar turbulent transition and he found that even for different duct shapes and aspect ratios that turbulent breakdown always occurred in the range $150 < R < 250$.

Very few experiments have been performed for PPMF but many have been undertaken for MHD duct or Hunt flow [53] [8] [4] due to its relevance to fusion blankets. Fusion blankets consist of rectangular ducts in which liquid metal flows in the presence of a strong transverse magnetic field of between 5T and 10T. The purpose of these devices is to cool the plasma and to breed and remove tritium. The most famous theoretical work of this type was conducted by Hunt *et al* [34]. His work concentrated on the stability characteristics of the laminar layers and the related heat transport across them. He predicted that at high Hartmann numbers in MHD duct flow that laminarization occurs on the boundaries parallel to the magnetic field. According to linear stability theory they posses very

different stability properties and their role in the transition to turbulence is still not well understood. This effect does not happen in PPMF as the boundaries are set to infinity although it is important to mention the effect especially in the context of experimental MHD. At high $M$ values the instability if found to originate in the laminar layers parallel to the magnetic field while the core flow remained stable and that the local velocity of the flow in the parallel layers can exceed that in the core [85]. This leads to a dual effect, the Lorentz force dampens the turbulence while at the same time the magnetic field alters the basic velocity profile in such a was to create inflection lines [37] and jets [34]. To experimentally verify this Baylis *et al* [4] used an imposed radial current perpendicular to the axial magnetic field to drive a (MHD) flow around a rectangular annulus with electrically conducting boundaries. Some alterations to the theory had to be made for the curvature of the duct. Two other experimental factors had to be factored in which were not considered by the theory. Firstly the contact resistance between the copper conducting walls and the mercury fluid and secondly the resistance of the walls. Their comparison between theoretical and experimental results was good for the side wall boundary layer with only a small systematic error being of the order of the terms not considered in the theoretical expressions.

## 1.5 Global numerical bifurcation analysis

In the field of *global numerical bifurcation analysis* Herbert [28] was the first to calculate numerical solutions of the non-linear modal equations formulated by Heisenberg [26], which are known today as the *method of spectral collocation*. Spectral methods use a sum of basis functions (usually Fourier series) to numerically solve a certain differential equation by using the coefficients of the sum to satisfy the differential equation as accurately as possible. By employing up to four modes and considering the constant pressure condition Herbert [29] found the critical Reynolds number for two-dimensional travelling waves to be $Re \approx 2900$. These calculations were repeated albeit with more modes in order to benchmark our PPF results. Orszag & Kells [70], Orszag & Patera [73] and Pugh [81] also used spectral methods and achieved high accuracy by using several streamwise harmonics, most of these computations were done for two-dimensional

travelling waves. Using the *mean field approximation* Grohne [21] and Zahn *et al* [115] considered three-dimensional disturbances. This work was to lead to the fully non-linear treatment of three-dimensional disturbances by Pugh [81], Koch [46] and Ehrenstein & Koch [16] with the express aim of calculating secondary bifurcation equilibria. Progress in numerical bifurcation theory has matched the advance of numerical methods along with computer technology. As previously mentioned the intermediate travelling wave solutions are unstable in open flow systems and therefore have not been observed in experiments. This led Saffmann [92] to hypothesise that the origins of turbulent flow are not forgotten and these intermediate states, which he termed vortical states, are responsible for the large scale coherent structure observed in fully turbulent flow. These large scale coherent structures can be though of as being lower dimensional manifolds in whose neighbourhood the dynamical system spends a substantial fraction of time [35]. This leads to the logical conclusion that if the flow is dominated by these large scale structures then the determination of the intermediate solutions may lead to a better understanding of transition. The greatest breakthrough in recent years has been to recognize that secondary instabilities of two-dimensional primary waves is the generic transition mechanism in shear flows [71], [29], [30]. They originate from a parametric resonance and help explain the abrupt route to transition [15] although it fails to provide transition criteria without experimental data.

## 1.6 Time dependent numerical simulations

Accurate time dependent numerical simulations have only been made possible by the development of spectral methods and the large increases in computing power that have been made over the last two decades. Again few laminar flows correspond to known solutions of the non-linear equations of motion so research has been concentrated on a few simple examples. The PPF high resolution simulations of Kim, Moin & Moser [42] are a testament to how far computer simulations have advanced and how much detail can be included. Rozhdestvensky & Simakin [90] extended the work of Orszag & Patera [73] to show that even low resolution simulations can closely approximate several overall quantities of engineering interest, such as the friction factor or the mean velocity profile. This ties in with the aforementioned lower dimensional vortical states and shows that flows which are dominated by large scale coherent structures can be adequately modelled at low resolution.

## 1.7 Plane Pressure-driven Magnetohydodynamic flow historical background

The steady two-dimensional motion of a conducting fluid between parallel planes under a transverse magnetic field was the first problem in magnetohydrodynamics to be solved, by Hartmann & Lazarus [25]. Stuart [102] then investigated the effect of a co-planar magnetic field and found that a parallel magnetic field led to a steady rise in $Re_c$ as the magnetic field strength was increased. Lock [51] then investigated the effect of a perpendicular magnetic field and found it had a far stronger stabilising effect because the principal effect of the magnetic field is to modify the velocity distribution where as in the parallel field case it only adds a Lorentz force term to the Orr-Sommerfeld equation. In all this early work as in this study the magnetic Prandtl number $Pr_m \ll 1$, thereby eliminating all the magnetic fluctuation terms from the Navier-Stokes equations which also removes the magnetic boundary conditions, considerably simplifying the calculations. The Alfven number $A_v$ must also be large enough for the Hartmann number M to retain its finite value when it is defined as $M = P_m^{1/2} \cdot Re \cdot A$ [88]. This approximation has been made by several authors for various stability problems such as the aforementioned Stuart, Lock, Takashima [105] as well as Kakutani, [37], Nagata [60], [61] to mention but a few. The magnetic Prandlt number is a dimensionless parameter that approximates the ratio of momentum diffusivity and magnetic diffusivity. Although this simplification had been called into question by Lock himself and later Takashima [106] for large M values due to the high Re involved making the $Re_m$ not so small compared with unity. Potter & Kutchey [78] repeated Locks work but without the simplifications and found that the fluid flow became more stable as $Pr_m$ is increased although there do appear to be some mistakes in their working. They also used the incorrect boundary conditions for the magnetic field perturbations, they used $\psi = 0$ at $\pm 1$ which correspond to the boundaries being perfectly electrically conducting. Whilst their initial steady state velocity profile is that for perfectly non-conducting boundary conditions. Takashima [106] eliminated the mistakes and found that the transverse magnetic field had both and stabilising and destabilising effect on the fluid flow when $Pr_m$ is sufficiently small and that at a fixed value of M the flow becomes more unstable as $Pr_m$ is increased.

# 2 Formulation of the problem

For PPMF a pressure-driven electrically conducting fluid between two infinite parallel boundaries in the presence of a homogeneous transverse magnetic field $B_0$ is considered. The viscous fluid is assumed to be incompressible and of constant density. The origin O is midway between the plates and using Cartesian coordinates x, y, z and their corresponding unit vectors $\hat{\mathbf{i}}, \hat{\mathbf{j}}, \hat{\mathbf{k}}$ with the x-axis in the direction of the flow and the z-axis is perpendicular to the plates, see Fig 2.1. All physical quantities except pressure $P$ are independent of x, $\nabla P$ is only a function of z so $\frac{\partial P}{\partial x}$ is constant. The plates at z=$\pm$1 and y=$\pm\infty$ are perfectly electrically insulating and smooth. For PPF the same conditions are considered excluding the magnetic field, thus the equations that govern the fluid motion are:

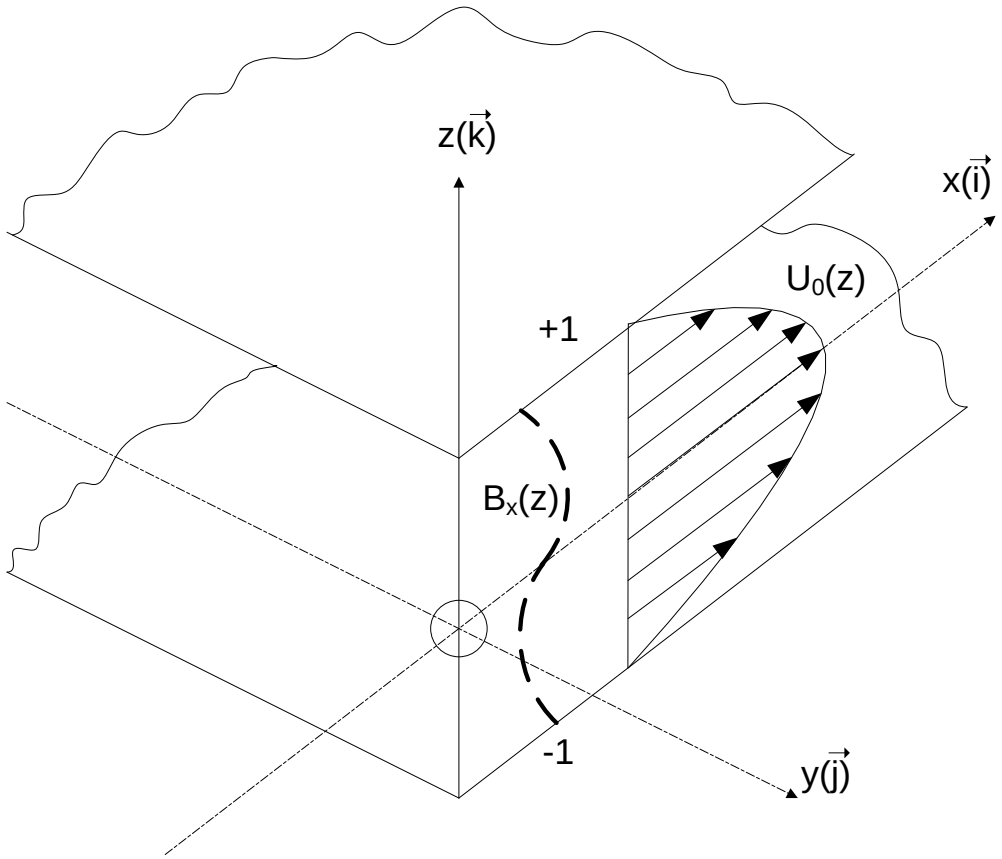


Figure 2.1: The geometrical configuration of PPF with a transverse magnetic field applied.

The incompressibilty condition

$$\nabla \cdot \mathbf{u} = 0 \tag{2.1}$$

The PPF Navier-Stokes equation

$$\frac{\partial \mathbf{u}}{\partial t} + (\mathbf{u} \cdot \nabla)\mathbf{u} = \frac{1}{\rho} \cdot \nabla P + \upsilon \nabla^2 \mathbf{u} \tag{2.2}$$

In order to derive the body force (Lorentz force) an electrically conducting fluid experiences when passing through a magnetic field Maxwell's equations are used, which govern the evolution of electric and magnetic fields. When a fluid contains an electric charge density $\rho_c$ there is a force per unit area $\mathbf{F} = \rho_c \mathbf{E}$. Similarly when a electric current density flows through the fluid it experiences a force per unit area $\mathbf{F} = \mathbf{J} \times \mathbf{B}$. It is fair to neglect the displacement current from 2.4 because the fluid flows that are considered are not relativistic and consequently the effects which are related to the propagation of electromagnetic waves are not relevant. The electric force can also be omitted as it is negligible in comparison to the Lorentz force.

Maxwell's equations

$$\nabla \cdot \mathbf{B} = 0, \tag{2.3}$$

$$\nabla \times \mathbf{H} = \mathbf{J} + \frac{\partial \mathbf{D}}{\partial t}, \tag{2.4}$$

$$\nabla \times \mathbf{E} = -\frac{\partial \mathbf{B}}{\partial t}. \tag{2.5}$$

$$\nabla \cdot \mathbf{D} = \rho_c \tag{2.6}$$

where in an isotropic medium $\mathbf{B} = \mu \mathbf{H}$ and $\mathbf{D} = \varepsilon \mathbf{E}$

Ohm's law states that the total electric current flowing in a conductor is proportional to the total electric field. In addition when the fluid is moving with velocity $\mathbf{u}$ in the presence of a magnetic field $\mathbf{B}$ it is subject to an additional electric field $\mathbf{u} \times \mathbf{B}$. Ohm's law is given by

$$\mathbf{J} = \sigma(\mathbf{E} + \mathbf{u} \times \mathbf{B}) \tag{2.7}$$

The Lorentz force

$$\mathbf{L} = \mathbf{J} \times \mathbf{B} = ((\nabla \times \mathbf{B}) \times \mathbf{B}) \tag{2.8}$$

Modified Navier-Stokes equation

$$\frac{\partial \mathbf{u}}{\partial t} + (\mathbf{u} \cdot \nabla)\mathbf{u} = \frac{1}{\rho} \cdot \nabla P + \upsilon \nabla^2 \mathbf{u} + ((\nabla \times \mathbf{B}) \times \mathbf{B}) \tag{2.9}$$

In order to eliminate $\mathbf{E}$ from the problem Ohm's law is used 2.7 in conjunction with 2.4 with the displacement current omitted and 2.5 and is known as the magnetic induction equation. It describes the evolution of the magnetic field. The first term on the right-hand side is the induction term and describes the interaction of the magnetic field and the flow, it is the only term that can generate a field. The second term on the right-hand side is

the diffusive term and causes the magnetic field to decay in the absence of a flow. The magnetic induction equation is given by

$$\frac{\partial \mathbf{B}}{\partial t} = \nabla \times (\mathbf{u} \times \mathbf{B}) + \eta \nabla^2 \mathbf{B} \tag{2.10}$$

where the magnetic diffusivity $\eta = \mu\sigma$

$\mathbf{u} = (u_x, u_y, u_z)$ is the fluid velocity, $\mathbf{B} = (B_x, B_y, B_z)$ is the magnetic induction, **H** and **E** are the magnetic and electric fields respectively, **J** is the current density vector, P is the pressure, $\rho$ is the fluid density, $\upsilon$ is the kinematic viscosity, $\sigma$ is the electrical conductivity and $\mu$ the magnetic permeability.

To write the above equations in dimensionless form the length is scaled with the half channel width h, the velocity with the maximum laminar velocity $U_0$ at the midchannel (z=0) and the magnetic field **B** is normalized with respect to $B_0$ the original transverse magnetic field. The Navier-Stokes equations and the Magnetic induction equations are non-dimensionalized with respect to kinematic viscosity $\upsilon$ as this is the cause of the instability, introducing the following dimensionless variables:
$(x^*, y^*, z^*) = (x/h, y/h, z/h)$, $u^* = \upsilon/h$, $t^* = h^2/\upsilon$
Eqs 2.2,2.9 and 2.10 become respectively

$$\frac{\partial \mathbf{u}}{\partial t} + (\mathbf{u} \cdot \nabla)\mathbf{u} = 2Re + \nabla^2 \mathbf{u} \tag{2.11}$$

$$\frac{\partial \mathbf{u}}{\partial t} + (\mathbf{u} \cdot \nabla)\mathbf{u} = 2Re + \nabla^2 \mathbf{u} + \frac{M^2}{P_m}(\nabla \times \mathbf{B}) \times \mathbf{B} \tag{2.12}$$

$$P_m\left(\frac{\partial \mathbf{B}}{\partial t} - \nabla \times (\mathbf{u} \times \mathbf{B})\right) = \nabla^2 \mathbf{B} \tag{2.13}$$

In many of the paper cited the Navier-Stokes equation for PPF is often non-dimensionalised with respect to a reference velocity $U^*_{ref}$(≡ maximum laminar velocity $U^*_{max}$ at midchannel) and is the equivalent of Eq 2.11. Where $\mathbf{u} \equiv (u, v, w) = \mathbf{u}^*/U^*_{ref}$ and $P = P^*/\rho^* U^{*2}_{ref}$ are the dimensionless velocity and pressure respectively, to give :
$\frac{\partial \mathbf{u}}{\partial t} + (\mathbf{u} \cdot \nabla)\mathbf{u} = -\nabla P + \frac{1}{Re}\nabla^2 \mathbf{u}$
In order to remove the boundary constrains on the magnetic field $\mathbf{u}, P$ and **B** are expanded in powers of $P_m$ for $P_m \ll 1$:

$$\mathbf{u} = u^{(0)} + P_m u^{(1)} + P_m^2 u^{(2)} + \ldots \tag{2.14}$$

$$P = p^{(0)} + P_m p^{(1)} + P_m^2 p^{(2)} + \ldots \tag{2.15}$$

$$\mathbf{B} = b^{(0)} + P_m b^{(1)} + P_m^2 b^{(2)} + \ldots \tag{2.16}$$

The leading order problem admits:

$$b^{(0)} \equiv \hat{k} \tag{2.17}$$

The next order equations are obtained in a closed form:

$$\nabla \cdot u^{(0)} = 0 \tag{2.18}$$

$$\frac{\partial u^{(0)}}{\partial t} + (u^{(0)} \cdot \nabla) u^{(0)} = -2Re + \nabla^2 u^{(0)} \tag{2.19}$$

$$\frac{\partial u^{(0)}}{\partial t} + (u^{(0)} \cdot \nabla) u^{(0)} = -2Re + \nabla^2 u^{(0)} + M^2 (\nabla \times b^{(1)}) \times \hat{k} \tag{2.20}$$

$$\nabla \cdot b^{(1)} = 0 \tag{2.21}$$

$$\nabla^2 b^{(1)} = -(\hat{k} \cdot \nabla) u^{(0)} \tag{2.22}$$

They must be solved subject to the boundary conditions at $z = \pm 1$

$$u^{(0)} = 0 \tag{2.23}$$

$$\hat{k} \cdot \nabla \times b^{(1)} = 0 \tag{2.24}$$

Re=$U_0 h/\upsilon$ is the Reynolds number, which is a dimensionless quantity and is the ratio between the inertial forces and the viscous forces, $M = Bh\sqrt{(\sigma/\rho\upsilon)}$ is the Hartmann number, which is the ratio of the electromagnetic force to the viscous force and is not dependent on the fluid velocity and $P_m = \mu\upsilon\sigma$ is the magnetic Prandatl number which is the approximate ratio between the viscous diffusion rate and the magnetic diffusion rate.

The velocity boundary conditions are $\mathbf{u} = 0$ at $z = \pm 1$ due to the non-slip condition. Since the condition must be satisfied for all x and y on the surface, it follows from the incompressibility condition that $\frac{\partial u_z}{\partial z} = 0$. The medium adjoining the fluid is non-conducting and therefore no current can cross the boundary. So $J_z = 0$ at $z = \pm 1$ and it is assumed that the external magnetic field is zero in the x-direction so $B_x = 0$ at $z = \pm 1$, although the magnetic field perturbation boundary conditions are now redundant.

The steady state solution of Eqn 2.11 consists of a basic velocity profile $\mathbf{u}_0 = U_0(z)\hat{\mathbf{i}}$ for PPF, of the form.

$$U_0(z) = Re(1 - z^2) \tag{2.25}$$

To find the basic velocity profile of PPMF the steady state solution of Eqn 2.12 is solved using the steady state of Eqs 2.13 to give:

$$U_0(z) = Re(\frac{\cosh(M) - \cosh(Mz)}{\cosh(M) - 1}) \tag{2.26}$$

$$\lim_{M\to 0} U_0(z) = Re(1 - z^2)$$

To explain the 'blunting' of the velocity profile as M increases it is best to think of the case when the conductivity of the fluid is infinite so the second term on the right-hand side of the magnetic induction equation Eqn 2.10 is zero. This makes the resistivity zero and will suffice for systems in which the variations of the field is short in comparison to the decay time, such as homogeneous fields and more physically cosmical and geophysical problems. In this form the magnetic induction equation is analogous to the vorticity equation as they are both solenoidal and it means the magnetic field lines and tubes can be treated the same as the vortex lines and tubes. So it is the equivalent of the Helmholtz-Kelvin theorem $\int_c \mathbf{B}d\mathbf{s} = const$. This implies the magnetic field lines consist of the same fluid elements, so it moves with the fluid like a material substance and behaves as though it is permanently attached to the fluid, this causes a drag on the fluid and flattens out the velocity profile. Applying the magnetic boundary conditions states above and using Eqn 2.26 then the streamwise magnetic field is of the form:

$$B_x(Z) = \frac{Re}{M}(\frac{\sinh(Mz) - z\sinh(M)}{\cosh(M) - 1}). \tag{2.27}$$

Next an infinitesimal disturbance is imposed on the steady velocity and magnetic fields described in Eqs 2.25, 2.26 and 2.27. The velocity deviations $\hat{\mathbf{u}}$ are separated from the basic flow $U_0(z)\hat{\mathbf{i}}$ and the magnetic deviations $\hat{b}$ from the basic magnetic profile $B_x(z)\hat{\mathbf{i}}$ and split into average parts $U(z,t) \equiv \bar{\hat{\mathbf{u}}}$ and $B(z,t) \equiv \bar{\hat{b}}$ and residuals $\hat{\mathbf{u}}$ and $\hat{\mathbf{b}}$ respectively:

$$\hat{\mathbf{u}} = \breve{U}(x,t)\hat{\mathbf{i}} + \breve{\mathbf{u}} \tag{2.28}$$

$$\hat{\mathbf{b}} = \breve{B}(x,t)\hat{\mathbf{i}} + \breve{\mathbf{b}} \tag{2.29}$$

The overbar denotes the average and is obtained by applying the operator $((\alpha\beta/4\pi^2)$ $\int_0^{2\pi/\alpha}\int_0^{2\pi/\beta} dxdy\cdot)$. The residuals $\breve{\mathbf{u}}$ and $\breve{\mathbf{b}}$ are then decomposed into poloidal and toroidal parts because they are solenoidal, by taking the double curl for the poloidal part and the

single curl for the toroidal part. The poloidal part for the velocity fluctuations comprises the Orr-Sommerfeld equation.

$$\breve{\mathbf{u}} = \boldsymbol{\delta}\phi + \boldsymbol{\varepsilon}\psi = \nabla \times \nabla \times (\hat{\mathbf{k}}\phi) + \nabla \times (\hat{\mathbf{k}}\psi) \tag{2.30}$$

$$\breve{\mathbf{b}} = \boldsymbol{\delta}g + \boldsymbol{\varepsilon}h = \nabla \times \nabla \times (\hat{\mathbf{k}}g) + \nabla \times (\hat{\mathbf{k}}h) \tag{2.31}$$

Where $\phi$ and $\psi$ are the streamwise and spanwise streamfunctions and g and h are poloidal and toroidal potentials of the magnetic fluctuations. The streamfunctions are used because they further simplify the equations and automatically satisfy the incompressibility equation Eqn 2.1 as well as being a convenient way of visualising fluid flow as they are constant along streamlines. This is demonstrated by substituting $u = \frac{\partial \phi}{\partial y}$, $v = -\frac{\partial \phi}{\partial x}$ into the simple two-dimensional example of the continuity equation $\frac{\partial u_x}{\partial x} + \frac{\partial u_y}{\partial y} = 0$, which gives $\frac{\partial \phi^2}{\partial x \partial y} - \frac{\partial \phi^2}{\partial x \partial y} = 0$. Eqs 2.1 and 2.3 and are automatically satisfied by Eqs 2.30 and 2.31 for the decomposition of the velocity and magnetic fields respectively. The total mean flow and the total mean magnetic induction are given by:

$$\hat{U}(z,t) = U_0(z) + \breve{U}(z,t), \tag{2.32}$$

$$\hat{B}(z,t) = U_0(z) + \breve{B}(z,t). \tag{2.33}$$

By applying $\boldsymbol{\delta}_i = \lambda_j \partial_i \partial_j - \lambda_i \Delta$ and $\boldsymbol{\varepsilon}_i = \varepsilon_{ijk}\lambda_k \partial_j$ to Eqs (2.10) and (2.11) the poloidal and toroidal parts of the motion equations for PPF and PPMF are obtained:

PPF

$$\hat{\mathbf{k}} \cdot \nabla \times \nabla \times (\breve{u} \cdot \nabla \breve{u}) = (\nabla^2 - \hat{U}\partial_x - \partial t)\nabla^2 \Delta_2 \phi + (\partial_z^2 \hat{U})\partial_X \Delta_2 \phi \tag{2.34}$$

$$\hat{\mathbf{k}} \cdot \nabla \times (\breve{u} \cdot \nabla \breve{u}) = (\nabla^2 - \hat{U}\partial_x - \partial t)\nabla^2 \psi + (\partial_z \hat{U})\partial_y \Delta_2 \phi \tag{2.35}$$

PPMF

$$\hat{\mathbf{k}} \cdot \nabla \times \nabla \times (\breve{u} \cdot \nabla \breve{u}) = (\nabla^2 - \hat{U}\partial_x - \partial t)\nabla^2 \Delta_2 \phi + (\partial_z^2 \hat{U})\partial_X \Delta_2 \phi + M^2 \partial_z \nabla^2 \Delta_2 g \tag{2.36}$$

$$\hat{\mathbf{k}} \cdot \nabla \times (\breve{u} \cdot \nabla \breve{u}) = (\nabla^2 - \hat{U}\partial_x - \partial t)\nabla^2 \psi + (\partial_z \hat{U})\partial_y \Delta_2 \phi + M^2 \partial_z \Delta_2 h \tag{2.37}$$

where $\Delta_2 = \partial_x^2 + \partial_y^2$ is the two-dimensional Laplacian operator or planform Laplacian.

To eliminate g and h they are expressed in terms of $\phi$ and $\psi$ by assuming that the magnetic Prandtl number $P_m$ is small and using $b^0 \equiv \hat{\mathbf{k}}$ in the steady state version of Eq 2.13 to give:

$$\nabla^2 b = -(\hat{\mathbf{k}} \cdot \nabla)\mathbf{u} \tag{2.38}$$

Applying the operations $\hat{\mathbf{k}} \cdot \nabla \times$ and $\hat{\mathbf{k}} \cdot$ to Eg 2.38 yields:

$$\nabla^2 \Delta_2 g = -\partial_z \Delta_2 \phi \tag{2.39}$$

$$\nabla^2 \Delta_2 h = -\partial_z \Delta_2 \psi \tag{2.40}$$

Substituting Eq 2.39 into Eq 2.36 and Eq 2.40 into Eq 2.37 gives:

$$\hat{\mathbf{K}} \cdot \nabla \times \nabla \times (\breve{u} \cdot \nabla \breve{u}) = (\nabla^2 - \hat{U}\partial_x - \partial t)\nabla^2 \Delta_2 \phi + (\partial_z^2 \hat{U})\partial_X \Delta_2 \phi + M^2 \partial_z^2 \Delta_2 \phi, \tag{2.41}$$

$$\hat{\mathbf{K}} \cdot \nabla \times (\breve{u} \cdot \nabla \breve{u}) = (\nabla^2 - \hat{U}\partial_x - \partial t)\nabla^2 \psi + (\partial_z \hat{U})\partial_y \Delta_2 \phi + M^2 \partial_z^2 \nabla^{-2} \psi. \tag{2.42}$$

The equations for the mean flow $\breve{U}(z,t)$ and the mean magnetic induction $\breve{B}(z,t)$ are obtained by taking the xy average of the x component of Eqs 2.34,2.41 and 2.38.

PPF

$$\partial_z^2 \breve{U} + \overline{\partial_z \Delta_2 \phi (\partial_x \partial_z \phi + \partial_y \psi)} = \partial_t \breve{U} \tag{2.43}$$

PPMF

$$\partial_z^2 \breve{U} - M^2 \breve{U} + \overline{\partial_z \Delta_2 \phi (\partial_x \partial_z \phi + \partial_y \psi)} = \partial_t \breve{U} \tag{2.44}$$

$$\partial_z^2 \breve{B} = -\partial_z \breve{U} \tag{2.45}$$

The boundary conditions now become $\phi = \partial_z \phi = \psi = \breve{U} = 0$ and there is no need to specify the boundary conditions for g and h as they have been eliminated.

# 3 Linear analysis

In linear analysis only infinitesimal disturbances are considered which are applied to the basic flow so any finite amplitude perturbations are neglected and consequently the non-linear terms are omitted. If the introduced linear perturbation dies away the flow is classed as stable, if it persists with a similar magnitude it is neutrally stable and if it grows enough so that it changes the basic flow to another laminar state or to a turbulent flow its unstable. In reality this determines whether it is a basin of attraction or repulsion with only attractors forming observable flows. To establish where the flow becomes unstable the locust of neutral stability points are plotted and is known as the neutral curve. This is because as a state passes from stable to unstable it becomes neutrally stable in a linear system. In physical terms a linear instability is initially localised in space and propagates like a wavepacket of the most unstable modes. Travelling with their group velocity and growing exponentially (although algebraically moderated through interference) as they travel in the direction of the basic flow. The disturbance decays rapidly up and down stream of the centre as it travels. So relative to an observer travelling at the group velocity the disturbance grows exponentially in time, but to an observer at a fixed stationary point the instability decays rapidly as its washed downstream. This sort of instability is called a convective instability. If on the other hand the group velocity is zero and the perturbation remains stationary as it grows exponentially then it is known as an absolute or non-convective instability.

In practice all small disturbances are possible, so for a flow to be called stable and therefore observable it must be stable to all possible disturbances. To this end the *method of normal modes* is used, whereby small wavelike disturbances are described by a superposition of normal modes, with each mode being treated separately as they each satisfy the linear system. The success of this method depends on finding a complete spectrum of normal modes to represent the development of any initial disturbance. The modes are normal in the sense they can move independently, that is to say the excitation of one mode will never cause the motion of another. For a disturbance to be considered linear it must be sufficiently small such that all non-linear terms can be neglected. This means the perturbation of the perturbation is neglected from the advection term in the governing equations. Shear flows can be divided into three categories according to their linear stability characteristics. The first case have inflectional mean-velocity profiles which are

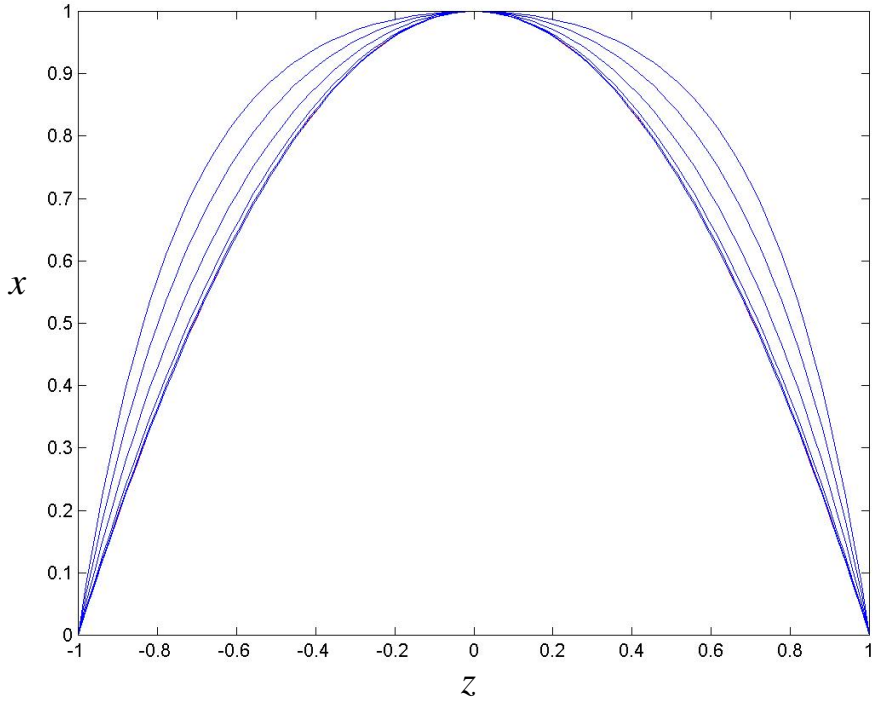


Figure 3.1: The basic velocity profile $U_0$ for M=0, M=0.1, M=0.5, M=1, M=2, M=3, M=4 at Re=1

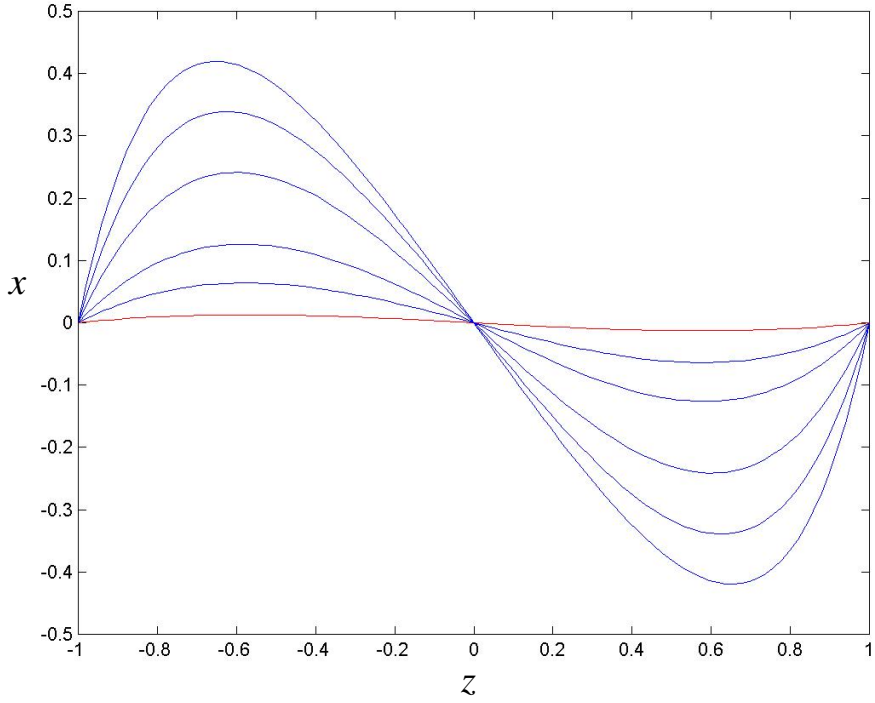


Figure 3.2: The magnetic velocity profile $B_0$ for M=0, M=0.1, M=0.5, M=1, M=2, M=3, M=4 at Re=1

inviscidly unstable according to the Rayleigh criteria or in other words these flows are unstable when viscosity is neglected from the governing equations. The second group are inviscidly stable but unstable to certain infinitesimal viscous disturbances which is the case for PPF, PPMF and Blasius flows. These flows have a finite critical Reynolds numbers $Re_c$, the critical Reynolds number is the lowest point on the neutral curve. This suggests that the linear instability in PPF and PPMF is driven by viscosity. The third group are linearly stable to both inviscid and viscous instabilities and examples include pipe Poiseuille flow and plane Couette flow (PCF). This third group is the least well understood especially pipe Poiseuille flow as no equilibrium solutions have been discovered. In this study only the second group are of concern as both PPF and PPMF exhibit this type of instability.

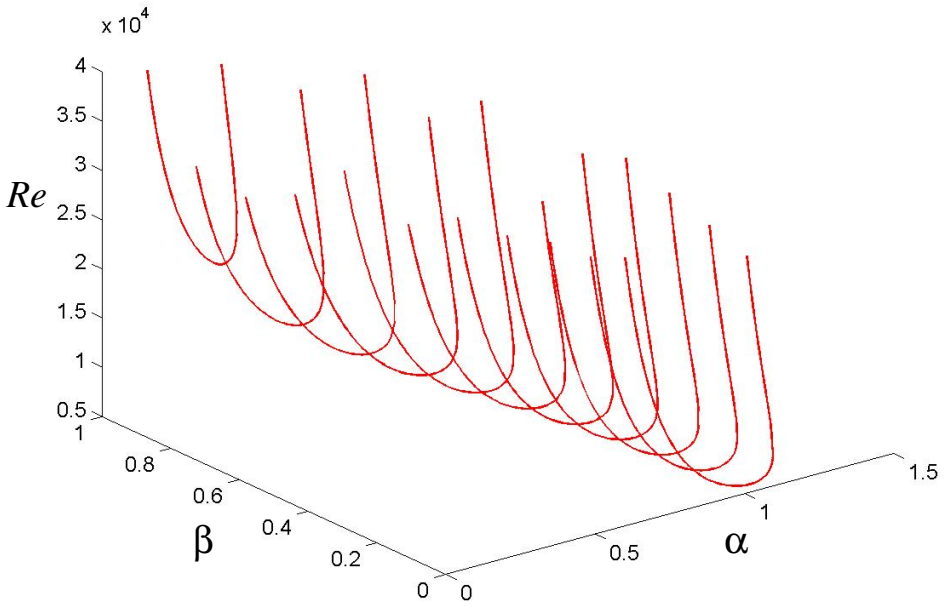


Figure 3.3: Neutral curve for PPF, $\beta = 0 - 1$.

In linear stability analysis only the interaction between an infinitesimal disturbances and the basic flow are considered so the mean flow is excluded Eqs 2.43, 2.44 along with the non-linear terms in Eqs 2.34, 2.35, 2.41 and 2.42. Both the polodial and toroidal parts of PPF and PPMF have been included for mathematical rigour, though two-dimensional

disturbances are of main concern.

PPF

$$\frac{\partial}{\partial t}\nabla^2\Delta_2\phi = (\nabla^2 - \hat{U}\partial_x)\nabla^2\Delta_2\phi + (\partial_z^2\hat{U})\partial_x\Delta_2\phi \tag{3.1}$$

$$\frac{\partial}{\partial t}\nabla^2\psi = (\nabla^2 - \hat{U}\partial_x)\nabla^2\psi + (\partial_z\hat{U})\partial_y\Delta_2\phi \tag{3.2}$$

PPMF

$$\frac{\partial}{\partial t}\nabla^2\Delta_2\phi = (\nabla^2 - \hat{U}\partial_x)\nabla^2\Delta_2\phi + (\partial_z^2\hat{U})\partial_x\Delta_2\phi + M^2\partial_z^2\Delta_2\phi \tag{3.3}$$

$$\frac{\partial}{\partial t}\nabla^2\psi = (\nabla^2 - \hat{U}\partial_x)\nabla^2\psi + (\partial_z\hat{U})\partial_y\Delta_2\phi + M^2\partial_z^2\nabla^{-2}\psi \tag{3.4}$$

Two-dimensional disturbances are the main focus because they are the most dangerous type as shown by Squire [98]. He stated "that, if any velocity profile is unstable for a particular Reynolds number, it will be unstable at a lower value of Reynolds number for two-dimensional disturbances". To demonstrate this, table 3.1 shows the stabilizing effect that longitudinal or β-type disturbances have on PPF and what is more, the larger the wavenumber of the longitudinal disturbance the greater the stabilizing effect, it also causes the $\alpha_c$ to decrease. Fig 3.3 shows the neutral curves for $\beta = 0-1$, this demonstrates the shape of the three-dimensional neutral surface for PPF and that the $\beta = 0$ plane is the most stable. Lock [51] showed an analogue of Squire's theorem to be true for PPMF. Eqs 3.1 - 3.4 together with the homogeneous boundary conditions $\phi = \partial_z\phi = \psi = \breve{U} = 0$ at $z = \pm 1$ constitute a generalized eigenvalue problem $Ax = \sigma Bx$ for PPF and PPMF. Using the fact that $P_m$ is extremely small, Lock simplified the governing equations, this simplification has been called into question for large M values [106] [78]. As this thesis is only concerned with small M values this simplification is considered to be valid. In order to solve the eigenvalue problem the Chebyshev collocation point method is employed across the channel with N+1 collocation points at $z_i = (\cos(i+1)\pi/(N+2))$, $i = 0,\ldots,N$ and expand in terms of a truncated Chebyshev series. A truncated power series is just a polynomial used to describe a function with the higher the truncation value the more accurate the description, but the computational time required rises so it is important to find an optimal level, although with the rapid increase in computing power this is not such an issue as it once was. This will be addressed in the next chapter in some detail, also see appendix 2 for details of how the Fourier power series is used to describe the modal disturbances. The disturbances is assumed to be wave like in nature and is set to:

$$\phi = exp[i\alpha(x - ct)]\sum_{n=o}^{N} a_n f_n(z) \tag{3.5}$$

where $\alpha$ is the wavenumber and c is the phase velocity and is generally complex, $f_n = (1-z^2)^2 T_n(z)$ with$T_n$ being the $n$th order type one Chebyshev polynomial and $a_0 - a_N$ are the complex coefficients. The factor $(1-z^2)^2$ is used so that the boundary conditions for $\phi$ are satisfied. The Eigenvalue problem $Ax = \sigma Bx$ where $\sigma = \sigma_r + i\sigma_i = i\alpha c$ and A and B are complex matrices. The QZ algorithm is employed by the IMSL libraries in Visual Fortran to invert the complex matrices and solve the generalized eigenvalue problem. The real part of the eigenvalue, $\sigma_r$ defines the rate of damping or amplification of the perturbations. If one $\sigma_r$ value is positive the system is unstable and the initial small perturbation grows exponentially with time, if all the $\sigma_r$ are negative the system is stable and the perturbations will die away. The imaginary part, $\sigma_i$ is associated with the phase velocity Re(c) of the propagating perturbations in the flow, where $\sigma_i = -\alpha Re(c)$. In order to achieve numerical accuracy for the results a high enough truncation number must be chosen in this case N=80 will suffice. For the linear bifurcation analysis the neutrally stable solutions are of primary interest so a Newton iteration method is used to find the curve of marginal stability. The neutral points are periodic in space and time so $\alpha$ and $\omega$ are real as there is no distinction between temporal and spatial instability.

In the case of PPF the eigenvalue spectrum is known to be discrete and complete with at most one unstable symmetric wall mode [49], usually termed the Tollmein-Schlichting mode which is the result of a Hopf bifurcation [14] which initiates a time periodic wave motion. Since the linear instabilities of PPF and PPMF are induced by viscosity the growth rates are small compared with the convective timescales observed experimentally. Orszag & Patera [73] state that for PPF the largest linear exponentially growing instability occurs at $Re_{opt} \approx 48000$ at $\alpha = 0.79$ with a growth rate of $Im\omega = 0.0076$, this was found using a time evolution program. This physically corresponds to the viscous or linear instability growing by a factor of 10 in the time it takes for a point on the center line to move 150 channel widths whereas the transition observed experimentally takes place in just a few channel widths. The distribution of the eigenvalue spectrum is shown in Fig 3.4 for the top 40 eigenvalues for $\alpha = 1.0$, $\beta = 0$ and $Re = 10000$ as this is the classic example initially used Thomas [110] and now quoted in most of the literature. It was calculated with N=80 collocation points and ordered by $\sigma_r$ as are all the eigenvalue spectrum plots. To benchmark the PPF eigenvalue spectrum against that of PPMF they are compared at $Re_c$, Figs 3.7 - 3.8. This is done because the absolute value $Re = 10000$ would not show a true reflection of how the eigenvalue spectrum changes as the magnetic field is

increased because $Re_c$ increases quickly with M so this point would fall far below the neutral curves for the higher M values and would therefore show the eigenvalue spectrum of a stable state. Mack [54] distinguishes the 3 classes of modes: the wall modes (A family), the centre modes (P family) and the mean velocity modes (S family). In Fig 3.4 the the different classes of mode are represented by different symbols with the wall modes denoted by circles $\bigcirc$, the center modes by triangles $\triangle$ and the mean velocity modes by squares $\square$. The modes are classed by there $\sigma_i$ which is closely related to the phase velocity, $\sigma_i = -\alpha Re(c)$. From Fig 3.4 it can be seen that the wall modes (A family) are travelling the slowest, as expected as this is the slowest part of the flow due to the non-slip condition. The center line velocity $U_0 = U_{max}$ so the center of the the flow is the fastest part because of the parabolic profile therefore the center modes (P family) have the highest velocity, with the mean velocity modes (S family) all having similar phase velocities as their name suggests. It should be noted for the generalized eigenvalue problem $Ax = \sigma Bx$ with $\sigma = -i\alpha c_i$ where as Mach has $\sigma = -i\alpha c_r$ so the eigenspectrum diagrams are the mirror image of those in Drazin & Reid [14]. Although the eigenvalue spectra look the same for PPF at $Re = 1000$ and $Re_c$ and in both cases it is the top wall mode number 80 that is the unstable mode (A1). For the second most dangerous mode P1 the mode number is different, at $Re_c$ P1 is mode 42 in Fig 3.4 P1 is mode 29, the mode numbers were found using the subroutine that orders the eigenvalues. Fig 3.5(a) shows the neutral curve for PPF with $Re_c = 5772.221816$ at $\alpha = 1.020547$ in good agreement with the literature. In Drazin and Reid [14] they cite Orszag results [69] who used the Lanczos's tau method rather than the more common Galerkin method. These results were later confirmed by Davey (unpublished) who utilized a shooting method. The results presented here were obtained using a Galerkin type projection method similar to those used by Ehrenstien & Koch [15] [16] and Orszag & Patera [72] [71] [73]. Galerkin methods are a way of converting continuous operators in this case partial differential equations to a discrete problem. The neutral curve is the locust of points with $\sigma_r = 0$ i.e. of neutral growth points and describes the stability boundary in the $Re, \alpha$ plane. From the diagram it can be seen that the neutral curve doubles back on itself as it tends to infinity on the right hand side with $\alpha_{max} = 1.0973$ so there is only a relatively narrow band of wave number values that the neutral curve covers so the system is linearly unstable to the related wavelengths. $Re_c$ is the lower Reynolds number value on the neutral curve and $\alpha_c$ is the corresponding wavenumber value.

Substituting Eq 3.5 into Eqs 3.1,3.3 gives the two dimensional form of the PPF and PPMF Orr-Sommerfeld equations.

$$-c(\alpha^4+\alpha^2)\phi = \alpha^6\phi + 2\alpha^4\phi'' + \alpha^2\phi'''' - \alpha^5\hat{U}\phi - \alpha\hat{U}\phi'' + \alpha^3\hat{U}''\phi \tag{3.6}$$

$$-c(\alpha^4+\alpha^2)\phi = \alpha^6\phi + 2\alpha^4\phi'' + \alpha^2\phi'''' - \alpha^5\hat{U}\phi - \alpha\hat{U}\phi'' + \alpha^3\hat{U}''\phi + M^2\alpha^2\phi'' \tag{3.7}$$

The basic velocity and magnetic profiles Eqs 2.26,2.27 are plotted inFigs 3.1,3.2 respectively, with increasing M, to show how the Hartmann number M effects the profiles between -1 and 1. From Fig 3.1 it is clear that as $M \to 0$ $U_0(z) \to (1-z^2)$. As M increases the basic velocity profile fattens out causing the velocity to be more uniform in the center of the channel, at the same time compressing the boundary layers against the outer surfaces giving rise to the Hartmann layers. It is this effect that is attributed for the majority of the stabilization. Fig 3.2 shows the magnetic field profile is almost horizontal to the flow at M=0.1, as M increases the profile becomes more pronounced with its two turning points being increasingly exaggerated. The magnetic field profile is treated as homogeneous because its fluctuations will be minimal at the flow rates considered.

Fig 3.5(b) shows the neutral curves of M=0.1-1.0. The critical Reynolds number $Re_c$ increases with increasing Hartmann number M, see Table 3.2. It is difficult to distinguish between the M=0.1 and M=0.2 curves but as M increases to M=1.0 the curves become more salient. The neutral curves for M=2.0 and M=3.0 are plotted on Fig 3.6(a) and the neutral curve for M=4.0 is plotted in Fig 3.6(b). They are plotted on separate graphs because of the large differences in $Re_c$ and aesthetically it looks better. For PPMF the eigenvalue spectrum is also discrete and complete and has one unstable wall mode due to a Hopf bifurcation which also leads to a time periodic wave motion. A Hopf bifurcation indicates the birth of a limit cycle, with a complex conjugate pair of eigenvalues becoming unstable although in this case only one becomes unstable, it is still classed as a Hopf bifurcation in the literature because it causes a similar sort of instability. Mathematically it is classed as a Hopf bifurcation because as $\sigma_{1r}$ passes through the zero growth rate point $\sigma_{1i} \neq 0$. At low Hartmann numbers the eigenvalue spectrum is similar to that of PPF, Fig 3.8(a). As the Hartmann number rises to M=1.0 the spectrum becomes more

Table 3.1: 3-D Linear results

| $\beta$ | $Re_c$ | $\alpha_c$ |
|---|---|---|
| 0.0 | 5772.22 | 1.02 |
| 0.1 | 5802.05 | 1.02 |
| 0.2 | 5886.66 | 1.00 |
| 0.3 | 6038.87 | 0.98 |
| 0.4 | 6273.23 | 0.94 |
| 0.5 | 6614.05 | 0.90 |
| 0.6 | 7113.61 | 0.84 |
| 0.7 | 7869.51 | 0.77 |
| 0.8 | 9093.74 | 0.68 |
| 0.9 | 11366.81 | 0.56 |
| 1.0 | 17156.43 | 0.41 |

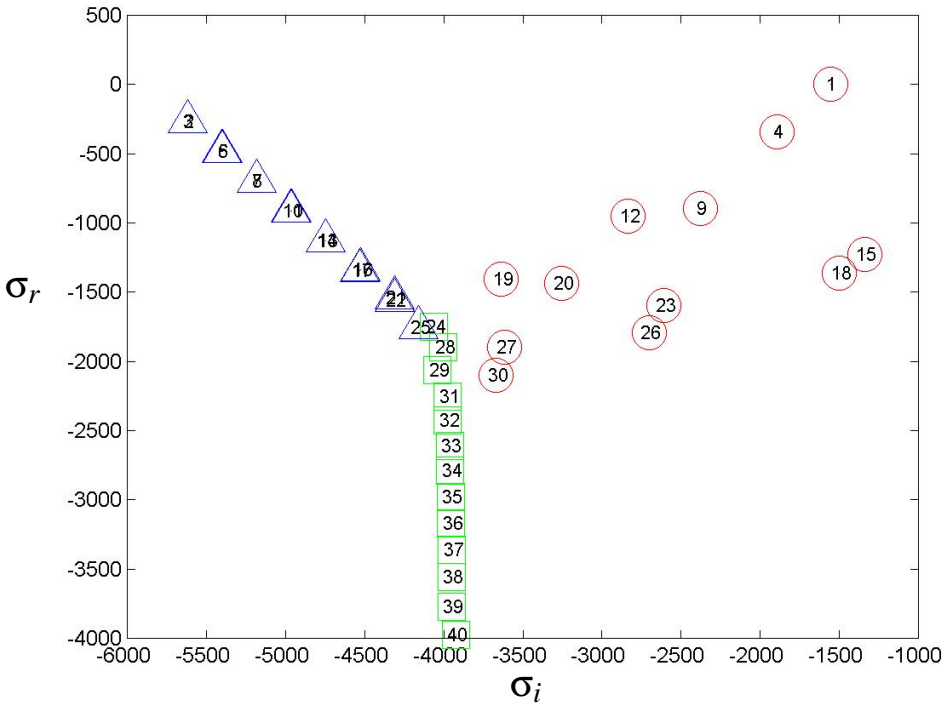


Figure 3.4: Eigenvalue spectrum at $\alpha = 1$, Re=10000 for PPF, M=0. ◯ - wall (A) modes, □ - mean velocity (S) modes, △ - center (P) modes

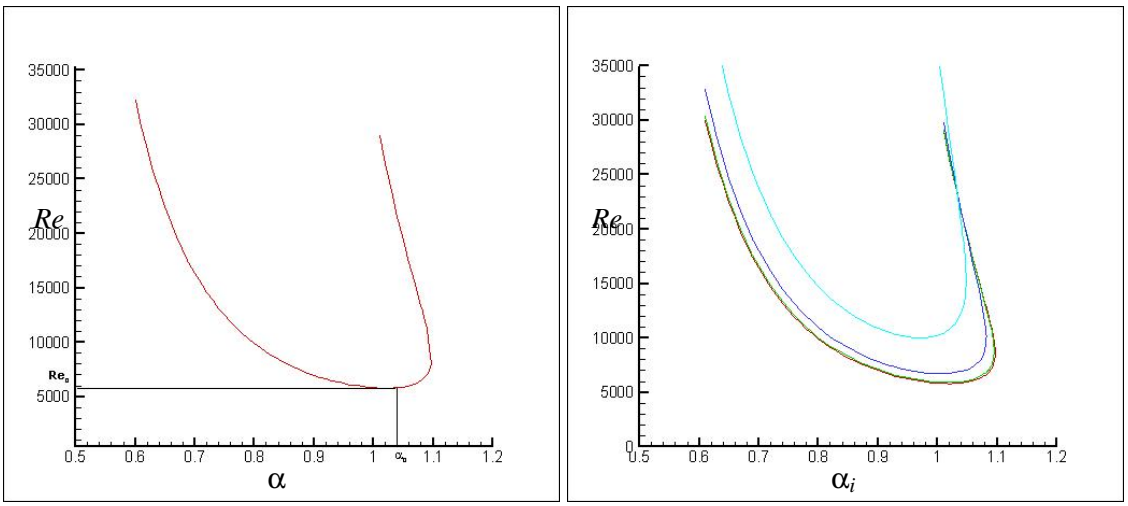


Figure 3.5: *a) PPF Neutral curve at $Re_c$. b) Neutral curve for PPMF, M=0.1 - M=1.0. at $Re_c$.*

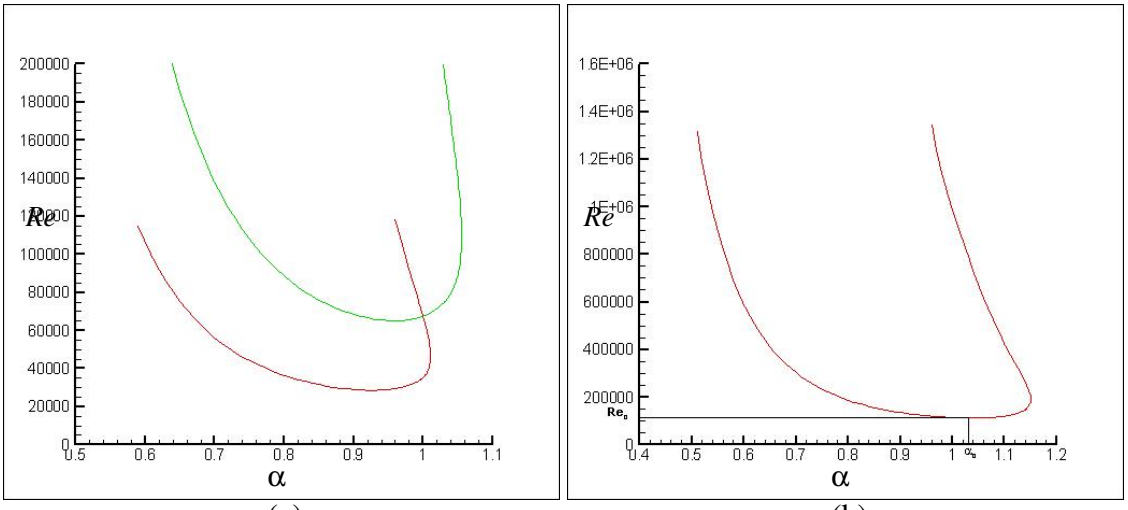


Figure 3.6: *a) Neutral curve for PPMF, M=2.0 and M=3.0 at $Re_c$. b) Neutral curve M=0.4 at $Re_c$.*

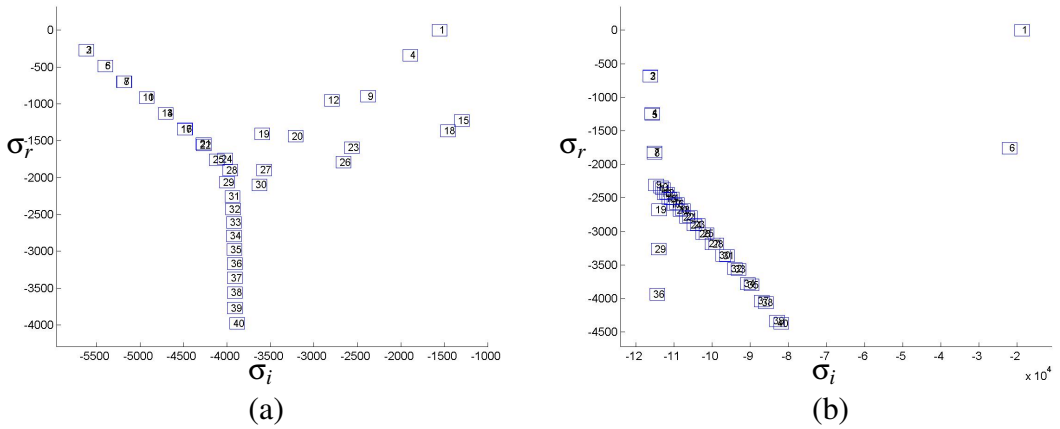


Figure 3.7: *a) Eigenvalue spectrum for M=0.0 at $Re_c$. b) Eigenvalue spectrum for M=4.0 at $Re_c$.*

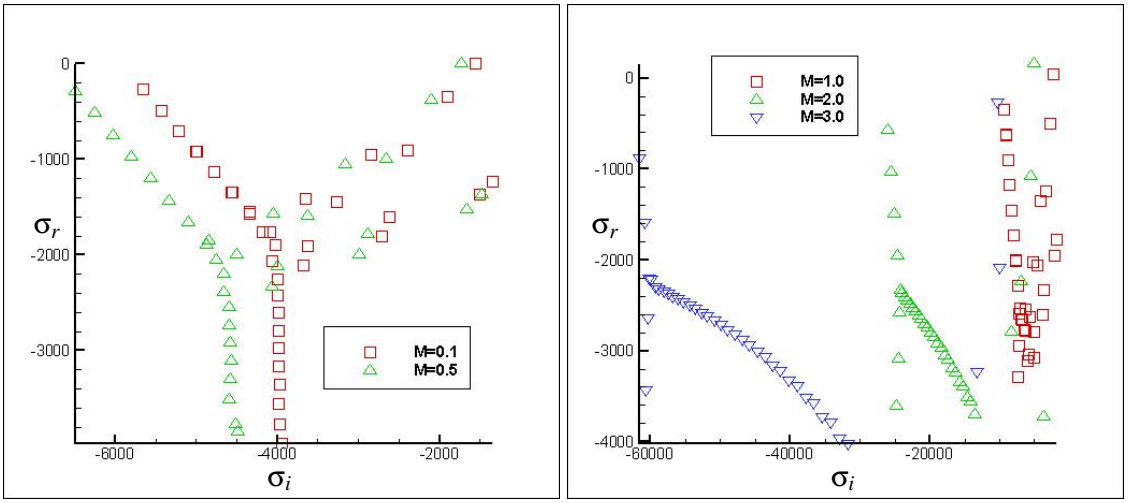


Figure 3.8: *a) Eigenvalue spectrum for M=0.1 and M=0.5 at $Re_c$. b) Eigenvalue spectrum for M=1.0, M=2.0 and M=3.0 at $Re_c$.*

Table 3.2: PPMF Linear results

| M | $Re_c$ | $\alpha_c$ | $\Delta Re_c$ |
|---|---|---|---|
| PPF | 5772.221816 | 1.020547 | 0.0 |
| 0.1 | 5807.870584 | 1.019917 | 35.648768 |
| 0.2 | 5915.675403 | 1.018044 | 143.453587 |
| 0.5 | 6706.091073 | 1.005734 | 933.870526 |
| 1.0 | 10016.262093 | 0.971829 | 4244.040277 |
| 2.0 | 28603.639354 | 0.927774 | 22831.41754 |
| 3.0 | 65155.213728 | 0.958249 | 59382.99191 |
| 4.0 | 112395.250686 | 1.035451 | 106623.0289 |

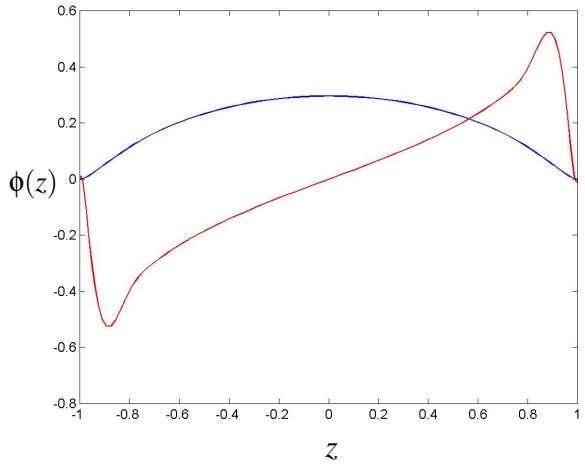


Figure 3.9: *Eigenfunction* $\phi(Z)$ *at Re=10000,* $\alpha = 1$ *for PPF, of the first symmetric and antisymmetric wall mode A1.*

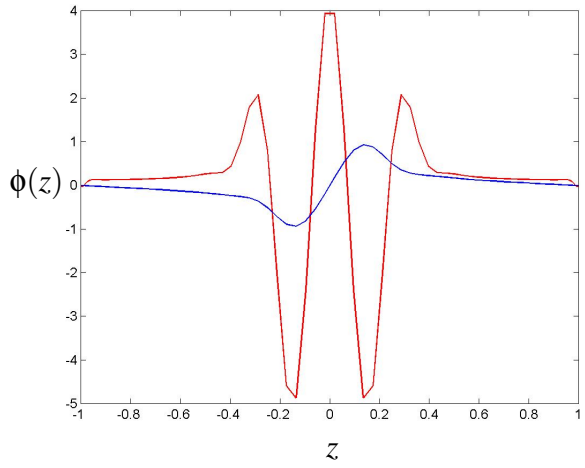


Figure 3.10: *Eigenfunction* $\phi(Z)$ *at Re=10000,* $\alpha = 1$ *for PPF, of the first symmetric and antisymmetric wall mode P1.*

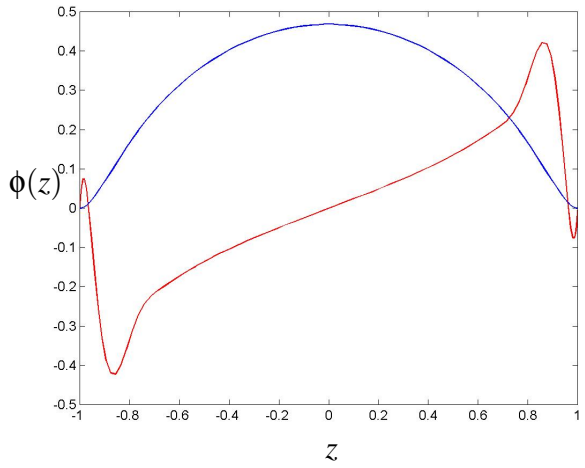


Figure 3.11: *Eigenfunction* $\phi(Z)$ *at Re=5773,* $\alpha = 1.02$ *for PPF, of the first symmetric and antisymmetric wall mode A1.*

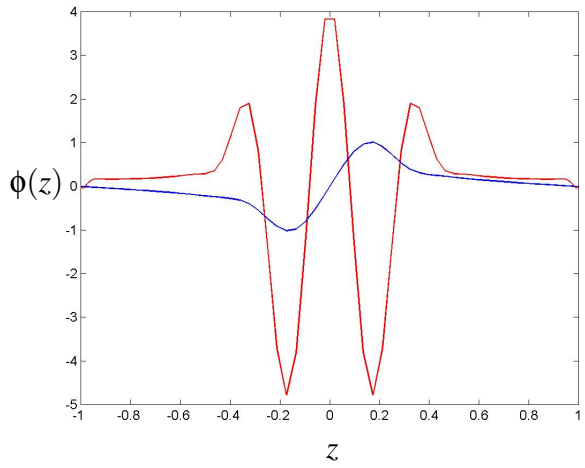


Figure 3.12: *Eigenfunction* $\phi(z)$ *at Re=5773,* $\alpha = 1.02$ *for PPF, of the first symmetric and antisymmetric wall mode P1.*

confused with no discernable mean velocity modes although unsurprisingly it is still wall mode 80 that becomes unstable. As the Hartmann number rises further the eigenvalue spectrum settles down with a distinct pattern that remains similar as the Hartmann number increases, although it bears no resemblance to that of PPF, see Figs 3.8(b). It is still possible to identify the wall and center modes but there appears to be no mean velocity modes as the $\sigma_i$ are no longer the same and can not be characterised as such because of their confused nature.

The PPF eigenfunctions correspond to the real part of the symmetric and antisymmetric modes for the top two eigenvalues. In all cases the most dangerous mode is the top

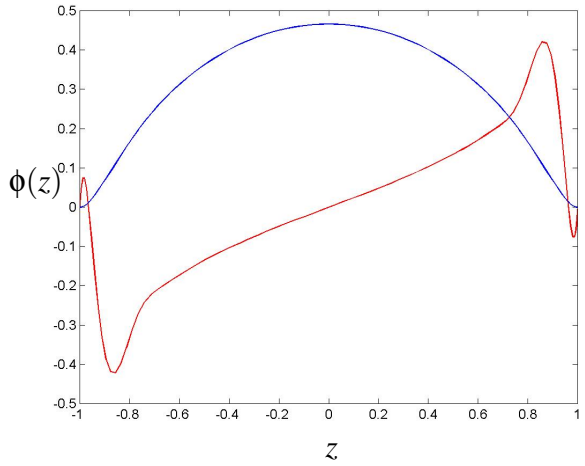


Figure 3.13: *Eigenfunction $\phi(Z)$ at $Re_c$, M=0.1 for PPMF, of the first symmetric and antisymmetric wall mode A1.*

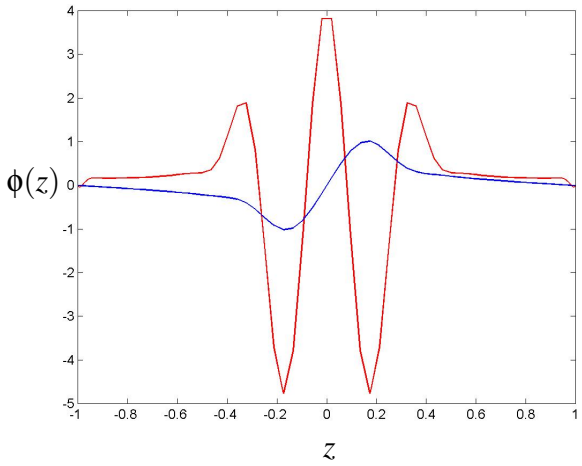


Figure 3.14: *Eigenfunction $\phi(Z)$ at $Re_c$, M=0.1 for PPMF, of the symmetric and antisymmetric center mode P1.*

wall mode 80 (A1), the second most dangerous is always a center mode (P1) but is not always the same mode because the P1 mode is sensitive to the Reynolds number. This qualitatively implies as the flow velocity increases the P1 mode is forced towards the back of the vortex. The modes have been calculated at $\alpha = 1$, Re=10000 as this has been used as a benchmark value starting from the work of Thomas [110] followed by Orszag [69] and most famously Mack [54]. The eigenfunction for the real part of the top two symmetric and antisymmetric modes are also calculated at just above $Re_c$, $\alpha = 1.02$, Re=5773 in order to compare the PPF with the PPMF. In the $\alpha = 1$, Re=10000 case P1 is the 29th mode and for the case just above $Re_c$ the P1 mode is the 42nd. Stuart [104] showed from the eigenfunctions it is possible to calculate the distribution of the Reynolds stress $S(z)$. As $S(z)$ is an odd function, the product SdU/dz is negative everywhere suggesting there is a transfer of energy from the basic flow to the disturbance at all values of z although the major contribution is at the two critical points. $S(Z) = \phi_r D\phi_i - \phi_i D\phi_r$ where $\phi_r = a_r cos(m\alpha x) - a_i sin(m\alpha x)$ and $\phi_i = i(a_r sin(m\alpha x) + a_i cos(m\alpha x)$

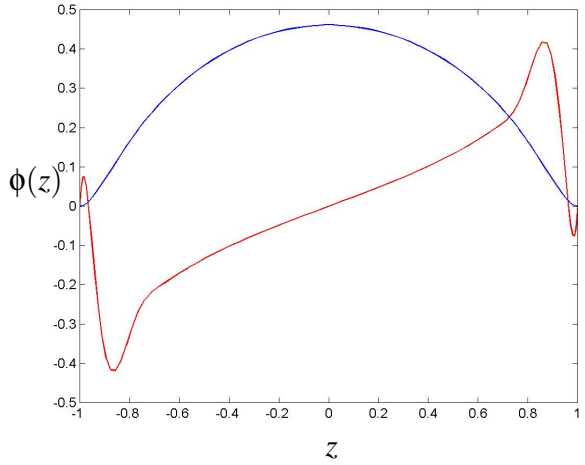


Figure 3.15: *Eigenfunction* $\phi(Z)$ *at* $Re_c$*, M=0.2 for PPMF, of the first symmetric and antisymmetric wall mode A1.*

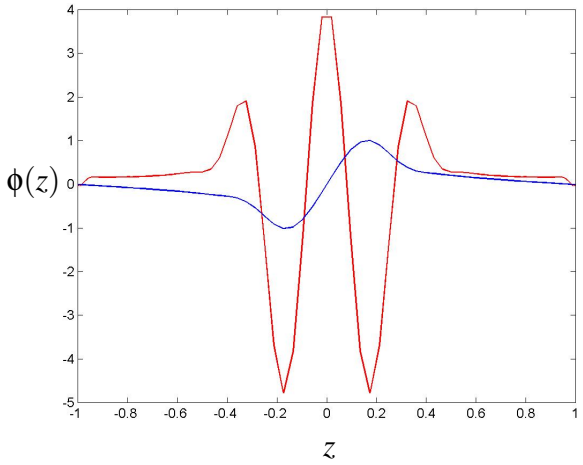


Figure 3.16: *Eigenfunction* $\phi(Z)$ *at* $Re_c$*, M=0.2 for PPMF, of the symmetric and antisymmetric center mode P1.*

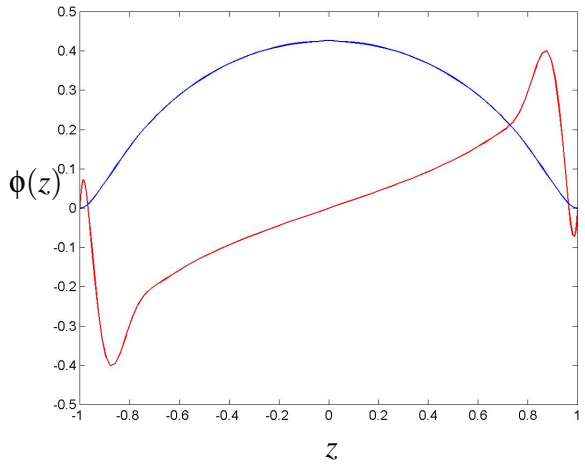


Figure 3.17: *Eigenfunction* $\phi(Z)$ *at* $Re_c$*, M=0.5 for PPMF, of the first symmetric and antisymmetric wall mode A1.*

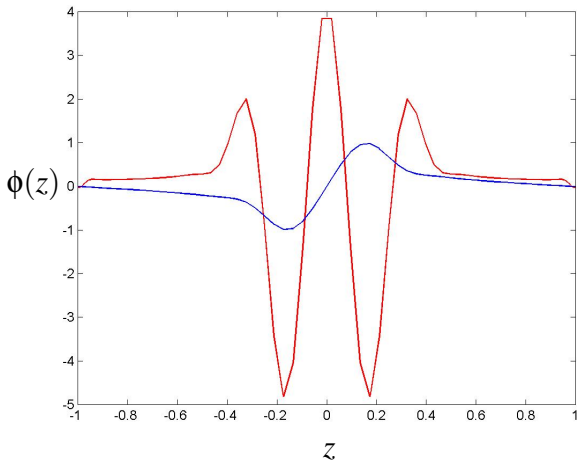


Figure 3.18: *Eigenfunction* $\phi(Z)$ *at* $Re_c$*, M=0.5 for PPMF, of the symmetric and antisymmetric center mode P1.*

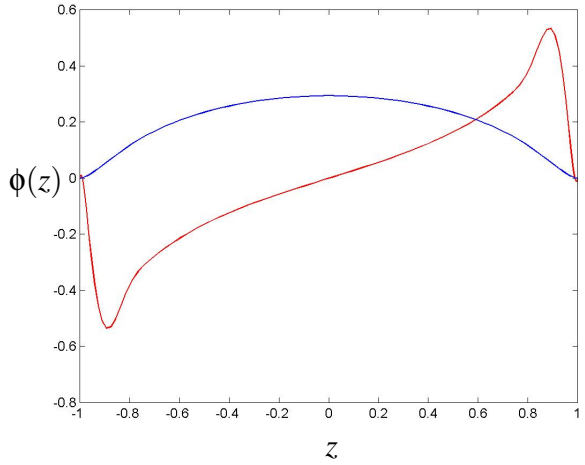


Figure 3.19: *Eigenfunction $\phi(Z)$ at $Re_c$, M=1.0 for PPMF, of the first symmetric and antisymmetric wall mode A1.*

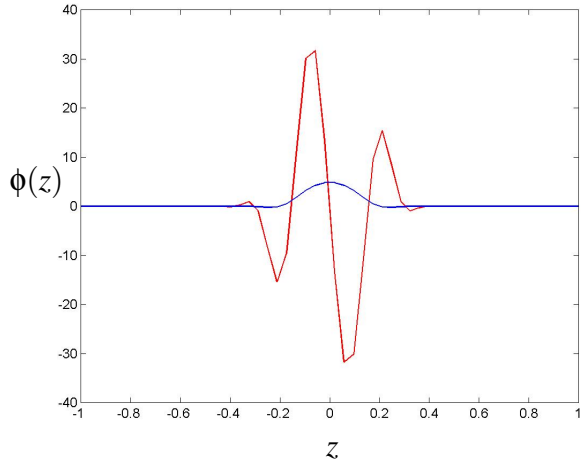


Figure 3.20: *Eigenfunction $\phi(Z)$ at $Re_c$, M=1.0 for PPMF, of the symmetric and antisymmetric center mode P1.*

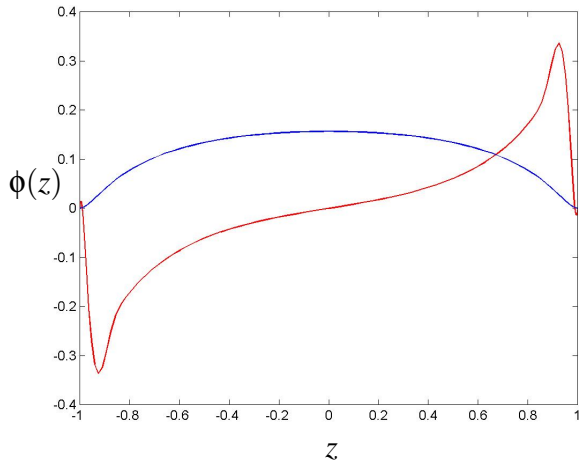


Figure 3.21: *Eigenfunction $\phi(Z)$ at $Re_c$, M=2.0 for PPMF, of the first symmetric and antisymmetric wall mode A1.*

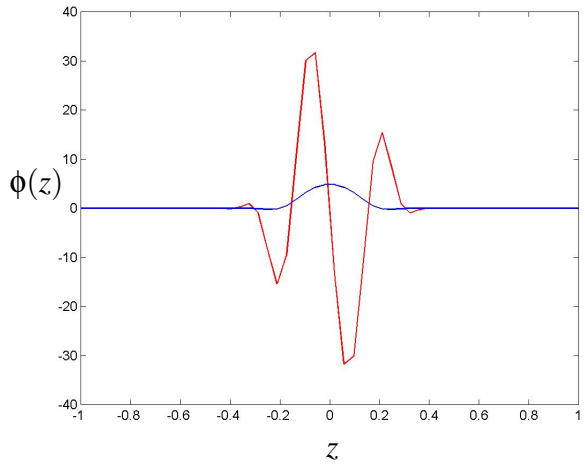


Figure 3.22: *Eigenfunction $\phi(Z)$ at $Re_c$, M=2.0 for PPMF, of the symmetric and antisymmetric center mode P1.*

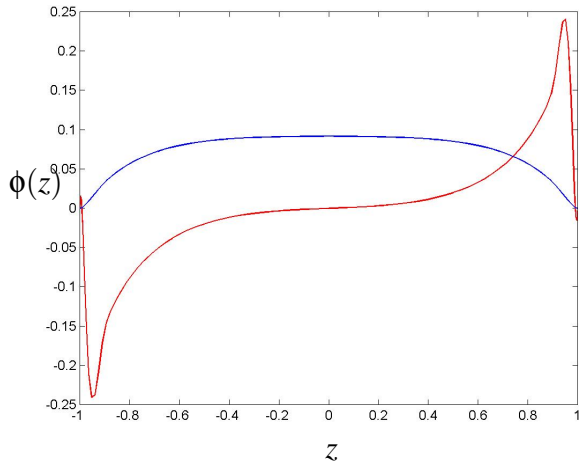


Figure 3.23: *Eigenfunction* $\phi(Z)$ *at* $Re_c$*, M=3.0 for PPMF, of the first symmetric and antisymmetric wall mode A1.*

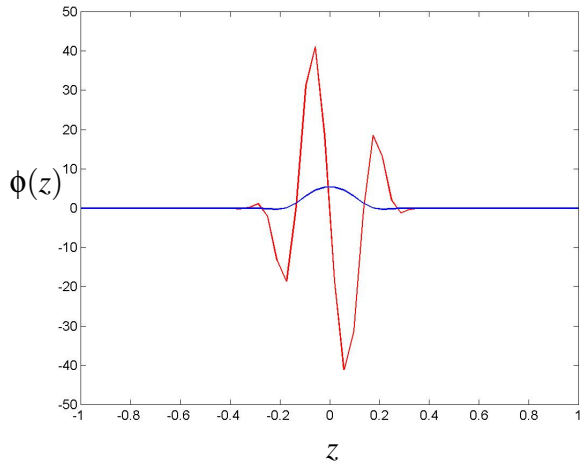


Figure 3.24: *Eigenfunction* $\phi(Z)$ *at* $Re_c$*, M=3.0 for PPMF, of the symmetric and antisymmetric center mode P1.*

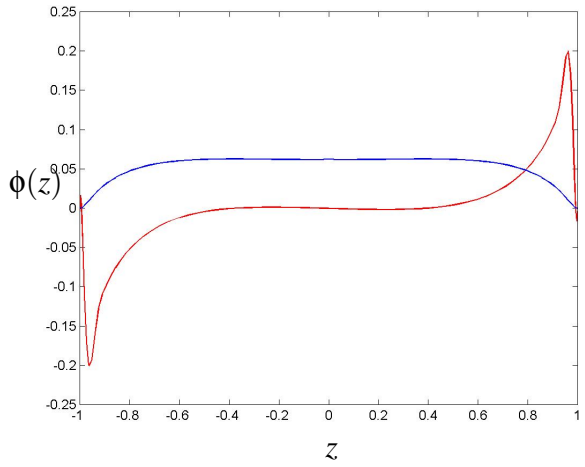


Figure 3.25: *Eigenfunction* $\phi(Z)$ *at* $Re_c$*, M=4.0 for PPMF, of the first symmetric and antisymmetric wall mode A1.*

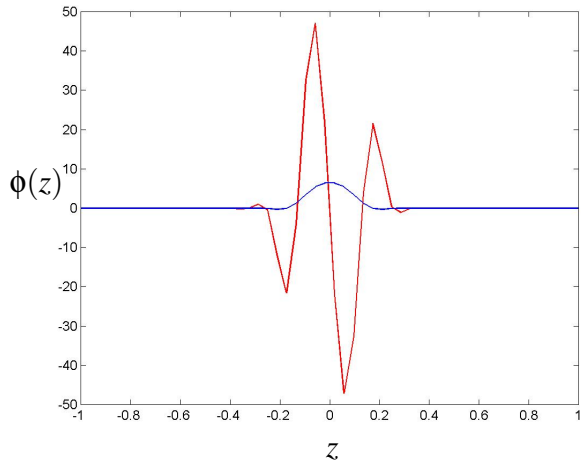


Figure 3.26: *Eigenfunction* $\phi(Z)$ *at* $Re_c$*, M=4.0 for PPMF, of the symmetric and antisymmetric center mode P1.*

# 4 Secondary equilibrium states

CONTENTS

Hydrodynamic instability is concerned with how the laminar flow breaks down, its subsequent development and the eventual transition to turbulence. In the case of linear stability the laminar solutions to the Navier-Stokes equations are perturbed sinusoidally. Then the expected solutions are substituted back into the hydrodynamic equations which allows the derivation of the disturbance equations. This provides a generalized eigenvalue problem, the literature refers to disturbances that grow in time as *absolute instabilities* and solutions that grow in space as *convective instabilities*. In this chapter the effect that finite amplitude disturbances have on the flow is analysed, where as in the linear results section only small first order perturbations were considered. This is done for both PPF and PPMF by including the perturbation of the perturbation in the governing Navier-Stokes equations (the non-linear terms can be seen in appendix 3). The mean flow part of the perturbations must also be included Eqs 2.43, 2.44. The disturbance is expanded using a Fourier series and then the resulting equations are truncated using a number of Fourier modes in the periodic direction. This operation can be performed because the two-dimensional travelling waves propagate with constant speed $c$. Using the material derivative the solutions appear as steady secondary flows in the moving frame, whereas in the laboratory frame they are limit-cycle solutions. This gives rise to periodicity in the streamwise direction and therefore the streamfunction $\phi$ can be expressed as a Fourier series in the moving frame $\tilde{x} = x - ct$. Then dropping the tilde $\phi$ can be written as.

$$\phi = \sum_{m=-\infty, m\neq 0}^{\infty} \sum_{n=0}^{\infty} a_{mn} exp(im\alpha x) f_n(z) \tag{4.1}$$

In the linear case only one mode is used but for non-linear case many modes are considered and it is their interactions that give rise to the non-linear equilibrium solutions. A Fourier's power spectra is used because it allows the expression of a periodic function as a sum of a constant term and a series of cosines and sine terms (see appendix 2). The frequencies associated with the sines and cosines are integer multiples (harmonics) of the fundamental frequency, in basic terms each coefficient determines how much of the original disturbance is associated with each harmonic. This analysis only examines weak magnetic fields for a Hartmann number range $M = 0 - 1$ because the same simplification that Lock used is applied which is only valid for low Hartmann numbers [105] and it more than covers the operating range of the Maxsys Fuel System (MFS). Due to the narrow range consider, all the cases display similar qualitative bifurcation characteristics. In this study two-dimensional travelling wave secondary equilibrium solutions are

computed. Fig 4.1 depicts the general PPF characteristics, which are as follows. The bifurcations are super-critically on the left-hand side of the neutral curve upto $\alpha \approx 0.9$. From this point the bifurcations become sub-critical with the limit point decreasing until they reach a minimum at $\alpha \approx 1.3$, after which the limit points start to increase again with the solutions vanishing at $\alpha \approx 1.5$. Al; these bifurcations in increasing $\alpha$ form a continuous surface. The term sub-critical refers to the fact that the non-linear solutions bifurcate from the linear neutral curve into the linearly stable region implying the existence of a finite threshold amplitude before the equilibrium solutions become unstable. Conversely a super-critical bifurcation continues into the linearly unstable region forming a locally stable state. Super-critical bifurcations indicate the birth of a stable limit cycle, Sub-critical bifurcations indicate the birth of an unstable limit cycle. Two important distinctions are made for sub-critical bifurcations, the first class which bifurcate from the neutral curve and the second that bifurcate from infinity. This distinction was made in order to examine the qualitative differences between the two types of bifurcation. The sub-critical bifurcation branches that originate from the neutral curve are exemplified by the $\alpha = 1.02$ results, the branches that bifurcate from infinity are typified by the $\alpha = 1.1$ results. Fig 3.5 a) shows that the PPF linear neutral curve reaches $\alpha_{max} \approx 1.09$ therefore it is the branches that bifurcate from infinity that have the lowest sub-critical limit points at $Re_{cP} = 2935$, $\alpha_c = 1.323$ [28], the subscript P indicates constant pressure. This lowers the $Re_c$ value by about a factor of two in comparison with the PPF linear results. The constant flux condition lowers the the limit point further by $\Delta Re \approx 300$. $\alpha = 1.02$ was chosen as the representative value for the family of solutions that bifurcate from the neutral curve because it is the $Re_c$ value for the linear PPF results and is close to the center of the $\alpha$ band for this type of bifurcations. The $\alpha = 1.1$ results were used as an example of the family of solution that appear to bifurcate from infinity in order to benchmark the PPF results presented in this chapter along with the two-dimensional secondary disturbance results in the next chapter with Pugh and Saffman's work [82]. Sub-critical bifurcations are the focus of the analysis because they reduce the $Re_c$, but the super-critical bifurcations will be discussed later in the chapter and again in relation to their stability. Sub-critical bifurcations are typical of pressure driven channels flows and occur when the system is more stable to infinitesimal disturbances than finite ones, this case is commonly known as metastability. This means that in the sub-critically bifurcating region, at a given Re value there will be two different shaped disturbances with different amplitudes $(L_2 - norm)$ val-

ues, i.e. two different states. The states on the lower branch are unstable with regards to two-dimensional infinitesimal secondary instabilities and the ones on the upper branch are stable in the same respect upto a certain threshold Reynolds number value. As with the linear case increasing the Hartmann number M increases the the limit point $Re_c$, below this point it is assumed the basic flow is globally asymptotically stable and thus this is the discrepancy between theoretical and experimental work. It is known from experimentation that the critical Reynolds number for substantial three-dimensional growth is $Re_c \approx 1000$ although small burst of instability have been observed as low as $Re_c \approx 500$ [65] [2] [9], so a lot of work has gone into the search for stable vortical states with limit points in this region.

The dynamics of the two-dimensional travelling waves at high Reynolds numbers is dominated by inertial processes. So the advection of vorticity by the flow is much stronger than viscous diffusion, this is self evident as the Reynolds number is a rough ratio of the inertial forces to the viscous forces. But this implies in the moving frame c, the vorticity is almost constant on each streamline [5] and the vorticity will be approximately uniform in the interior of any region of closed streamlines [3]. The evolution of a finite amplitude wave to its final equilibrium state is a complex process and involves two separate time scales. Initially a non-linear wave distorts and stirs the vorticity field, with viscosity having very little effect. This happens on a convective time-scale with the end result being such that the vorticity has become almost constant on each streamline. Next the viscosity of the fluid causes the vorticity to diffuse across the streamlines until it is almost uniformly distributed over regions of closed streamlines, this happens on a viscous time-scale. So the equilibration of two-dimensional travelling waves can be thought of as a fast initial relaxation to quasi-equilibrium states which can be considered as steady waves in regards to the inertial processes [71]. Followed by their slow evolution through a series of quasi-equilibria until they reach their final true equilibrium. The Stuart-Watson weakly non-linear expansions [103], [114] also describe the slow evolution of quasi-equilibria. They showed the vast majority of the modes are dampened rapidly by viscosity, leaving only the fundamental mode and the modes excited by its self-interaction. After the initial period of inertial adjustments all the higher modes are essentially phase-locked to the fundamental, giving rise to a quasi-equilibrium structure whose evolution proceeds on the slow time-scale of the first harmonic. Orszag and Patera [73] have also shown that such

quasi-equilibria evolve over long viscous time-scales and they exist well below the critical Reynolds number of the two-dimensional travelling waves. They found at Re=1500, $\alpha = 1.32$ the decay of the quasi-equilibrium states is four times slower that that of the corresponding linear mode. They concluded that quasi-equilibria are the dominant feature of the non-linear two-dimensional states of PPF. The time evolution of these flows was found to be smooth and regular with no hint of turbulent features and was determined using direct numerical solutions of the PPF Orr-Sommerfeld equations.

It has been suggested [92] that finite amplitude steady waves are simple members of a class of vortical states whose three-dimensional features may model properties of fully developed turbulence and that the physical existence of turbulent flow depends upon the mathematical existence of these vortical states. This line of thought reasons that secondary bifurcation branches can be used to predict transitions without any empirical input. Rozhdestvensky and Simakin [90] independently found that their three-dimensional secondary flows have profiles similar to those of turbulent flows. This suggests that the formulation of vortical states, solutions of the Navier-Stokes equations are intermediate stages between laminar and turbulent states, indicating the origins of turbulent flow are not forgotten and the large scale coherent structures of turbulent flow are the remnants of the vortical states from which they were formed. These coherent structures can be thought of as being lower dimensional manifolds in whose neighbourhood the dynamical system spent a substantial fraction of time [35]. This suggests that if the flow is controlled by these large scale structures the mean quantities of engineering interest might be determined by these intermediate solutions [46]. Some of these vortical states may be stable and therefore observable but the vast majority will be unstable braking into states from which turbulence is made. Although all these theories are well developed the true nature of turbulence and the mechanisms that cause its onset are hotly debated so the search for stable equilibrium solutions with a limit point in the experimentally observed region continues. The approach adopted in this thesis is dependent on the hypothesis that the transition from laminar flow to turbulence is based on the existence of intermediate vortical states and their complex interactions [92] and that the transition is the three-dimensional secondary instabilities of these states. The exact nature of the vortical states remains to be determined. Neither the two or three-dimensional travelling wave solutions have been ruled out as candidates for the stable vortical states that are primarily responsible for the

spike stage transition, especially as non-linear theory develops and new states of this type are discovered. At the same time it is quite possible another type of vortical state proves to be responsible for the early stage transition, such as three-dimensional hairpin vortical states that are observed in the onset of turbulence in the boundary layer [43].

Ehrenstein [15] conducting a detailed study of both and two and three-dimensional equilibrium solutions, using a similar method to our analysis, albeit across half the channel. Firstly he investigated three-dimensional travelling wave solutions that bifurcate from the linear three-dimensional neutral surface and found they do not lead to a reduction in $Re_c$ below the two-dimensional travelling wave solutions and they are both merely a staging ground for secondary instabilities. Next he studied three-dimensional travelling waves that bifurcate from their two-dimensional counterparts, the bifurcation points are the neutral points of the three-dimensional secondary instability of the two-dimensional travelling waves, see chapter 5. However these saturated states do not exist below the non-linear two-dimensional solutions either. Finally he found a partially isolated branch of three-dimensional equilibrium states that bifurcate bi-critically that do in fact exist to $Re \approx 1000$. Ehrenstein & Koch [16] further examined these states. They found two neutral, symmetric secondary phase locked modes with one being the second unstable phase locked mode and the other being the spanwise sub-harmonic of the first unstable phase-locked mode. A linear analysis around this bi-critical point showed interesting modal interactions. Consequently a non-linear analysis lead to the discovery of the aforementioned states. These states only contain even spanwise modes and contain twice as many streamwise vortices as the states that contain all the Fourier modes, this sort of pattern has been observed in PPF [48]. The fact that not all the spanwise modes are considered has called the validity of these results into question. Another drawback of this family of vortical states is that they only exist above $\beta$=3. Other candidates for the early onset of turbulence include non-phase locked branches which correspond to quasi-periodic solutions and may lead to a reduction in $Re_c$ although they are not possible to compute using the method presented in this thesis as they do not travel at the same speed as the frame of reference $c$. Sub-harmonic branches could also play an important in the laminar/turbulent transition process.

This investigation only considers the non-linear evolution of two-dimensional travelling waves. This approach was taken because most of the early investigations were done in

two-dimensions [71][72] [73][29]. The rational behind this starting point is that linear theory predicts that two-dimensional disturbances are unstable at lower Reynolds numbers than their three-dimensional versions [98] so the flow becomes practically two-dimensional by the time non-linearity becomes important, although this came from a misunderstanding of Squires theorem. To date it is the two-dimensional travelling waves that have the lowest $Re_c$ of all saturated steady vortical states studied for PPF which are the simplest equilibrium solutions to compute. The three-dimensional bi-critical states that exist at $Re \approx 1000$ are difficult to find and may not exist when a transverse magnetic field is applied. So the PPF two-dimensional travelling waves are the obvious candidate for comparison with their PPMF counterparts. It is generally accepted that the two-dimensional disturbances are the first to grow but as soon as there amplitude reaches a certain threshold they themselves become unstable to much faster three-dimensional secondary instabilities and quickly lead to turbulent breakdown in the convective time scales observed in the experiments [73], making it extremely difficult to study the original two-dimensional travelling waves. Milinazzo & Saffman [58] had a somewhat negative conclusion about the relevance of two-dimensional calculations and felt that three-dimensionality must be incorporated to describe the true nature of the transitions. Jimenez [35] used time dependant numerical simulations to examine the original non-linear two-dimensional disturbances exclusively and showed they exhibit chaotic properties such as ejections, wall sweeps, large scale intermittency and quasi-periodic bursting, all of which are observed in fully turbulent three-dimensional flows albeit at large Re values.

Pugh & Saffman [82] showed there are two different types of Reynolds number, constant pressure and constant flux. They arise from a lack of uniqueness in the parameterization of the flow, so the form of non-dimensionalzation of the centre line velocity $U_0$ must be fixed. The Constant flux centre line velocity corresponds to the flow being normalized by mass flux $U_0 = U_Q$ and constant pressure condition by the mean pressure gradient $U_0 = U_P$. These two different forms of the centre line velocity give rise to two Reynolds numbers $Re_Q = \frac{hU_Q}{\upsilon} = \frac{3Q}{4\upsilon}$ and $Re_P = \frac{hU_P}{\upsilon} = \frac{-h^3P}{2\upsilon^2}$. In this thesis two different solution types have been distinguished arising from the different parameterization because at the same parameter values they have different solutions. This is not strictly true the different non-dimensionalization conditions alter the scaling of the problem but not the underlying physics, they differ by a multiple of the base PPF and the scaling factor $\frac{U_Q}{U_P}$. It is impor-

tant to note these two Reynolds numbers represent the extremes of a continuous range, constant flux having no flux perturbations but finite pressure perturbations with flux perturbations increasing and pressure perturbations decreasing until the constant pressure condition remains. For linear and laminar flows the two conditions are identical with $Re_Q = Re_P$. Most numerical work up to date has used the constant pressure condition, whereas the literature states that in experimental work it is easier to keep the flux constant, in naturally occurring flows neither condition will be constant. The constant flux condition has the lower limit point of the two, Fig 4.3. The top eigenvalue passing through zero at the 'nose', consequently there is a stability change at the limit point with regards to two dimensional super-harmonic disturbances, this suggests nature prefers the constant flux condition. On the $Re_P$ curve the transition occurs on the upper branch because the transitions take place when the amplitude of the disturbance is the same, this will be discussed in more detail in the next chapter. In this work both the constant flux and constant pressure conditions have been calculated for $\alpha = 1.02$ and $\alpha = 1.1$ for values of Hartmann number $M = 0 - 1$. To calculate the constant flux condition an extra term must be added to the governing equations, Eqs 4.5 - 4.8, for this it is assumed:

$$\int_{-1}^{+1} \breve{U} dz = 0 \tag{4.2}$$

The mean flow distortion is written as:

$$\breve{U} = \sum_{n=0}^{N} C_n (1 - z^2) T_n(z) \tag{4.3}$$

substituting Eq 4.3 into Eq 4.2 with $T_n$=even if l=even and $T_n$=odd if l=odd the constant flux condition becomes:

$$\sum_{l=0}^{L} \frac{12}{(9 - l^2)(1 - l^2)} C_n = 0 \tag{4.4}$$

Pugh and Saffman [82] used a Chebychev tau method where the boundary conditions are incorporated into the Orr-Somerfeld equation. For the constant flux condition they set $[\tilde{\Psi}_P + \tilde{\hat{\psi}}_0]_{-h}^{+h} = Q$, where $\tilde{\Psi}_P = U_Q(y - y^3/3h^2)$ and setting $U_0 = U_Q$ along with $\hat{\psi}_0(-1) = 0$ to give the boundary condition $\hat{\psi}(+1) = 0$. Similarly for the constant pressure condition they set $[\tilde{\Psi}_{P,yy} + \tilde{\hat{\psi}}_{0yy}]_{-h}^{+h} = \frac{2Ph}{\upsilon}$ and setting $U_0 = U_P$ with the same upper boundary condition as before to give the boundary condition $[\tilde{\psi}_{0,yy}]_{-1}^{+1}$.

To calculate the two-dimensional travelling wave equilibrium solutions the non-linear terms are added to Eqs 2.34, 2.35, 2.41 and 2.42, to give:

PPF

$$\frac{\partial}{\partial t}\nabla^2\Delta_2\phi = (\nabla^2 - \hat{U}\partial_x)\nabla^2\Delta_2\phi + (\partial_z^2\hat{U})\partial_x\Delta_2\phi - \delta\cdot(\delta\phi+\varepsilon\psi)\cdot\nabla(\delta\phi+\varepsilon\psi) \tag{4.5}$$

$$\frac{\partial}{\partial t}\nabla^2\psi = (\nabla^2 - \hat{U}\partial_x)\nabla^2\psi + (\partial_z\hat{U})\partial_y\Delta_2\phi - \delta\cdot(\delta\phi+\varepsilon\psi)\cdot\nabla(\delta\phi+\varepsilon\psi) \tag{4.6}$$

PPMF

$$\frac{\partial}{\partial t}\nabla^2\Delta_2\phi = (\nabla^2 - \hat{U}\partial_x)\nabla^2\Delta_2\phi + (\partial_z^2\hat{U})\partial_x\Delta_2\phi + M^2\partial_z^2\Delta_2\phi - \delta\cdot(\delta\phi+\varepsilon\psi)\cdot\nabla(\delta\phi+\varepsilon\psi) \tag{4.7}$$

$$\frac{\partial}{\partial t}\nabla^2\psi = (\nabla^2 - \hat{U}\partial_x)\nabla^2\psi + (\partial_z\hat{U})\partial_y\Delta_2\phi + M^2\partial_z^2\nabla^{-2}\psi - \delta\cdot(\delta\phi+\varepsilon\psi)\cdot\nabla(\delta\phi+\varepsilon\psi) \tag{4.8}$$

The equations for the mean flow $\breve{U}(z,t)$ for PPF and PPMF and the mean magnetic induction $\breve{B}(z,t)$ are obtained by taking the xy average of the x component of Eqs 2.34, 2.41 and 2.38 to give:

PPF

$$\partial_z^2\breve{U} + \overline{\partial_z\Delta_2\phi(\partial_x\partial_z\phi + \partial_y\psi)} = \partial_t\breve{U} \tag{4.9}$$

PPMF

$$\partial_z^2\breve{U} - M^2\breve{U} + \overline{\partial_z\Delta_2\phi(\partial_x\partial_z\phi + \partial_y\psi)} = \partial_t\breve{U} \tag{4.10}$$

$$\partial_z^2\breve{B} = -\partial_z\breve{U} \tag{4.11}$$

The above equations are subject to the same homogeneous boundary conditions as the linear system. $\phi = \partial_z\phi = \psi = \breve{U} = 0$ at $z = \pm 1$. The Chebychev collocation point method is again employed to obtain the non-linear secondary equilibrium solutions. $\phi$ is expanded in terms of type 1 Chebyshev polynomials $T_n$ which are orthogonal, along with the addition of $(1-z^2)^2$ to Eq 4.1 to satisfy the boundary conditions, $\phi$ becomes:

$$\phi = \sum_{m=-\infty}^{\infty}\sum_{n=0}^{\infty} exp[i\alpha(x-ct)](1-z^2)^2 a_{mn}T_n(z) \tag{4.12}$$

For $\phi$ to be real the reality condition must be satisfied $a_{mn} = a*_{-mn}$ where * denotes the complex conjugate. Due to the symmetrical basic velocity profile of the system it allows the additional constraint that the complex coefficients $a_{mn} = 0$ when m+n=even. This reduces the calculation time as half of the coefficients are zero. To calculate the non-linear equilibrium solutions the wavefunction $\phi$ Eq 4.12 and the mean flow distortion Eq 4.3 are substituted into Eqs 4.5, 4.6 for PPF and Eqs 4.7, 4.8 for the PPMF case. The resulting equations are multiplied by $\langle(\alpha/2\pi)\rangle\int_0^{2\pi/\alpha} dx\ exp(i\gamma\alpha x)$ for the mean flow contribution

and evaluated at $z_i = cos((i+1)\pi/(N+1))i = 0\ldots,N$. The system is transformed into a moving frame of reference in the x-direction with speed c $(\tilde{x},\tilde{y},\tilde{z})$ so that $\tilde{x} = x - ct, \tilde{z} = z, \tilde{t} = t$ and dropping the tilde here after. A system of (N+1)(2M+1) non-linear equations is obtained with $A_{ij}x_j + B_{ijk}x_jx_k = 0$. Where matrix $A_{ij}$ and tensor $B_{ijk}$ are functions of $\alpha$ and Re for PPF and $\alpha$, Re and M for the PPMF case. The vector $x_i$ has $(a_{mn}, c, C_n)$ as elements for the unknown amplitudes. When transforming the system into analytical form the time term becomes $c\partial x\nabla^2\Delta_2\phi$ so care has to be taken when dealing with the phase velocity. In our numerical work c is allocated a position in $x_i$ that is not reserved for a complex coefficient $a_{mn}$, i.e and odd value in this case m=2 n=1. Where m are the streamwise fourier modes and n the spanwise fourier modes. This is achieved by introducing t such that $Im(a_{21}exp(-i2act) = 0$ and setting $\hat{a}_{mn} = a_{mn}exp(-imact)$. The Newton-Raphson iterative method is employed in order to obtain solutions to the resulting finite system of equations [62]. The Newton-Raphson method is an iterative method to calculate the root of a function, it works by taking an initial approximation of the root and calculating the tangent of the function at that point, the x-intercept of the tangent will be closer to the true root so the process is then repeated. However this single parameter continuation fails at the limit point where the gradient becomes infinite. So in order to pass through the limit point a subroutine is used to find a non-converged solution after five iterations at the limit point then the Reynolds number is slightly decreases or increased depending which way along the curve you are travelling to try and obtain a converged solution.

## 4.1 Results

To establish the secondary equilibrium solutions the vector normal $L_2 - norm$ is used which represents the amplitude of the disturbance, for the complex coefficient $a_{mn}$ it is defined as $\mid L_2 \mid = \left( \sum_{n=0}^{N} \sum_{m=-M,m\neq 0}^{M} a_{mn}a_{mn}^{*} \right)^{1/2}$. In the majority of literature cited the disturbance energy is used rather than the $L_2 - norm$ as a measure of non-linearity although experimentally rms values of the fluctuation in the streamwise velocity component are used. The disturbance energy is given by $E = \sum_{n=0}^{N} \sum_{m=-M,m\neq 0}^{M} E_{mn}$ where $E_{mn} = \frac{15}{4(1+\delta_{n0}(1+\delta_{m0})} \int_{-1}^{1} \left[\hat{\mathbf{u}}_{mn} \cdot \bar{\hat{\mathbf{v}}}_{mn}\right] dz$ and is normalised with respect to the basic velocity $U_0(z)$ equal to one $E = 15/16 \int_{-1}^{1} U_0(z)^2 dz \equiv 1$. The disturbance amplitude $\varepsilon$ is related

to the disturbance energy $E$ by $\varepsilon = \sqrt{8E/15}$ where $\varepsilon\hat{u}_0 = \partial_z^2\breve{U} + \overline{\partial_z\Delta_2\phi(\partial_x\partial_z\phi + \partial_y\psi)} = \sum_{\substack{n=even \\ n=0}}^{\infty} C_n(1-z^2)T_n(z)$. The calculations of the secondary equilibrium solutions were initially performed at a Truncation level m=7 Fourier modes with each Fourier component expanded into a Chebyshev series of k=95. When the stability analysis was performed with an input of this size on a desktop computer using visual Fortran it was found to take too long for practical purposes. Unfortunately these jobs could not be done in batches on the Cray XD1 as stability programme used the NAG subroutine F02GJF and the university no longer held the licences for the NAG libraries. In an attempt to solve this problem the programmes were parallelized which significantly reduced the run time. The parallel programmes use PARPACK libraries to invert the matrices and therefore could be used on the Cray. When the results from the Serial and Parallel programmes were compared a small discrepancy was found in the imaginary part of the eigenvalues, the cause of which is still unresolved to date. This proved particularly problematic as it is not possible to determine if a given mode was phase-locked or not. Another major drawback with the parallel code was that the eigenvalues are calculated around a point in the complex plane and not globally. This is fine if you know where to look or are comparing data but generally this is not the case. Therefore the calculation must be performed on a grid of points in the complex plane which proves time consuming so the speed advantages of parallel programming are lost. Consequently it was realized that the university does hold the licence to the LAPACK libraries, so the IMSL subroutine DGVLCG which computes the entire eigenvalue spectrum and the corresponding eigenvectors to double precision of a generalized complex eigensystem $Az = \lambda Bz$ was exchanged with AMCL subroutine ZGGEV. The problem with using the DGVLCG or ZGGEV subroutines is that the vectors are normalised to have Euclidean length equal to the value one. Where as the F02GJF subroutine does not actually produce the eigenvalue $\lambda_j$ but instead returns $\alpha_j$ and $\beta_j$ such that $\lambda_j = \alpha_j/\beta_j$, for $j = 1,2\ldots,n$. This means the absolute values of the eigenvalues are different and as the majority of the cited papers had used the NAG subroutine or similar methods this made direct comparison of the growth rates impossible and therefore they have to be compared qualitatively. Although this made it possible to run the jobs in batches but unfortunately a lot of time had elapsed during this process. For these reasons the decision was made to use the serial programme but with a data Truncation level of m=5 and k=39. Using this lower truncation level made it harder for solutions to converge at high Reynolds especially

on the upper branch which was another reason why the non-linear analysis was restricted to a lower Hartmann number range M=0-1.

Table 4.1 shows the beginning of a typical converged equilibrium solution which are also the input files for the secondary stability programme. In the first row the 39 represents the number of collocation points used k, the 5 is the number of streamwise modes m, the 0 is the number of spanwise modes n and the 99 is the number of Newton iterations. In the second row the first value is the tolerance delta and the second the angle of inclination. In the third row the first value is $\alpha$, the second $\beta$, the third the Hartmann number M, the fourth is the Reynolds number Re and the fifth is the Grashof number Gr. In the fourth row the 200 is the number of complex coefficients $a_{mn}$ in the block, which is $(39+1)\times 5 = 200$ the one is added to the thirty nine because the first collocation point is zero. The next two hundred rows have the same layout where the first column is the k values, the second column is the m values, the third is the n values and the final column are the $a_{mn}$ complex coefficient values. In the three-dimensional case there are four blocks of two hundred the first being the real part of the poloidal the second being the real part of the toroidal the third being the imaginary part of the poloidal and the fourth being the imaginary part of the toroidal. The mean flow contributions is included using four block of twenty, the first being the even collocation points for the real poloidal the second being the even collocation points for the real toroidal the third being the odd collocation points for the imaginary poloidal and the fourth being the odd collication points for the imaginary toroidal. In the two-dimensional case the toroidal parts are zero and this explains the number of complex coefficients $a_{mn}$ in Table 4.2. The truncation Table 4.2 shows the quantitative difference between the k=95, m=7 truncation level and that of the k=39 m=5 level. This shows that the number of overall complex coefficients does not affects the $L_2 - norm$ value in a significant way but this does greatly reduce the computation time required. It also helps to shows that number of modes does not make a large difference to the quantitative results. The justification for this is that the second and subsequent modes make a very small contribution to the $L_2 - norm$ value and consequently the over all disturbance energy [58], this also explains why the mean flow approximation accounts for the majority of the sub-critical effects.

Table 4.1: Example equilibrium solution

| | | | | |
|---|---|---|---|---|
| 39 | 5 | 0 | 99 | |
| 0.00001000 | 0.0000 | | | |
| 1.10000 | 0.00000 | 0.500000000E+00 | 0.972000000E+04 | 0.000000000E+00 |
| 200 | | | | |
| 0 | 1 | 0 | -0.7472227379167037E+02 | |
| 0 | 2 | 0 | 0.7518415714910863E-14 | |
| 0 | 3 | 0 | -0.1570187368766355E+00 | |
| 0 | 4 | 0 | 0.2274556356590954E-15 | |
| 0 | 5 | 0 | 0.2133132955884305E-03 | |
| 1 | 1 | 0 | 0.5556599179187888E-13 | |
| 1 | 2 | 0 | -0.5023650478046953E+01 | |
| 1 | 3 | 0 | 0.2272167311563014E-14 | |
| 1 | 4 | 0 | -0.1447256859577161E-01 | |
| 1 | 5 | 0 | 0.4215823563380048E-16 | |
| 2 | 1 | 0 | -0.9183842482247529E+02 | |
| 2 | 2 | 0 | 0.6296584773541605E-14 | |
| 2 | 3 | 0 | -0.2722011020932570E+00 | |
| 2 | 4 | 0 | 0.3805456421299489E-15 | |
| 2 | 5 | 0 | 0.1962263935633619E-03 | |

Table 4.2: Truncation results

| $L_2 - norm(\times 10^3)$ | M | k | $a_{mn}$ |
|---|---|---|---|
| 0.5911692046 | 7 | 95 | 1440 |
| 0.5911692046 | 7 | 91 | 1380 |
| 0.5911692046 | 7 | 85 | 1290 |
| 0.5911692046 | 7 | 81 | 1230 |
| 0.5911692047 | 7 | 75 | 1140 |
| 0.5911692049 | 7 | 71 | 1080 |
| 0.5930492650 | 6 | 71 | 936 |
| 0.5930492653 | 6 | 65 | 858 |
| 0.5930492723 | 6 | 61 | 806 |
| 0.5930491299 | 6 | 55 | 728 |
| 0.5930484874 | 6 | 51 | 676 |
| 0.5930524700 | 6 | 45 | 598 |
| 0.5930695294 | 6 | 39 | 520 |
| 0.5888653687 | 5 | 39 | 440 |
| 0.5889070973 | 5 | 35 | 396 |

### 4.1.1 PPF

Two families of non-linear equilibrium solution are distinguished by way of their bifurcation origin, along with the two types of equilibrium solution constant pressure and constant flux that have been previously outlined. The first family of solutions bifurcate from infinity and occupy a narrow band to the right of the neutral curve from $\alpha \approx 1.1 - 1.5$, see Fig 4.2. They have the lowest sub-critical Reynolds number $Re_c \approx 2950$ at $\alpha \approx 1.3$ and are exemplified by the $\alpha = 1.1$ results. The second family of solutions bifurcate from the neutral curve and are exemplified by $\alpha = 1.02$ results, this $\alpha$ value was chosen as it is the wavenumber that corresponds to the linear critical Reynolds number. The non-linear equilibrium solutions start bifurcating super-critically from the left-hand side of the neutral curve until they reach $\alpha \approx 0.9$. From the bifurcation table, Table 4.3 it can be seen that from then on they start to bifurcate sub-critically with the limit point becoming lower as $\alpha$ increases until $\alpha \approx 1.3$ where they start increasing again and the solutions vanish at $\alpha \approx 1.5$. At $\alpha \approx 1.09$ the neutral curve starts to double back on itself as it tends to infinity (see Fig 3.5 a)) but the sub-critical bifurcations still take place with the limit point becoming lower until they reach a minimum at $\alpha = 1.323$, this is depicted in Fig 4.1. The results in the tables were calculated using the constant pressure condition $Re_P$, the constant flux $Re_Q$ branches have a lower limit points. The two families of solution do not show any qualitative differences they are distinguished because of their point of bifurcation. These results are best summed up by saying no two-dimensional vortical state have been found below $Re \approx 2900$ for the constant pressure condition and below $Re = 2600$ for the constant flux condition. For $Re > 2900$, neutral finite amplitude solutions exist for a finite band of $\alpha$ centred about $Re \approx 1.25$ of width $\Delta\alpha \approx 0.5$ forming a continuous cigar shaped neutral surface with upper and lower sheets. The lower sheet is known to be unstable to all two-dimensional super-harmonic disturbances with x-period $2\pi/\alpha$, while the higher energy upper sheet solutions on the $Re_Q$ surface are stable to all the super-harmonic two-dimensional perturbations up to a threshold $Re$ value. For $Re \leq 5772$ there are either zero or two finite amplitude equilibria depending on whether the bifurcation type is sub-critical or super-critical. Using the k=95, m=5 truncation level for constant pressure the limit point is found at $Re_{cP} = 2939.02$ with the corresponding $\alpha = 1.319$ and for constant flux $Re_{cQ} = 2607.40$ at $\alpha = 1.352$. The $Re_{cP}$ value is slightly higher than Herberts [29] equivalent result because more modes were used in its calculation which

adds a small amount of energy to the system thereby increasing the limit point.

Table 4.3: Bifurcation results

| α | Start point | Limit point | Bifurcation type |
|---|---|---|---|
| 0.75 | 12461.2 | none | super-critical |
| 0.80 | 9882.4 | none | super-critical |
| 0.85 | 8140.8 | none | super-critical |
| 0.90 | 6965.3 | 6894.7 | sub-critical |
| 0.95 | 6207.5 | 5771.0 | sub-critical |
| 1.00 | 5814.8 | 4922.1 | sub-critical |
| 1.01 | 5783.9 | 4778.9 | sub-critical |
| 1.02 | 5772.2 | 4643.6 | sub-critical |
| 1.03 | 5782.7 | 4516.0 | sub-critical |
| 1.04 | 5819.6 | 4394.6 | sub-critical |
| 1.05 | 5890.0 | 4280.2 | sub-critical |
| 1.06 | 6005.1 | 4172.2 | sub-critical |
| 1.07 | 6186.0 | 4070.2 | sub-critical |
| 1.08 | 6478.0 | 3973.8 | sub-critical |
| 1.09 | 7022.0 | 3883.0 | sub-critical |
| 1.10 | ∞ | 3798.0 | sub-critical |
| 1.20 | ∞ | 3186.0 | sub-critical |
| 1.30 | ∞ | 2944.9 | sub-critical |
| 1.40 | ∞ | 30915.5 | sub-critical |
| 1.50 | ∞ | 3918.4 | sub-critical |

The constant pressure and constant flux equilibrium solutions bifurcate from the same place on the neutral curve because in the linear case they are identical. The lower branches mirror one another no matter where they bifurcate from, until they start to approach the limit point. At this point the two curves start to diverge with the constant flux equilibrium curve having the lower limit point of the two (see Fig 4.3). Although the two curves diverge on the upper branch if the two $L_2 - norm$ values are the same the two states are the same. This is demonstrated in Fig 4.4, it depict the eigenvalue spectrum of a con-

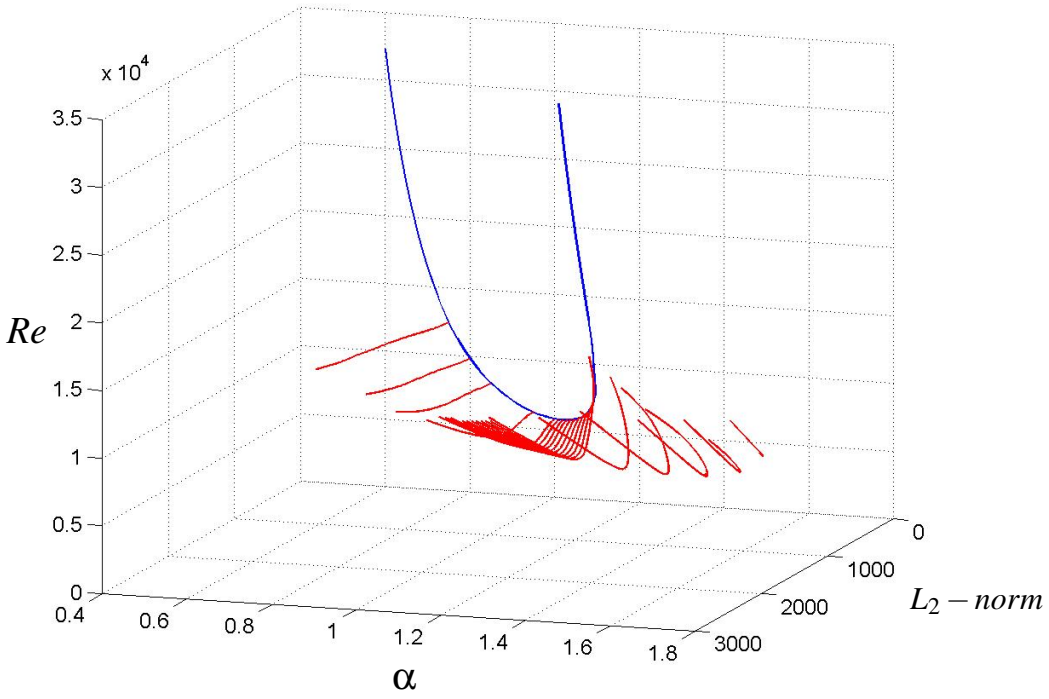


Figure 4.1: The 2D equilibrium solutions bifurcating from the neutral curve

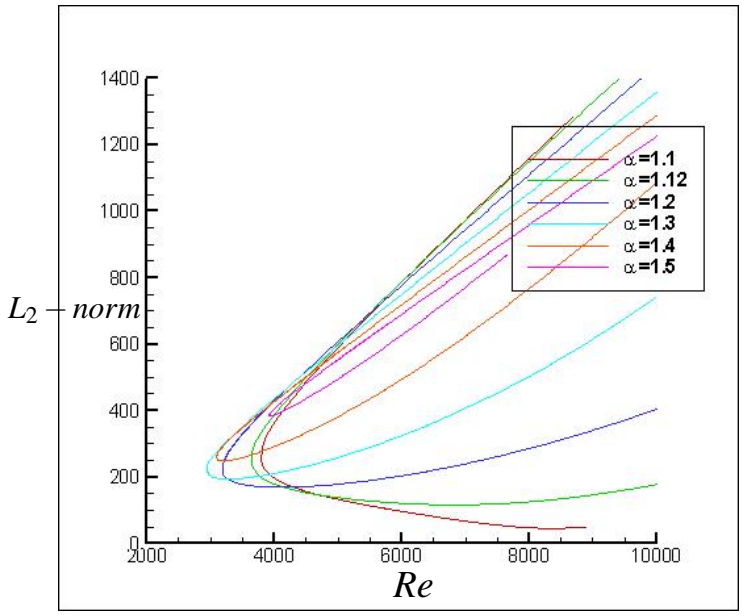


Figure 4.2: Stable two-dimensional equilibrium curves that bifurcate from infinity for PPF.

stant pressure and a constant flux disturbance with similar $L_2 - norm$ values, with the two spectra being identical. The constant pressure equilibrium state has a Re=6360 with $L_2 - norm = 830.74$ and constant flux Re=5117, $L_2 - norm = 830.56$. This implies that a constant flux equilibrium solution on the upper branch with the same $L_2 - norm$ value as a constant pressure solution are equivalent despite having different Reynolds numbers which suggests the two only differ by a scaling factor. To visualise the nature of the steady state equilibrium solutions Figs 4.5-4.13 show, a) the streamfunction of the velocity fluctuations $\partial\phi/\partial x$ or in other words the x-component of the velocity u. b) the streamfunction of the disturbance $\partial\phi/\partial x + \int_{-1}^{z} \breve{U} dz$ and this represents the u component of the velocity plus the average part of the velocity fluctuation, c) the total flow $\partial\phi/\partial x + \int_{-1}^{z} \hat{U} dz$ . These are plotted for the constant pressure and flux condition at $\alpha = 1.1$, $Re = 4000$ on the lower and upper branch and at $Re = 8000$. The three values of Re represent points on the unstable lower branch, the stable part of the upper branch and the unstable part of the upper branch with respect to two-dimensional super-harmonic secondary disturbances. From the diagrams it is clear that the different Reynolds numbers do not make a qualitative difference to the flow plots as secondary disturbances are not considered. The streamfunction of the the velocity fluctuations shows the two-dimensional vortical states aligned in the streamwise direction. The constant pressure streamfunctions of the disturbances show a meandering central flow with the vortices being pushed towards the channel walls. This is in contrast to the constant flux case which are similar to the velocity fluctuation plots because the average part of the mean flow distortion across the channel is set to zero Eqn 4.2. Consequently when the streamfunction of the disturbance is considered the forward flow must be the equal to the backward flow. Therefore the meandering flow is not possible and only the transverse vortices aligned with the x-axis remain, they are rotating faster than the velocity fluctuations due to the extra flow, this demonstrates the merit of distinguishing the constant pressure and constant flux equilibrium solutions. For the total flow plots the basic flow is also included which is far stronger than the mean flow due to the high Reynolds numbers the equilibrium solutions exist at. This has the effect of 'washing' away the vortical features and almost straightening out the 'snake-like' pattern although it is just about discernible.

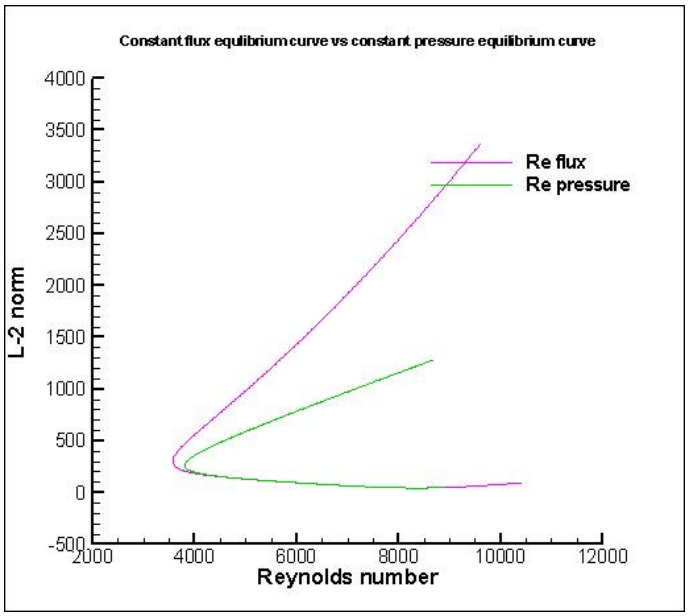


Figure 4.3: Constant flux equilibrium curve vs constant pressure equilibrium curve for PPF.

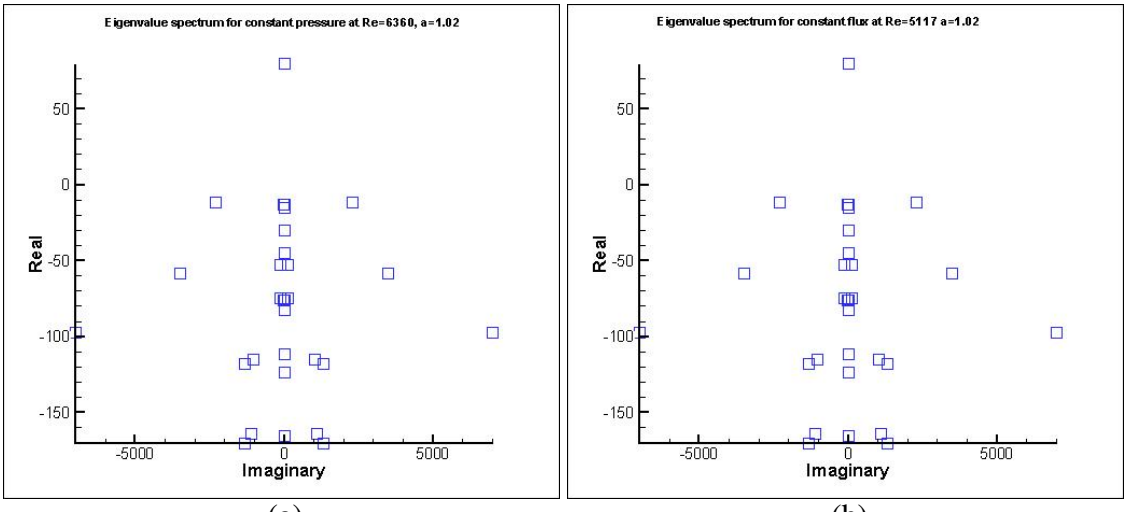


(a) (b)

Figure 4.4: *a) Eigenvalue spectrum for constant pressure at Re=6360.* $\alpha = 1.02$ *for PPF. b) Eigenvalue spectrum for constant flux at Re=5117.* $\alpha = 1.02$ *for PPF.*

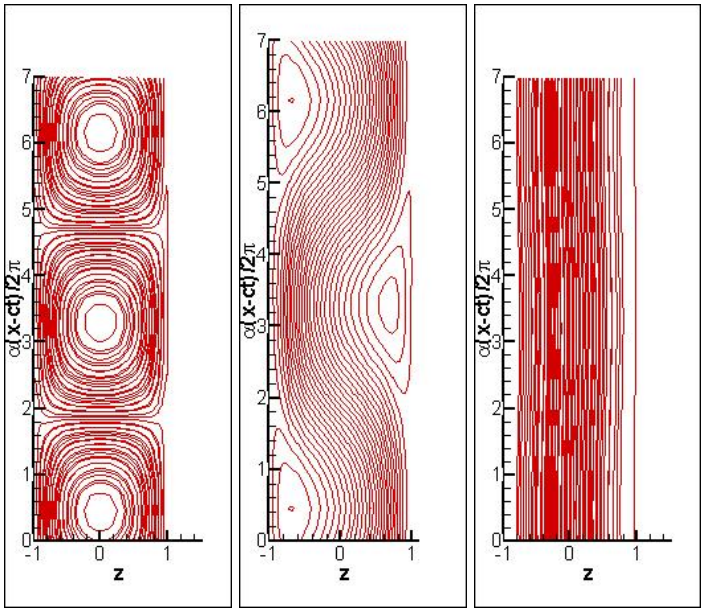


Figure 4.5: *The stream-function of (a) the velocity fluctuations* $\partial\phi/\partial x$*, (b) the disturbance* $\partial\phi/\partial x + \int_{-1}^{z} \check{U}\,dz$ *and (c) the total flow* $\partial\phi/\partial x + \int_{-1}^{z} \hat{U}\,dz$*, for the constant pressure condition of PPF at* $\alpha = 1.1$*,* $Re = 4000$ *on the lower branch.*

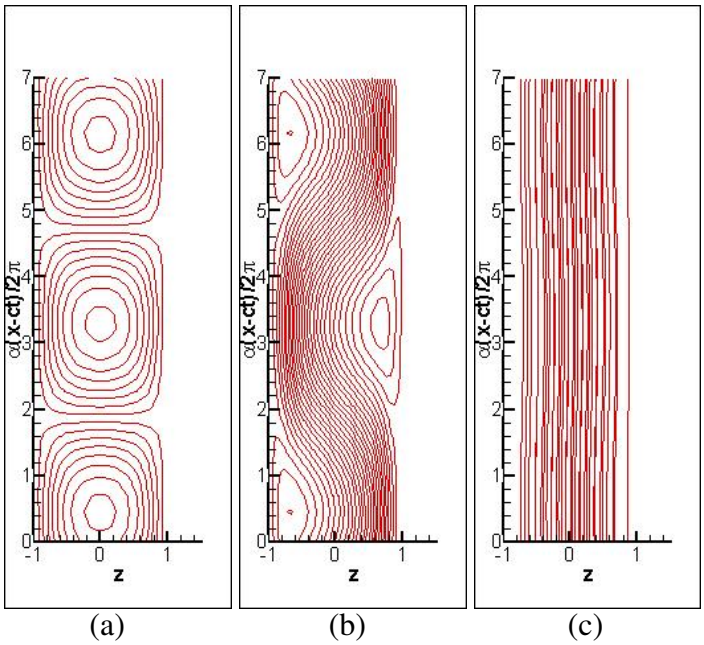


Figure 4.6: *The stream-function of (a) the velocity fluctuations* $\partial\phi/\partial x$*, (b) the disturbance* $\partial\phi/\partial x + \int_{-1}^{z} \check{U}\,dz$ *and (c) the total flow* $\partial\phi/\partial x + \int_{-1}^{z} \hat{U}\,dz$*, for the constant pressure condition of PPF at* $\alpha = 1.1$*,* $Re = 4000$ *on the upper branch.*

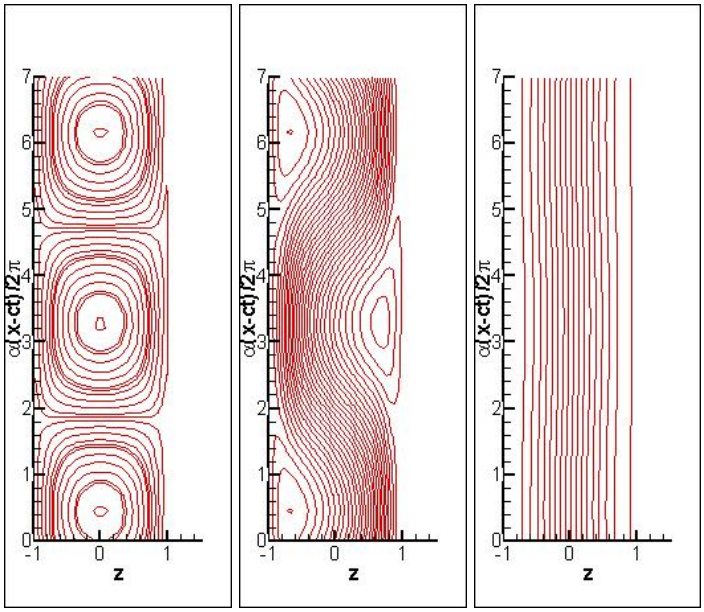


Figure 4.7: *The stream-function of (a) the velocity fluctuations* $\partial\phi/\partial x$*, (b) the disturbance* $\partial\phi/\partial x + \int_{-1}^{z} \check{U}\,dz$ *and (c) the total flow* $\partial\phi/\partial x + \int_{-1}^{z} \hat{U}\,dz$*, for the constant pressure condition of PPF at* $\alpha = 1.1$*,* $Re = 8000$ *on the upper branch.*

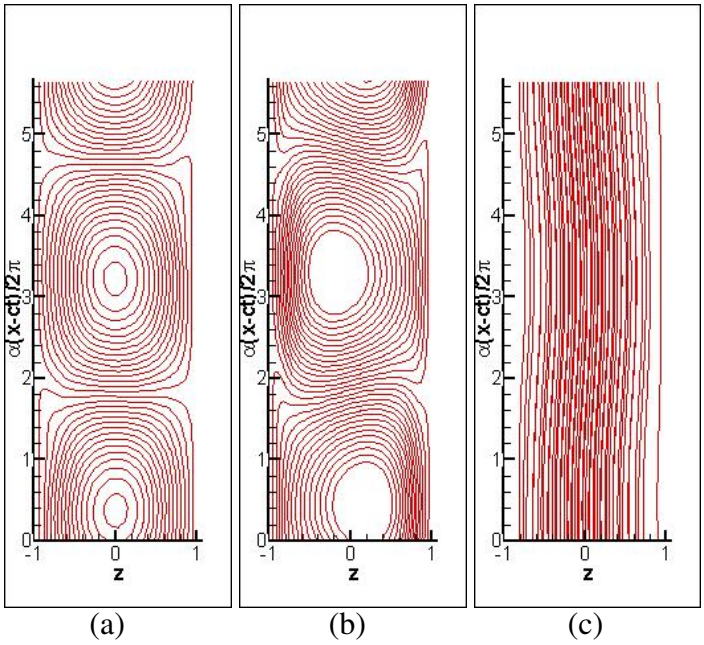


Figure 4.8: *The stream-function of (a) the velocity fluctuations* $\partial\phi/\partial x$*, (b) the disturbance* $\partial\phi/\partial x + \int_{-1}^{z} \check{U}\,dz$ *and (c) the total flow* $\partial\phi/\partial x + \int_{-1}^{z} \hat{U}\,dz$*, for the constant flux condition of PPF at* $\alpha = 1.1$*,* $Re = 4000$ *on the lower branch.*

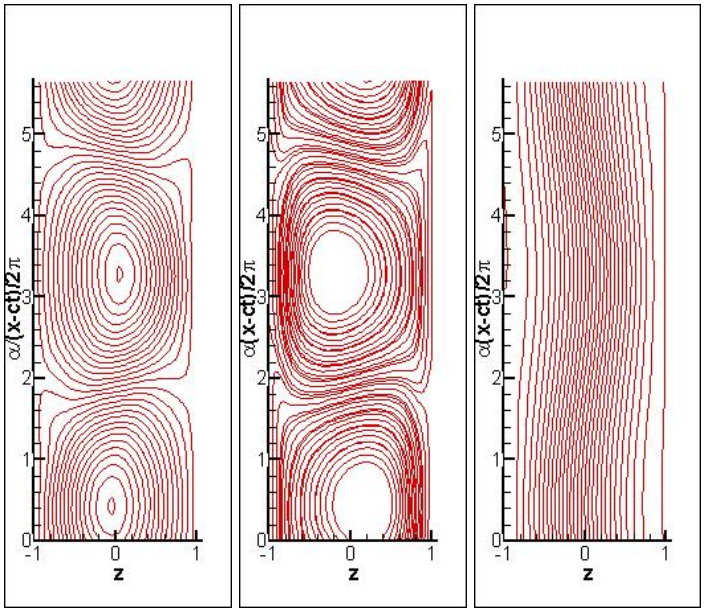


Figure 4.9: *The stream-function of (a) the velocity fluctuations* $\partial\phi/\partial x$*, (b) the disturbance* $\partial\phi/\partial x + \int_{-1}^{z} \breve{U}\,dz$ *and (c) the total flow* $\partial\phi/\partial x + \int_{-1}^{z} \hat{U}\,dz$*, for the constant flux condition of PPF at* $\alpha = 1.1$*,* $Re = 4000$ *on the upper branch.*

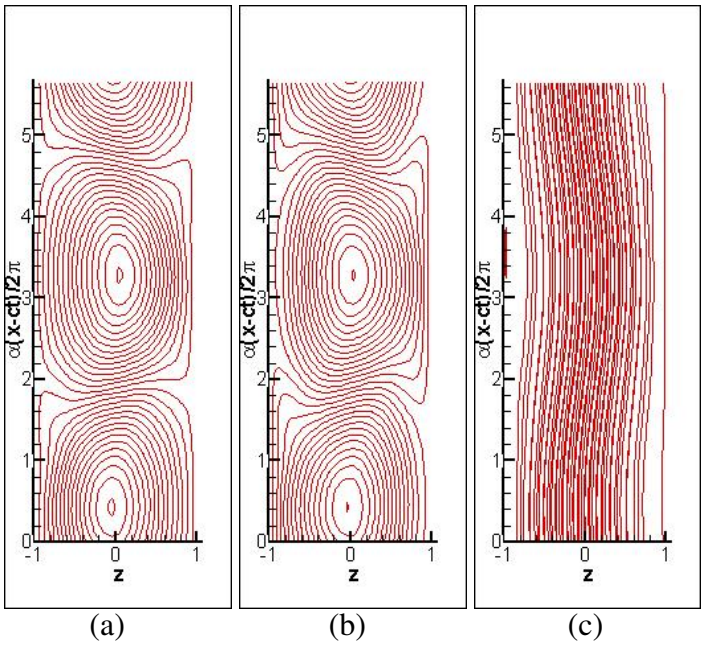


Figure 4.10: *The stream-function of (a) the velocity fluctuations* $\partial\phi/\partial x$*, (b) the disturbance* $\partial\phi/\partial x + \int_{-1}^{z} \breve{U}\,dz$ *and (c) the total flow* $\partial\phi/\partial x + \int_{-1}^{z} \hat{U}\,dz$*, for the constant flux condition of PPF at* $\alpha = 1.1$*,* $Re = 8000$ *on the upper branch.*

### 4.1.2 PPMF

To the best of the authors this is the first attempt to calculate the travelling wave equilibrium solutions for PPMF. The solutions have been computed upto $M = 1.0$ and have similar bifurcation characteristics to those of the PPF case. Once again they bifurcate super-critically from the left-hand side of the neutral curve upto $\alpha \approx 0.9$. After which point they bifurcate sub-critically with the critical value $Re_c$ of the limit point decreasing as $\alpha$ increases. This reaches a minimum at $\alpha \approx 1.3$, the states vanish at $\alpha \approx 1.5$. Once again the constant flux and constant pressure conditions are equivalent if the $L_2 - norm$ values are the same. This is shown in Fig 4.12 with $L_2 - norm \approx 743$ which corresponds to a constant flux secondary equilibrium solution at $Re = 5000$ on the upper branch and a constant pressure on at $Re = 5780$ on the upper branch. The calculations were performed at a truncation level of k=95 collocation points with m=7 streamwise modes. The critical Reynolds number value $Re_c$ of the sub-critical limit point increases as the Hartmann number increases due to the stabilising effect of the magnetic field, shown in Tables 4.4, 4.5 for the constant pressure condition and constant flux condition respectively. The limit point increase in a rapid fashion as Hartmann number M increases but less so than in the linear case, (see Table 3.2). As the absolute differences in $Re_c$ between PPF and a given M value is smaller in the non-linear case than the linear case, the PPMF sub-critical bifurcations extend further into the linearly stable region. This proves that the overall stabilising effect is due to linear disturbances of which the vast majority is attributed to the 'blunting' of the basic velocity profile. It also shows as non-linearity is introduced it relatively has a grater destabilising effect on the system than is the case for PPF due to the extent the equilibrium solutions extend into the linear stable region. This indicates the mean flow contribution is counteracting the affect the homogeneous magnetic field has on the basic flow.

The $Re_c$ value is far higher at $M = 1.0 \times 10^{-4}$ than the trend would suggest and produces an unnatural initial step value. This suggests an error is introduced in the PPMF basic flow profile at such small M values, in order to correct this the PPMF basic velocity profile should be expressed as a power series. To visualise the flow the same procedure is used as for the PPF case. The flow plots in Figs 4.14 - 4.19 again show a) the streamfunction of the velocity fluctuation, b) the streamfunction of the disturbance and c) the total flow. For the PPMF case they are plotted at $Re = 5000$ on the lower and upper branches and at

$Re = 9500$ on the unstable part of the upper branch as $Re = 4000$ is too close to the limit point at $M = 1.0$ and this point would therefore be stable in respect to two-dimensional secondary disturbances in the constant pressure case. The results are qualitatively the same as the PPF plots although of greater magnitude due to the higher Re values at which they are plotted. Again their is a distinction between the constant pressure and constant flux case for the streamfunctions of the disturbance. In the constant pressure case there is a meandering flow between the vortices and in the constant flux case there is no such flow. This is because of the same reasons outlined for the PPF case.

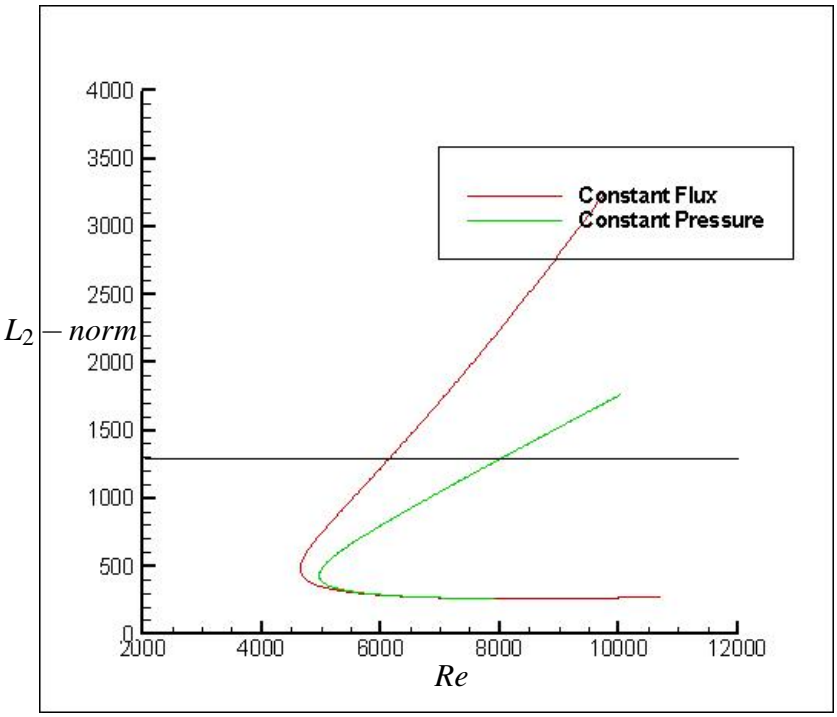


Figure 4.11: Constant flux equilibrium curve vs constant pressure equilibrium curve for PPMF at $M = 1.0$.

Table 4.4: PPMF Bifurcation results for constant pressure

| $\alpha_c$ | $Re_c$ | M | $\Delta Re_c$ |
|---|---|---|---|
| 1.319 | 2939.02 | 0.0 | 0.0 |
| 1.317 | 2948.17 | $1 \times 10^{-4}$ | 9.15 |
| 1.317 | 2957.61 | 0.1 | 18.59 |
| 1.319 | 2986.24 | 0.2 | 47.22 |
| 1.310 | 3189.90 | 0.5 | 250.88 |
| 1.291 | 3983.36 | 1.0 | 1044.34 |

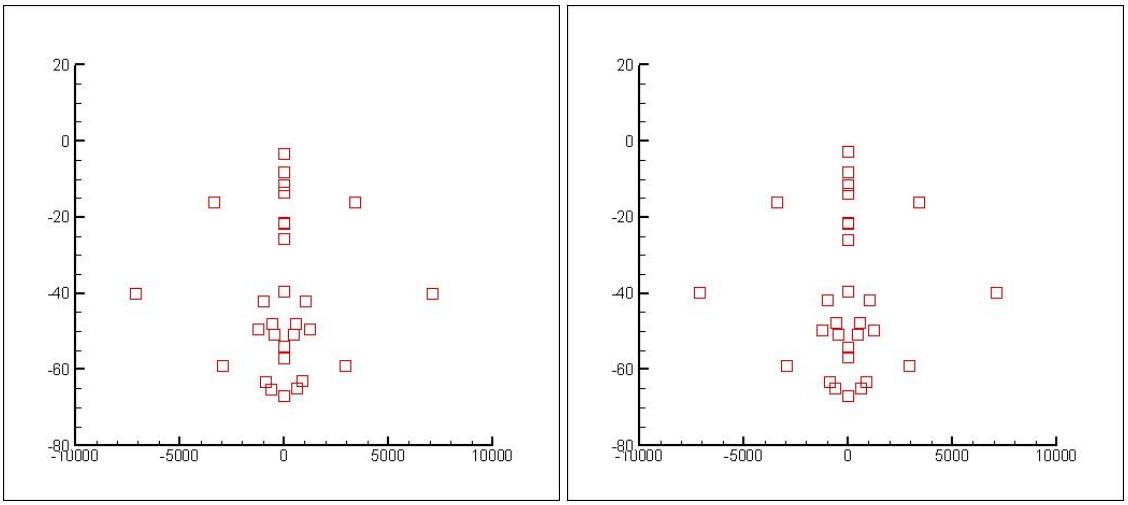


(a) (b)

Figure 4.12: *a) Eigenvalue spectrum for constant pressure at Re=5780.* $\alpha = 1.1$ *at* $M = 1.0$*. b) Eigenvalue spectrum for constant flux at Re=5000.* $\alpha = 1.1$ *for PPF.*

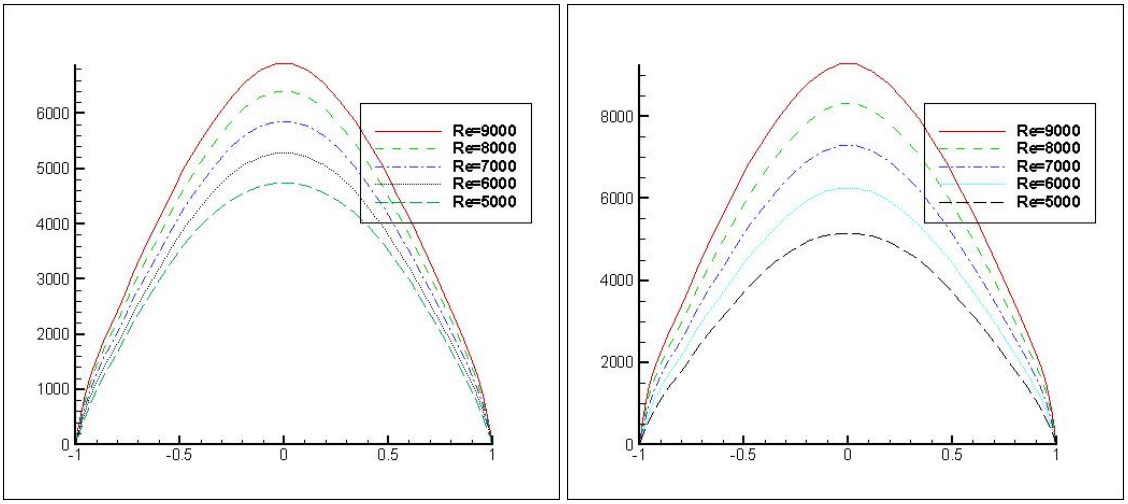


(a) (b)

Figure 4.13: *a) Total mean flow profile* $(\hat{U})$ *for various Reynolds numbers for fix* $\alpha = 1.1$ *M=1 for a) constant pressure condition, b) the constant flux condition.*

Table 4.5: PPMF Bifurcation results for constant flux

| $\alpha_c$ | $Re_c$ | M | $\Delta Re_c$ |
|---|---|---|---|
| 1.352 | 2607.40 | 0.0 | 0.0 |
| 1.354 | 2618.26 | $1 \times 10^{-4}$ | 10.86 |
| 1.354 | 2626.93 | 0.1 | 19.89 |
| 1.353 | 2653.06 | 0.2 | 45.66 |
| 1.347 | 2840.26 | 0.5 | 232.86 |
| 1.326 | 3568.08 | 1.0 | 960.68 |

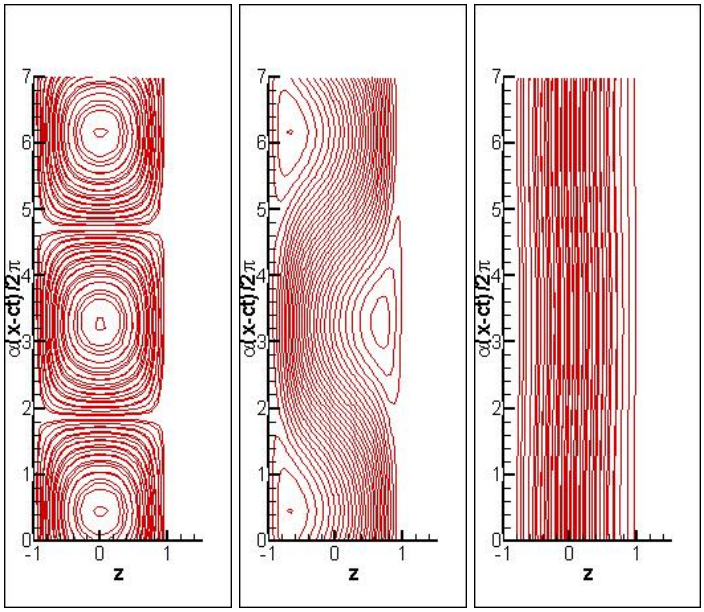


(a) (b) (c)

Figure 4.14: *The stream-function of (a) the velocity fluctuations* $\partial\phi/\partial x$*, (b) the disturbance* $\partial\phi/\partial x + \int_{-1}^{1} \check{U}\,dz$ *and (c) the total flow* $\partial\phi/\partial x + \int_{-1}^{1} \hat{U}\,dz$*, for the constant pressure condition of PPMF at* $M = 1$ $\alpha = 1.1$*,* $Re = 5000$ *on the lower branch.*

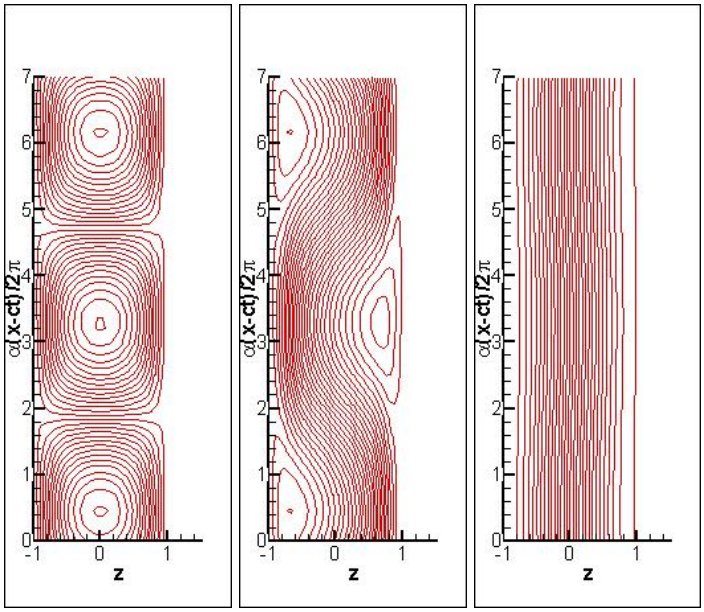


(a) (b) (c)

Figure 4.15: *The stream-function of (a) the velocity fluctuations* $\partial\phi/\partial x$*, (b) the disturbance* $\partial\phi/\partial x + \int_{-1}^{1} \check{U}\,dz$ *and (c) the total flow* $\partial\phi/\partial x + \int_{-1}^{1} \hat{U}\,dz$*, for the constant pressure condition of PPMF at* $M = 1$ $\alpha = 1.1$*,* $Re = 5000$ *on the upper branch.*

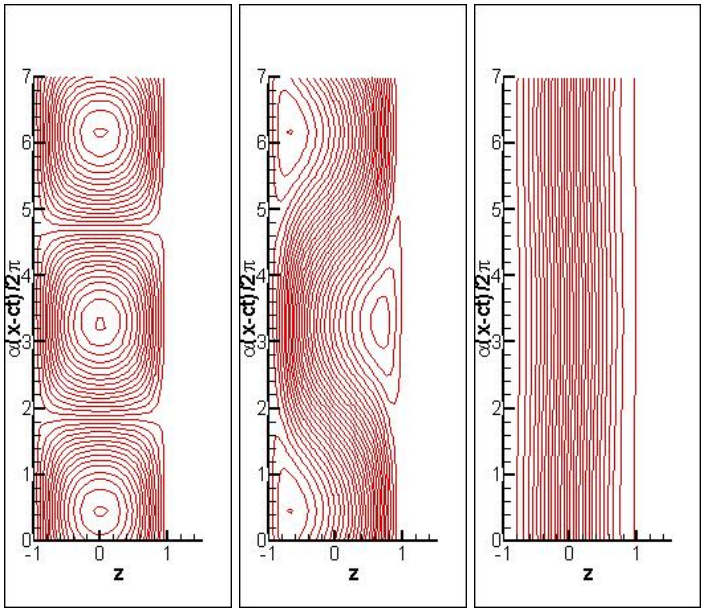


Figure 4.16: *The stream-function of (a) the velocity fluctuations* $\partial\phi/\partial x$*, (b) the disturbance* $\partial\phi/\partial x + \int_{-1}^{1} \check{U}\,dz$ *and (c) the total flow* $\partial\phi/\partial x + \int_{-1}^{1} \hat{U}\,dz$*, for the constant pressure condition of PPMF at* $M = 1$ $\alpha = 1.1$*,* $Re = 10000$ *on the upper branch.*

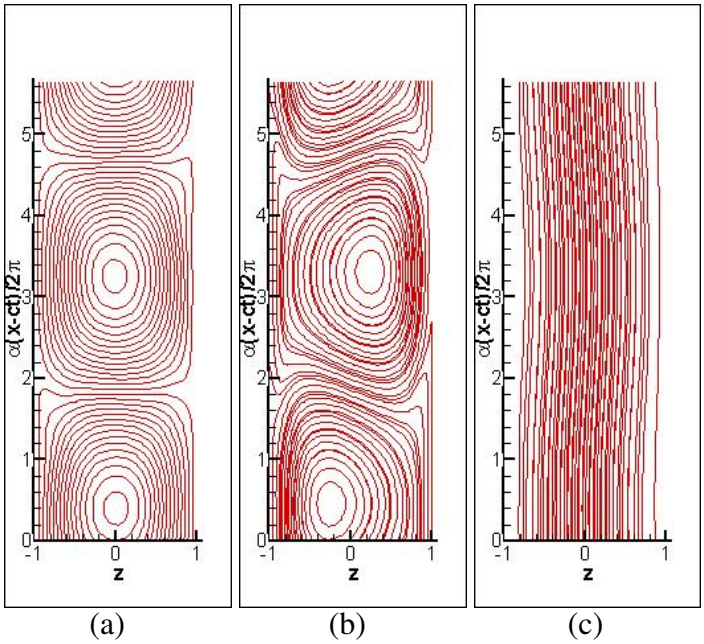


Figure 4.17: *The stream-function of (a) the velocity fluctuations* $\partial\phi/\partial x$*, (b) the disturbance* $\partial\phi/\partial x + \int_{-1}^{1} \check{U}\,dz$ *and (c) the total flow* $\partial\phi/\partial x + \int_{-1}^{1} \hat{U}\,dz$*, for the constant flux condition of PPMF at* $M = 1$ $\alpha = 1.1$*,* $Re = 5000$ *on the lower branch.*

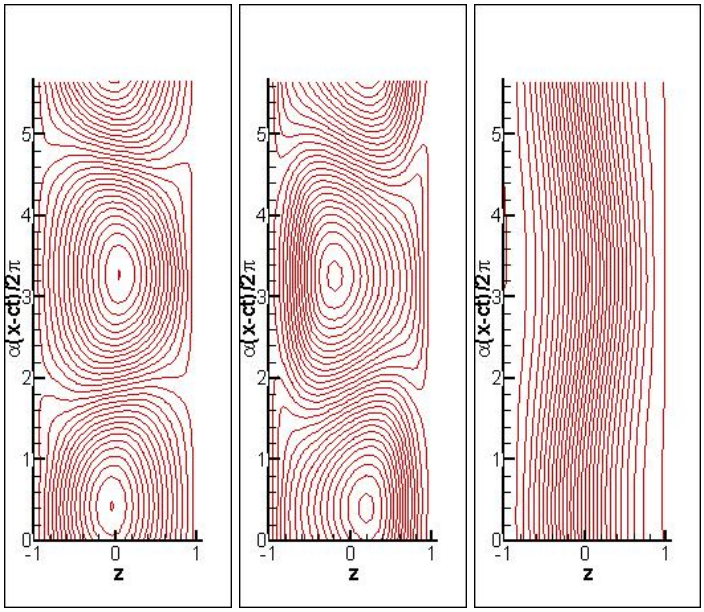


Figure 4.18: *The stream-function of (a) the velocity fluctuations* $\partial\phi/\partial x$*, (b) the disturbance* $\partial\phi/\partial x + \int_{-1}^{1} \check{U}\,dz$ *and (c) the total flow* $\partial\phi/\partial x + \int_{-1}^{1} \hat{U}\,dz$*, for the constant flux condition of PPMF at* $M = 1$ $\alpha = 1.1$*,* $Re = 5000$ *on the upper branch.*

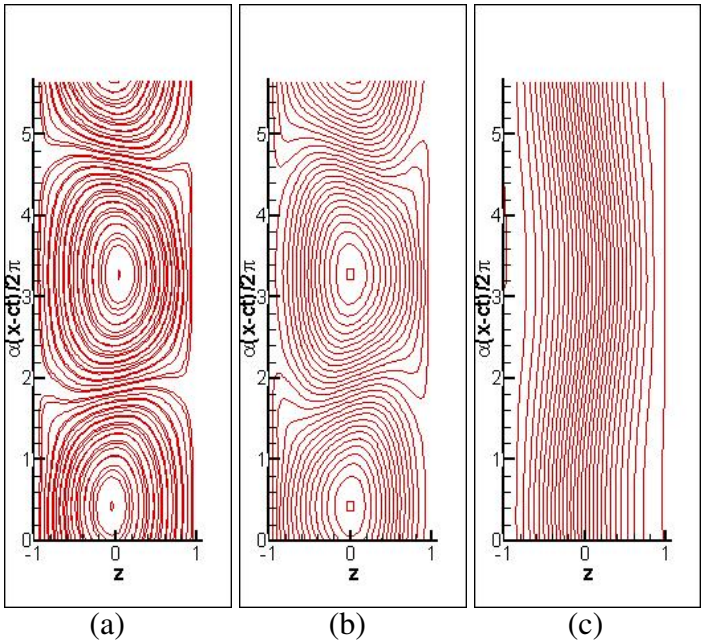


Figure 4.19: *The stream-function of (a) the velocity fluctuations* $\partial\phi/\partial x$*, (b) the disturbance* $\partial\phi/\partial x + \int_{-1}^{1} \check{U}\,dz$ *and (c) the total flow* $\partial\phi/\partial x + \int_{-1}^{1} \hat{U}\,dz$*, for the constant flux condition of PPMF at* $M = 1$ $\alpha = 1.1$*,* $Re = 9500$ *on the upper branch.*

# 5 Secondary Instability

*CONTENTS*

To find transitions to tertiary flows and other higher order bifurcations in the two-dimensional travelling wave equilibrium solutions Floquet theory is applied and a stability change is sought in the eigenvalues. Floquet theory states that in a linear differential equation or a system of linear differential equations there exists a set of fundamental solutions (from which one can build all other solutions) where all solutions can be written in the form $\varphi(t) = c(t)exp(\lambda t)$, where c(t+1/f)=c(t). The exponent $\lambda$ is called the Floquet or characteristic exponent and are the eigenvalues of the system. It is not uniquely defined because any factor $exp(2\pi it/f)$ can be either absorbed in c(t) or in $exp(\lambda t)$, thereby transforming a periodic system into a linear one. As before the solution is stable if the real part of all Floquet exponents are negative, also known as the Lyapunov exponents. In the case of solid-state physics Floquet theorem is analogous to Bloch theorem. Floquet theory is applicable because the two-dimensional non-linear secondary equilibrium states are periodic, this process can be thought of as applying a secondary linear instability to the non-linear states. It is generally accepted that three-dimensional secondary instability is the generic mechanism for transition in shear flows [73] as the bifurcations occur on the convective time-scale observed in experiments. The unsteady disturbance is divided into the finite amplitude contribution plus an infinitesimally small secondary disturbance. Both two-dimensional and three-dimensional infinitesimal secondary disturbances $\tilde{\mathbf{u}}$ are superimposed onto the travelling wave equilibrium solutions $\widehat{U}\,\mathbf{i} + \breve{\mathbf{u}}$ in the form:

$$\tilde{\mathbf{u}} = \delta\tilde{\phi} + \varepsilon\tilde{\psi} \tag{5.1}$$

and then the corresponding growth rates $\sigma$ are numerically evaluated. There is no explicit dependence on y or t so it is assumed to be periodic because the dependence on x is periodic. The complex disturbance is denoted on $\phi, \psi$ by $\tilde{\phi}, \tilde{\psi}$ respectively and then applying Floquet theory by setting:

$$\tilde{\phi} = \sum_{m=-\infty}^{\infty} \sum_{n=0}^{\infty} exp\{im\alpha(x-ct) + id(x-ct) + iby + \sigma t\} \times (1-z^2)^2 \tilde{a}_{mn} T_n(z) \tag{5.2}$$

$$\tilde{\psi} = \sum_{m=-\infty}^{\infty} \sum_{n=0}^{\infty} exp\{im\alpha(x-ct) + id(x-ct) + iby + \sigma t\} \times (1-z^2) \tilde{b}_{mn} T_n(z) \tag{5.3}$$

the same boundary conditions are used as before

$\tilde{\phi} = \partial\tilde{\phi}/\partial z = \tilde{\psi} = 0$, at $z \pm 1$

In order to derive the corresponding equations for the disturbance field $\{\tilde{\Phi}, \tilde{\Psi}\}$, $\{\phi, \psi\}$ is replaced with $\{\phi + \tilde{\phi}, \psi + \tilde{\psi}\}$ in Eqs 2.34, 2.35 and 2.41, 2.42 for PPF and PPMF

respectively, then the equations for the secondary solutions $\{\phi, \psi\}$ are subtracted while at the same time ignoring terms that are non-linear in the disturbances, arriving at:
PPF

$$(-\nabla^2 + \widehat{U}\,\partial_x + \partial t)\nabla^2\Delta_2\tilde{\varphi} = (\partial_z^2\,\widehat{U}\,\tilde{\varphi} + c\nabla^2\tilde{\phi})\partial_X\Delta_2 - \delta\cdot\{(\delta\tilde{\phi} + \varepsilon\tilde{\psi})\cdot\nabla(\delta\phi) + (\delta\phi)\cdot\nabla(\delta\tilde{\phi} + \varepsilon\tilde{\psi})\} \quad (5.4)$$

$$(-\nabla^2 + \widehat{U}\,\partial_x + \partial t)\Delta_2\tilde{\psi} = \{(\partial_z\,\widehat{U})\partial_y)\phi + (c - \widehat{U})\partial_x\tilde{\psi}\}\Delta_2 - \varepsilon\cdot\{(\delta\tilde{\phi} + \varepsilon\tilde{\psi})\cdot\nabla(\delta\phi) + (\delta\phi)\cdot\nabla(\delta\tilde{\phi} + \varepsilon\tilde{\psi})\} \quad (5.5)$$

PPMF

$$(-\nabla^2 + \widehat{U}\,\partial_x + \partial t)\nabla^2\Delta_2\tilde{\varphi} = \{(\partial_z^2\,\widehat{U}\,\tilde{\varphi} + c\nabla^2\tilde{\phi})\partial_X) - M^2\cdot\partial_z^2\tilde{\varphi}\}\Delta_2 - \delta\cdot\{(\delta\tilde{\phi} + \varepsilon\tilde{\psi})\cdot\nabla(\delta\phi) + (\delta\phi)\cdot\nabla(\delta\tilde{\phi} + \varepsilon\tilde{\psi})\} \quad (5.6)$$

$$(-\nabla^2 + \widehat{U}\,\partial_x + \partial t)\Delta_2\tilde{\psi} = \{(\partial_z\,\widehat{U})\partial_y)\phi + (c - \widehat{U})\partial_x\tilde{\psi}\}\Delta_2 - M^2\nabla^{-2}\partial_z^2\tilde{\psi} - \varepsilon\cdot\{(\delta\tilde{\phi} + \varepsilon\tilde{\psi})\cdot\nabla(\delta\phi) + (\delta\phi)\cdot\nabla(\delta\tilde{\phi} + \varepsilon\tilde{\psi})\} \quad (5.7)$$

The PPF and PPMF equations are the same if M=0. It is assumed that that $d^2 \neq b^2 \neq 0$, and as the disturbances are linear there will be no contribution to the mean flow. Eqs 5.2-5.3 are substituted into Eqs 5.4-5.5 for PPF and into Eqs 5.6- 5.7 for PPMF. The new coefficients $\tilde{\tilde{a}}_{mn} = \tilde{a}_{mn}exp(-imact - icdt)$, $\tilde{\tilde{b}}_{mn} = \tilde{b}_{mn}exp(-imact - icdt)$ (for the ease of notation the second tilde will be dropped from here on in) are operated on by $((\alpha b/4\pi^2)\int_0^{2\pi/a} dx \int_0^{2\pi/b} dy\, exp(-\sigma t - iby - i(\gamma\alpha x + dx))\cdot)$ to form a complex eigenvalue problem.

## 5.1 Two-dimensional results

### 5.1.1 PPF

In this section the stability characteristics of the $\alpha = 1.1$ class are examined with regards to two-dimensional super-harmonic secondary disturbances and compared to those of $\alpha = 1.02$. The $\alpha = 1.1$ secondary equilibrium states are indicative of solutions that

bifurcate from infinity and were used by Pugh and Saffman [82] to show the heuristic arguments employed by Orszag & Patera [72] were incorrect. Orszag & Patera used a one-dimensional phase representation of the energy to claim the lower branch was unstable to two-dimensional super-harmonic perturbations with a stability transition occurring at the limit point as the top real eigenvalue ($\sigma_{1r}$) passes through zero, with the upper branch becoming stable from this point. Pugh & Saffman showed that a much richer picture of bifurcation exists in which quasi-periodic flows form. Their insight was to realise the stability transition was complicated by the lack of uniqueness in the parameterization of the two-dimensional flow and went on to show that by differentiating between the constant flux condition and the constant pressure condition the picture becomes clear. ($Re_P = f(Re_Q, \alpha)$ with $Re_P > Re_Q$ [92], [90]). What they found was that $\sigma_{1r}$ passes through zero at the limit point for the constant flux condition at $Re_{cQ} = 2800$ with a second eigenvalue becoming zero at the nose. This corresponds to a phase-shifted eigenfunction which represents the trivial two-dimensional disturbance caused by shifting a known two-dimensional equilibrium solution along the x-axis. The phase shifted zero eigenvalue has algebraic multiplicity 2 and geometric multiplicity 1 so there is a one-dimensional null space [20]. They also showed the upper branch does not stay stable, with a Hopf bifurcation occurring at $Re_Q = 6300$, which is contrary to Orszag & Patera [72] findings who claimed the upper branch remained stable. As $\sigma_i \neq 0$ at the second zero growth rate point ($\sigma_{r1} = 0$) the bifurcation produces a family of travelling wave solution which are spatially periodic with two frequencies (quasi-periodic) in time. If Orszag & Patera energy argument is then applied the $Re_P$ transition occurs on the upper branch where the amplitude of the flows are the same.

The $Re_P$ case demonstrates similar behaviour on the lower branch up until the limit point where upon a second eigenvalue becomes zero. These two eigenvalues coalesce at $Re = 3500$ to form a stable complex conjugate pair. This suggest that a sub-critical bifurcation from this point would produce a stable quasi periodic flow which may well lead to states with lower Reynolds number than the $Re_c$ of the minimum two-dimensional secondary equilibrium solution [56]. Pugh & Saffman highlight the fact that the second eigenvalue becoming neutrally stable at the nose of the $Re_P$ curve but this does not constitute a stability transition, rather it is a second mode becoming unstable. Their value for the limit point of the is $Re_P = 3041$ with the first transition occurring at $Re_P = 3500$

on the upper branch. They state their two-dimensional flows were calculated using m=1 Fourier modes in the streamwise direction and k=50 Chebysehev collocation points across half the channel. The secondary stability analysis was performed at m=1, k=30 and m=1 k=50 at higher Reynolds numbers. They also performed a number of calculations with m=2 for both the secondary flows and stability analysis. They point out the bifurcation points changed from m=1 to m=2 but the nature of the bifurcations and the $\sigma_i$ values at the bifurcation remained the same. Although this is rather confusing it is safe to say they used a rather low truncation level due to hardware limitations.

The first part of the two-dimensional non-linear stability analysis is to recreate Pugh & Saffman work at $\alpha = 1.1$ but at a significantly higher truncation level. The second part is to perform a similar two-dimensional super-harmonic stability analysis for $\alpha = 1.02$ to see if there are any qualitative differences in the transition characteristics between the equilibrium solutions that bifurcate from the neutral curve and ones that bifurcate from infinity. Although the majority of recent work has concentrated on three-dimensional secondary instabilities, the two-dimensional super-harmonic problem is not without interest as it may prove to be a staging ground for stable quasi-periodic flows with $Re_c$ lower than that of two-dimensional travelling wave solutions [56]. In this work m=5 Fourier modes in the x-direction along with k=39 Chebyshev collocation points across the channel in the z-direction are used. The first difference is that in this analysis the limit points occur at $Re_{cQ} = 3565$ and $Re_{cP} = 3798$ opposed to the $Re_{cQ} = 2800$ and $Re_{cP} = 3041$ they state. This discrepancy may be explained by the extra modes included in this analysis, which adds energy to the system, although in PPF the majority of the flow is accounted for by the basic velocity profile so the difference is larger than expected. Despite this the results agree qualitatively with Pugh & Saffman with the first transition taking place at the limit point of the $\alpha = 1.1$ constant flux curve at $Re_c = 3565$, $L_2 - norm \approx 308$, the curve then remains stable on the upper branch until $Re = 5324$, $L_2 - norm \approx 1111$. After which the system becomes highly chaotic with $\sigma_{r1}$ rising rapidly, with other eigenvalues including many complex conjugate pair becoming highly unstable. On the constant pressure curve the first transition takes place on the upper branch at $Re = 3843$, $L_2 - norm = \approx 304$, with the second bifurcation occurring at $Re = 7735$, $L_2 - norm \approx 1111$. This demonstrates that both the first and second bifurcations on the constant flux curve and the constant pressure curve happen when the disturbances have the same $L_2 - norm$ values. This suggests the

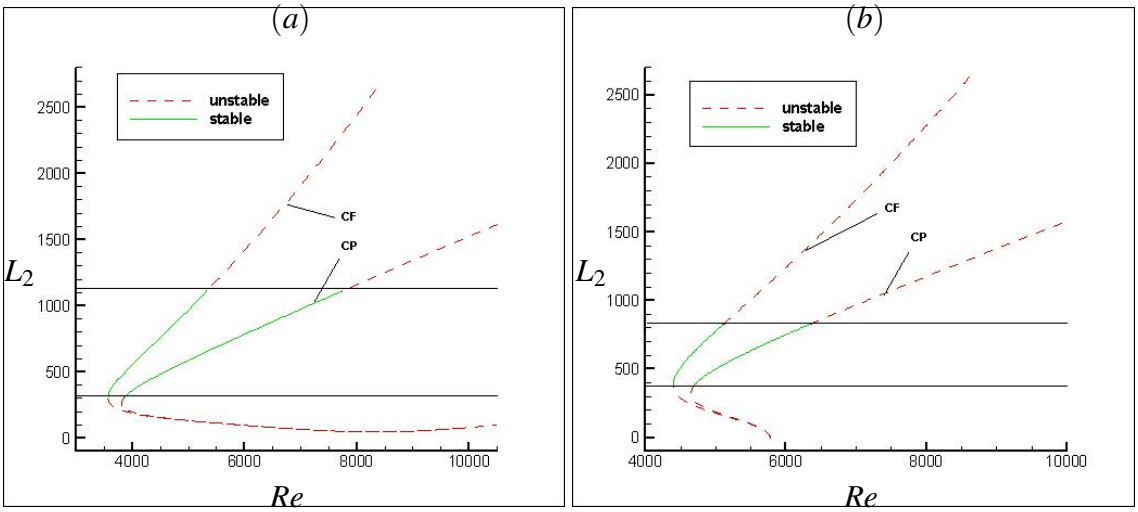


Figure 5.1: *The stable and unstable regions of the constant pressure and flux secondary equilibrium curves for PPF at (a)* $\alpha = 1.10$ *(b)* $\alpha = 1.02$

bifurcations arise when the disturbances reach a certain threshold energy and is shown in Fig 5.1(a). The graph also demonstrates that the $Re_Q$ curve has the lower limit point and therefore how the bifurcation occurs on the upper branch for the constant pressure curve. The two line through the curves show the $L_2 - norm$ value of the bifurcation points and consequently why the bifurcation takes place at a higher Re value on the constant pressure curve. Fig 5.1(b) shows the bifurcation points for the $\alpha = 1.02$ on the constant pressure and constant flux curves, which again exhibit similar qualitative behaviour. In the constant flux case the first bifurcation again befalls at the limit point $Re = 4396$ $L_2 - norm \approx 388$ with the upper bifurcation manifesting at $Re = 5118$, $L_2 - norm \approx 831$. In the constant pressure case the lower bifurcation occurs at $Re = 4694$, $L_2 - norm \approx 380$ with the upper bifurcation taking place at $Re = 6362$, $L_2 - norm \approx 831$. Although from the figures stated above it may appear the lower bifurcation take place at different $L_2 - norm$ values, this is due to the bifurcation points only being calculated to an accuracy of $Re = 1$. This is accentuated near the limit point as the gradient is at it's greatest so $L_2 - norm$ range between one Reynolds number is larger but they do overlap.

Fig 5.2 shows the growth rate $\sigma_{r1}$ of the most dangerous eigenvalue vs $Re$ on the lower and upper branches for constant flux and constant pressure. This demonstrates that the top eigenvalue in each case behave similarly on the lower branch. From the graph it can be seen that the lower branches in the two cases mirror one another and are at their lowest $L_2 - norm$ value at $Re \approx 8360$ which is the closest point to the neutral curve, after which the system becomes more unstable as the Reynolds number increases to infinity.

Moving down the lower branch the system again becomes increasingly unstable reaching a maximum at $Re \approx 4500$ after which point they rapidly stabilise. The top eigenvalue on the lower branch is purely real. The points on the upper branch which are stable are only slightly so, therefore the disturbances are only marginally dampened so the disturbances die away slowly. At the point of the second transition the systems become rapidly and highly unstable. By looking at the eigenvalue spectra for the constant flux case, all along the lower branch the second most dangerous eigenvalue has zero growth rate and is phase-locked. This changes just before the bifurcation point where a relatively fast moving complex conjugate pair become unstable and the stationary zero growth rate eigenvalue is to demoted to third. After the bifurcation point the complex conjugate pair become stable again promoting the phase-locked zero growth rate eigenvalue to the top. Just before the second bifurcation point a complex conjugate pair with a large phase velocity become less stable than the slow moving eigenvalue and at the transition point become unstable. In the constant pressure case the system behaves almost identically on the lower branch until the limit point where a complex conjugate pair become unstable with the phase-locked zero growth rate eigenvalue becomes the third most dangerous eigenvalue. At the bifurcation point the complex conjugate pair become stable and the system behaves as in the case of the constant flux condition. As the complex conjugate pairs begin to stabilise or destabilise they move rapidly through the spectrum. The qualitative behaviour of the system demonstrates the conditions constant flux and constant pressure only differ by a scaling factor. This is particularly well highlighted by the fact that at the limit point of the constant pressure curve a previously stable complex conjugate pair becomes unstable and even though this does not constitute a stability change the same behaviour occurs on the constant flux curve at the corresponding $L_2 - norm$ value. As the bifurcation takes place at the limit point of the constant flux curve this suggests that nature prefers the constant flux condition.

Both the constant flux and constant pressure non-linear solutions for $\alpha = 1.02$ bifurcate sub-critically from the linear curve of neutral stability at $Re = 5772.22$ by way of a Hopf bifurcation as they are identical for the linear case. In both cases at $Re = 5772$, a point close to the neutral curve, the real part of top eigenvalue is slightly positive and therefore unstable and is phase-locked $\sigma_i = 0$. The second eigenvalue has zero growth rate and is also phase-locked as both parts of the eigenvalue are zero. Fig 5.3 shows the states

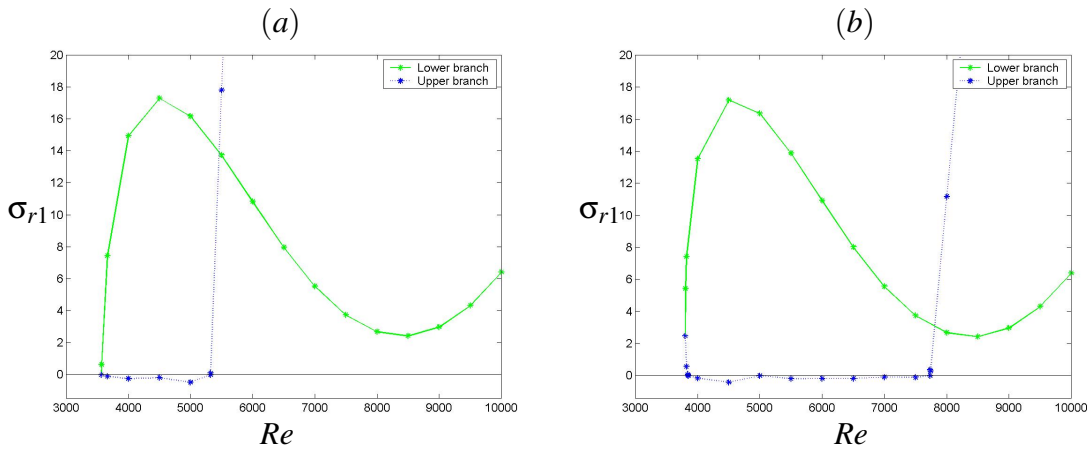


Figure 5.2: *The maximum growth rate of PPF at* $\alpha = 1.1$ *for (a) constant flux, (b) constant pressure*

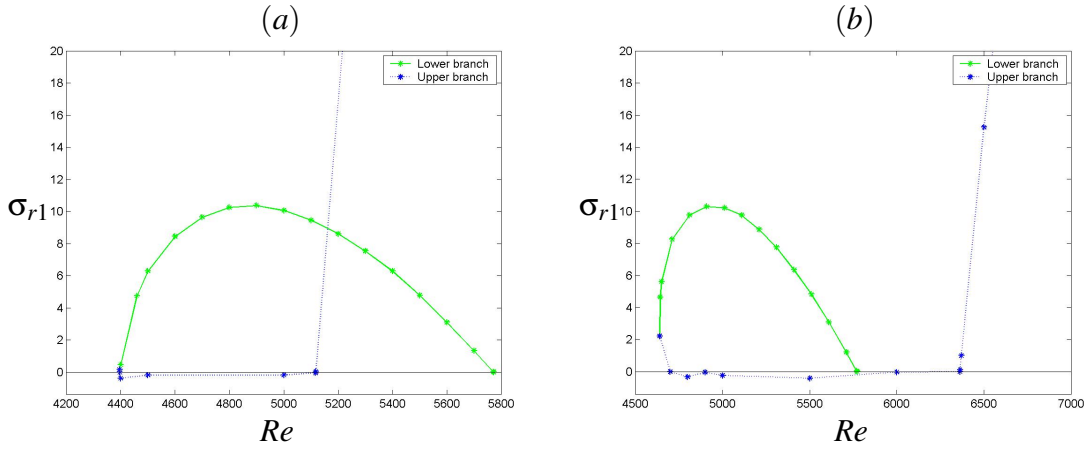


Figure 5.3: *The maximum growth rate of PPF at* $\alpha = 1.02$ *for (a) constant flux, (b) constant pressure*

become increasingly unstable as they precede down the lower branch until they reach $Re \approx 5000$, after which point they start to stabilise. In both cases, on the lower branch the second eigenvalue remains of zero growth rate and phase-locked until in the constant flux case at $Re \approx 4400$, $L_2 - norm \approx 370.94$ after which point a complex conjugate pair become the most unstable eigenvalues. This point has the same disturbance amplitude as the limit point of the constant pressure curve. At the bifurcation point at the limit point the complex conjugate pair stabilise and the top eigenvalue is phase-locked. In the constant pressure case the complex conjugate pair become the most dangerous at the limit point and stabilise at the first bifurcation point on the upper branch. Qualitatively this is exactly the same behaviour as the $\alpha = 1.1$ case, this was to be expected as Jimenez [35] used an unsteady code for $\alpha = 1.0$ and found quasi-periodic flows, period doubling and evidence of chaos in good agreement with the finding outlined above.

### 5.1.2 PPMF

To examine the effect that a transverse magnetic field has on the two-dimensional stability characteristics of the system, the two-dimensional stability results for PPMF are contrasted with those of PPF. As previously shown Fig 5.1 compares the stable and unstable regions of the travelling wave equilibrium solutions between the constant flux and constant pressure conditions for PPF at $\alpha = 1.02$ and $\alpha = 1.1$. This demonstrates that the transitions occur when the $L_2 - norm$ values are the same, the bifurcation point are highlighted by the horizontal lines. The first bifurcation takes place at the limit point of the constant flux curve for both $\alpha = 1.1$ and $\alpha = 1.02$ and on the corresponding $L_2 - norm$ value on the upper branch in the constant pressure case. The second transition also takes place when the $L_2 - norm$ values are identical. The fact that the bifurcation takes place at the limit point for the constant pressure condition suggests it is preferred in nature. The figure also shows that the constant pressure condition stays stable to a higher Reynolds number value and that the stable region is greater in the $\alpha = 1.1$ case as it is more subcritical.

The PPMF case is more complex, Fig 5.4 demonstrates the stable and unstable regions of the travelling wave equilibrium solutions at $M = 0.1$, $M = 0.5$ and $M = 1.0$ for $\alpha = 1.1$. Firstly concentrating on part (a) of the diagram, the constant flux case, the first bifurcations now take place on the lower branch before the limit point and not only that for the $M = 0.2, 0.5, 1.0$ curves are stable at $Re > 10000$ on the lower branch although it can not be assumed they are stable to infinity. The fact that regions of the lower branch are stable is in stark contrast to the PPF case. Looking at the constant pressure case, even the $M = 0.1$ lower branch is also initially stable in the range considered, these results suggest the magnetic field has a stabilising effect on the lower branch. Tables 5.1, 5.2 show the bifurcation data for $\alpha = 1.1$ and $\alpha = 1.02$ for constant flux and constant pressure respectively, accurate to one Reynolds number. They show that on the lower branch when the magnetic field is weakest, $M = 0.1 - 0.2$, that the points at which the curves become stable the $L_2 - norm$ values are different, this is best highlighted by the $M = 0.1$ case because the lower branch of the constant flux curve is unstable while for the constant pressure gradient it is stable. As the magnetic field strength is increased to $M = 0.5 - 1.0$ the first bifurcation on the lower branch happens when the $L_2 - norm$ values are the same. Moving on to the next bifurcation point, the point where the curves become stable occurs before the limit point.

The bifurcations all take place when the $L_2 - norm$ values are equivalent between the constant flux and constant pressure gradient. At the bifurcation point on the upper branch it is again found that for the Hartmann number range $M = 0.1 - 0.2$ the $L_2 - norm$ values differ a little, it is difficult to know if this is significant or the truncation level used is to low, although this seems improbable as the bifurcations occur at lower Reynolds number values for lower Hartmann number values. As the magnetic field strength increases to $M = 0.5 - 1.0$ the disturbance amplitudes are the same at the bifurcation points. Looking at the overall trend firstly it is shown that the majority of the lower branch is unstable for the constant flux case at $M = 0.1$ and $M = 0.2$, while for the constant pressure gradient case it is mainly stable. As the magnetic field is increased more of the lower branch becomes stable. On the upper branch once the magnetic field has been applied the system becomes unstable at higher $L_2 - norm$ values as the field strength is increased because the limit points are higher. Surprisingly the upper bifurcation point for the PPF case is higher than the trend would suggest, the equivalent of between $M = 0.5 - 1.0$, implying the weak magnetic field is destabilising the upper branch.

The $\alpha = 1.02$ case behaves as expected with all the bifurcations occurring when the $L_2 - norm$ values are equivalent. Fig 5.5 shows the stable and unstable regions of the travelling wave equilibrium solutions for $M = 0.1, 0.5, 1.0$ at $\alpha = 1.02$. The whole of the lower branch is unstable as in the PPF case except for the $M = 1.0$ curve which begins stable from the linear neutral curve until a transition takes place on the lower branch and remains unstable until it has passed the limit point. From Tables 5.1, 5.2 it can be seen that the only bifurcations on the lower branch takes place when the disturbance amplitudes are the same. On the upper branch the constant flux bifurcation no longer takes place at the limit point as in the PPF case but rather is delayed until further along the upper branch. All the bifurcations take place when the $L_2 - norm$ values correspond between the constant flux condition and the constant pressure gradient as with PPF. The overall trend is as expected with the $L_2 - norm$ values rising on the upper branch with increasing $M$ at both bifurcation points. In the PPF case the $\alpha = 1.1$ and $\alpha = 1.02$ branches had qualitatively similar bifurcation characteristic but this is not the case for PPMF. In the $\alpha = 1.1$ case the bifurcations happen earlier on the lower branch but in the $\alpha = 1.02$ case they are delayed until the upper branch. Also in the $\alpha = 1.02$ case the upper bifurcation point increases with $M$, so the magnetic field delays the upper bifurcation point. This is in contrast to the

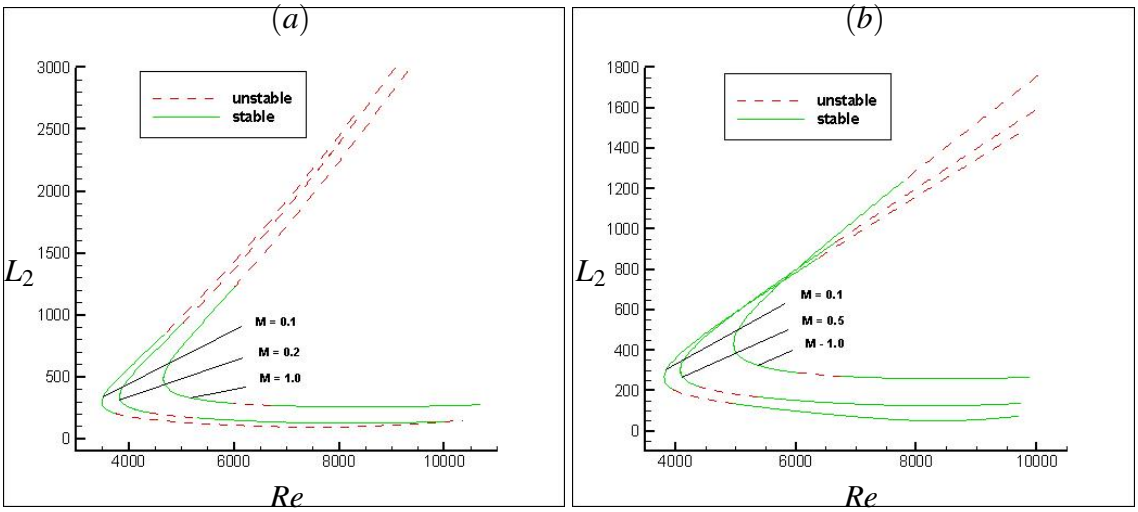


Figure 5.4: *The secondary equilibrium curves for M=0.1,0.2,1.0 at* $\alpha = 1.1$ *for (a) constant flux, (b) constant pressure*

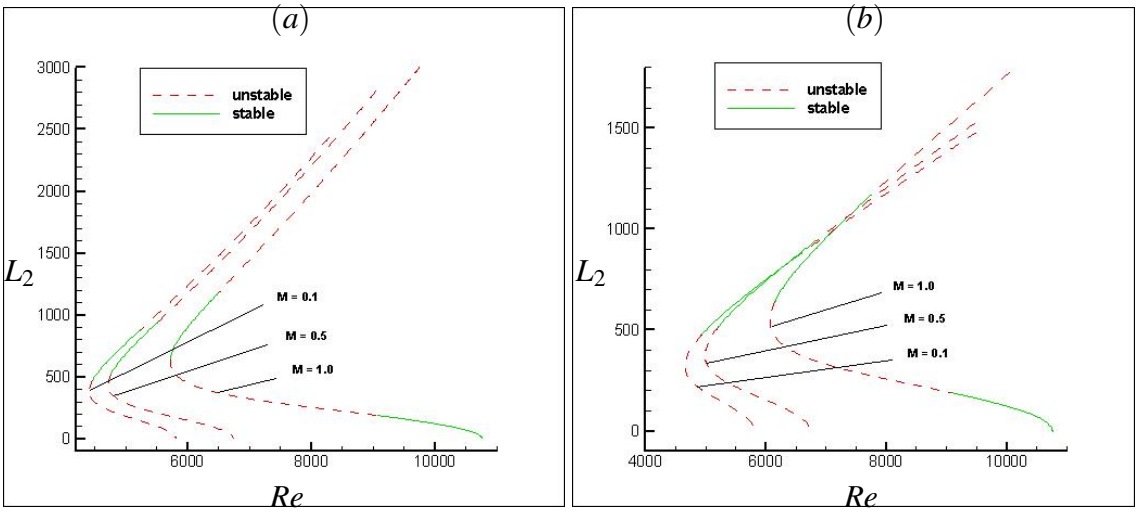


Figure 5.5: *The secondary equilibrium curves for M=0.1,0.2,1.0 at* $\alpha = 1.02$ *for (a) constant flux, (b) constant pressure*

$\alpha = 1.1$ case as the PPF case had a higher bifurcation point than the $M = 0.5$ case. The qualitative differences between the $\alpha = 1.02$ case which bifurcates from the neutral curve and the $\alpha = 1.1$ case which bifurcates from infinity are unexpected.

To gain some insight into the strange behaviour of the $\alpha = 1.1$ results the eigenvalue spectra will be examined at $Re = 7000$ for $M = 0.0, 0.1, 1.0$ on the lower branch. Fig 5.6 illustrates the real part of the top 30 eigenvalues vs the imaginary part at $Re = 7000$ for PPF on the lower branch for (a) constant flux, (b) constant pressure. On the lower branch the two cases are indistinguishable and as expected the eigenvalue diagram patterns are equivalent. The eigenvalue spectral pattern is shaped like an aeroplane, with the top eigenvalues being stationary. As $\sigma_r \approx -75$ complex conjugate pair become preva-

Table 5.1: Constant flux bifurcation results

| | | lower branch | | | | upper branch | | | |
|---|---|---|---|---|---|---|---|---|---|
| | | 1 | | 2 | | 1 | | 2 | |
| $M$ | α | $Re$ | $L_2$ | $Re$ | $L_2$ | $Re$ | $L_2$ | $Re$ | $L_2$ |
| 0.0 | 1.02 | - | - | - | - | 4396 | 387.85 | 5118 | 831.02 |
| 0.1 | 1.02 | - | - | - | - | 4465 | 475.99 | 5235 | 882.06 |
| 0.2 | 1.02 | - | - | - | - | 4500 | 480.51 | 5269 | 889.40 |
| 0.5 | 1.02 | - | - | - | - | 4751 | 513.90 | 5516 | 944.37 |
| 1.0 | 1.02 | 9068 | 189.65 | - | - | 5719 | 641.64 | 6473 | 1169.35 |
| 0.0 | 1.10 | - | - | - | - | 3565 | 308.04 | 5324 | 1111.15 |
| 0.1 | 1.10 | 3753 | 204.94 | - | - | 4661 | 843.39 | - | - |
| 0.2 | 1.10 | 5836 | 120.72 | 3801 | 206.88 | 4697 | 853.35 | - | - |
| 0.5 | 1.10 | 5304 | 170.09 | 4278 | 221.55 | 5022 | 935.78 | - | - |
| 1.0 | 1.10 | 6683 | 272.05 | 5960 | 288.85 | 6018 | 1234.49 | - | - |

Table 5.2: Constant pressure bifurcation results

| | | lower branch | | | | upper branch | | | |
|---|---|---|---|---|---|---|---|---|---|
| | | 1 | | 2 | | 1 | | 2 | |
| $M$ | α | $Re$ | $L_2$ | $Re$ | $L_2$ | $Re$ | $L_2$ | $Re$ | $L_2$ |
| 0.0 | 1.02 | - | - | - | - | 4694 | 380.08 | 6362 | 831.17 |
| 0.1 | 1.02 | - | - | - | - | 4930 | 475.90 | 6594 | 881.93 |
| 0.2 | 1.02 | - | - | - | - | 4962 | 480.33 | 6623 | 889.49 |
| 0.5 | 1.02 | - | - | - | - | 5206 | 514.07 | 6837 | 944.18 |
| 1.0 | 1.02 | 9087 | 189.57 | - | - | 6143 | 636.65 | 7747 | 1169.1 |
| 0.0 | 1.10 | - | - | - | - | 3843 | 304.27 | 7735 | 1111.11 |
| 0.1 | 1.10 | 4956 | 136.75 | 3972 | 204.01 | 6343 | 851.43 | - | - |
| 0.2 | 1.10 | 5002 | 141.09 | 4021 | 205.96 | 6382 | 861.65 | - | - |
| 0.5 | 1.10 | 5347 | 169.78 | 4378 | 221.62 | 6663 | 937.61 | - | - |
| 1.0 | 1.10 | 6747 | 272.07 | 6045 | 288.87 | 7769 | 1234.73 | - | - |

lent with the phase velocity increasing as the system becomes more stable, forming the 'wings' of the plane. The overall pattern is symmetrical with the top eigenvalue being stationary and unstable as it is all along the lower branch for PPF. Fig 5.7 depicts the eigenvalue spectrum of the top 30 eigenvalues for $M = 0.1$ at $Re = 7000$ on the lower branch. It has a similar pattern and range to the PPF case except the top two eigenvalues are not phase locked, this complex conjugate pair is stable in the constant pressure case and unstable in the constant pressure gradient case. This is quite telling as again both the (a) constant flux and (b) the constant pressure eigenvalue spectra appear similar except one is stable and one is not resulting in very different flows. Fig 5.8 is another eigenvalue spectrum graph on the lower branch at $Re = 7000$ but this time at $M = 1.0$. The most dangerous eigenvalues are again a complex conjugate pair but are both stable for (a) the constant flux and (b) the constant pressure conditions. Although the range of the graph is similar to that of PPF and $M = 0.1$ cases the pattern has changed slightly. This makes (a) the constant flux and (b) the constant pressure case appear unsymmetrical as they are a mirror image of one another. This is misleading due to the fact only the top 30 eigenvalues are includes and therefore only one eigenvalue of the bottom complex conjugate pair is included. From these results it seems the overall eigenvalue pattern is not altered a great deal as Hartmann number increases on the lower branch. The obvious difference is that the magnetic field changes the top unstable stationary mode into a more stable complex conjugate pair. From these results it is still unclear why in the $M = 0.1$ case the constant flux condition is unstable while the constant pressure case is stable despite having such similar spectra.

To try and find out the reason for the disparity of the $L_2 - norm$ values at the upper bifurcation point for $M = 0.1$ the eigenvalue spectra is inspected for clues. Fig 5.9 shows the eigenvalue spectrum of the top 30 eigenvalues for PPF at the second or upper bifurcation point on the upper branch which occurs at $Re = 5324$ on the constant flux curve and $Re = 7735$ on the constant pressure gradient curve. It demonstrates a symmetrical pattern although it is rather different to that on the lower branch. This time the most dangerous eigenvalues are an unstable complex conjugate pair with the overall pattern appearing more scattered and without complex conjugate pairs with such large phase velocities. This is in contrast to the linear system where at most there is at most one unstable wall mode. Again the constant pressure and flux cases appear similar. Fig 5.10 shows the eigenvalue

spectrum for $M = 0.1$ at the upper bifurcation point on the upper branch at $Re = 4661$ for the constant flux case and $Re = 6343$ in the constant pressure gradient case. This was the point that the $L_2 - norm$ values did not match up and this can be seen from the fact that the two spectra are not identical, why this should be is unclear. The spectra themselves are quite different from the PPF case although again the two most dangerous eigenvalues are a complex conjugate pair. Fig 5.4 depicts the same but at $M = 1.0$ and the two cases appear similar as expected, the bifurcation points are at $Re = 6018$ for the constant flux case and $Re = 7769$ for the constant pressure case where the $L_2 - norm$ values are equivalent. The eigenvalue spectra patterns are similar to those of the $M = 0.1$ case.

Looking deeper into the effects of the magnetic field the MAGPHI subroutine was removed from the program which is responsible for the magnetic or Lorentz term in the poloidal equation. This did not have much effect on the system as the stability characteristics remained similar to the true magnetic results although they were slightly more unstable than the true results. The transitions retained the same qualitative behaviour with the bifurcation again occurring on the lower branch and at the bifurcation point the top stable eigenvalue becomes phase-locked. Next the magnetic velocity profile Eq 2.26 was replaced with the PPF velocity profile Eq 2.25 while retaining the MAGPHI subroutine in the magnetic secondary stability program. This caused the top eigenvalue to become highly unstable and phase-locked with the system remaining unstable even on the upper branch. Thirdly a PPF secondary equilibrium solution was used as an input in the magnetic secondary stability program and as a result that the top eigenvalues are a unstable complex conjugate pair. Conversely a PPMF secondary equilibrium solution was used as an input in the PPF secondary stability code with the affect of the most dangerous eigenvalue being unstable and phase-locked. These alterations were performed on the PPF constant pressure $\alpha = 1.1$ secondary equilibrium solutions and the constant flux $\alpha = 1.1$, $M = 0.1$ PPMF secondary equilibrium solutions. From this it can be deduced that the magnetic basic velocity profile is responsible for the emergence of complex-conjugate pair in the magnetic results and that it requires a combination of the MAGPHI subroutine, the magnetic velocity profile and a PPMF secondary equilibrium input to stabilise the system although the majority of the stabilisation effect can again be attributed to the basic magnetic velocity profile. This is in agreement with the linear results.

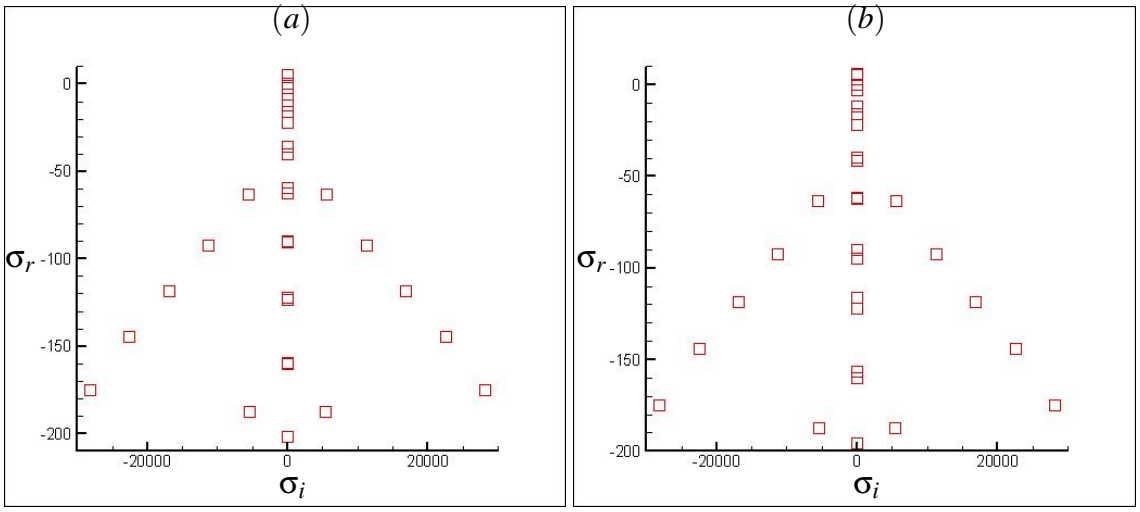


Figure 5.6: *The eigenvalue spectrum of the top 30 modes at Re=7000 on the lower branch at* $\alpha = 1.1$, *PPF for (a) constant flux (b) constant pressure*

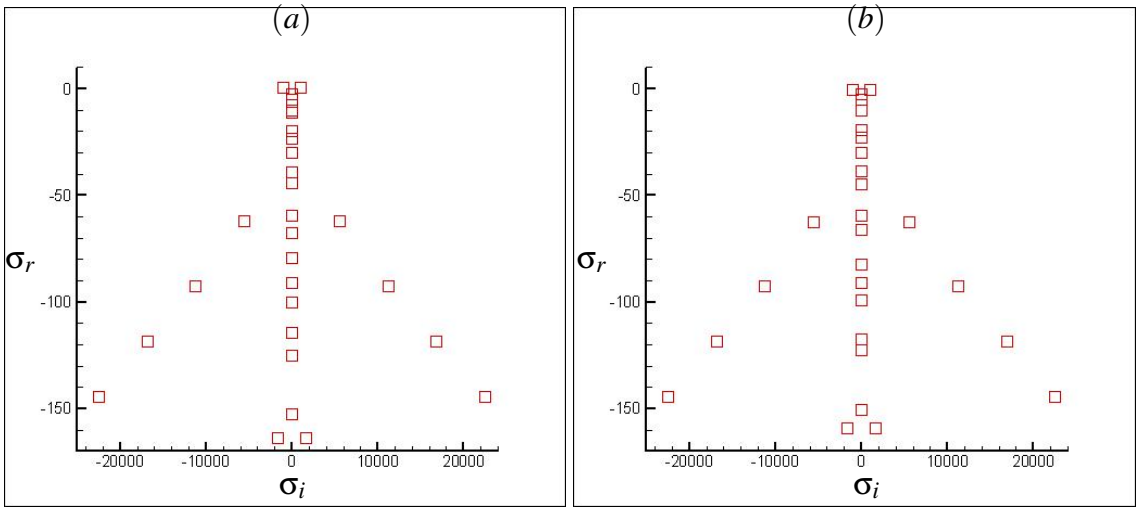


Figure 5.7: *The eigenvalue spectrum of the top 30 modes at Re=7000 on the lower branch for* $\alpha = 1.1$, $M = 0.1$ *for (a) constant flux (b) constant pressure*

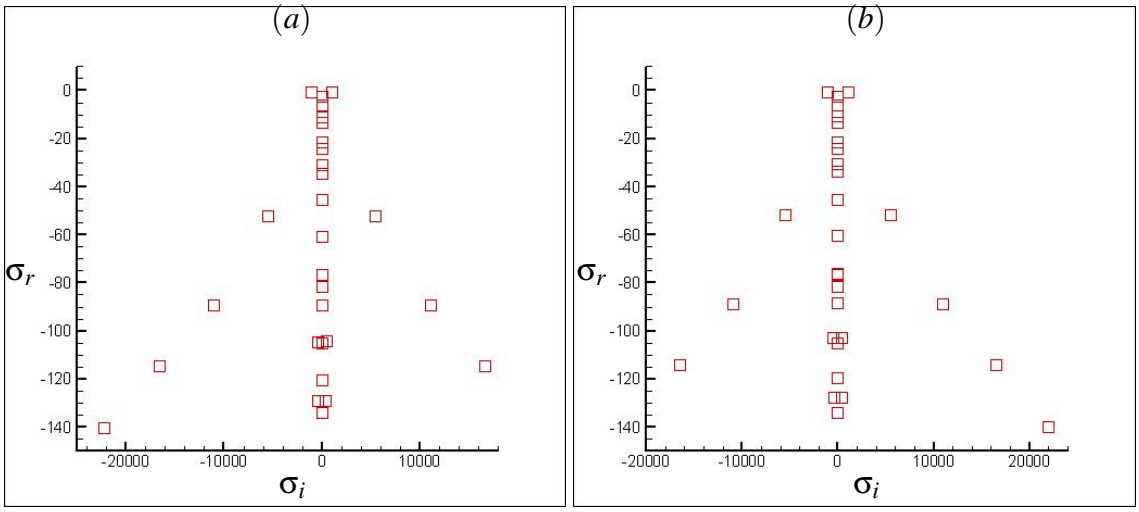


Figure 5.8: *The eigenvalue spectrum of the top 30 modes for at Re=7000 on the lower branch for* $\alpha = 1.1$, $M = 1.0$ *for (a) constant flux (b) constant pressure*

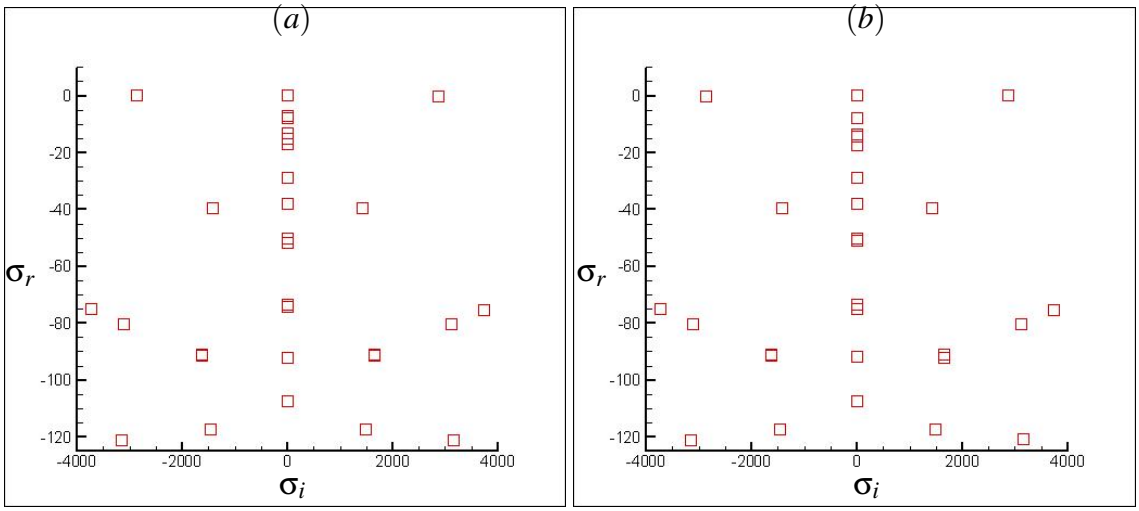


Figure 5.9: *The eigenvalue spectrum of the top 30 modes at the upper bifurcation point on the upper branch for* $\alpha = 1.1$, *PPF for (a) constant flux (b) constant pressure*

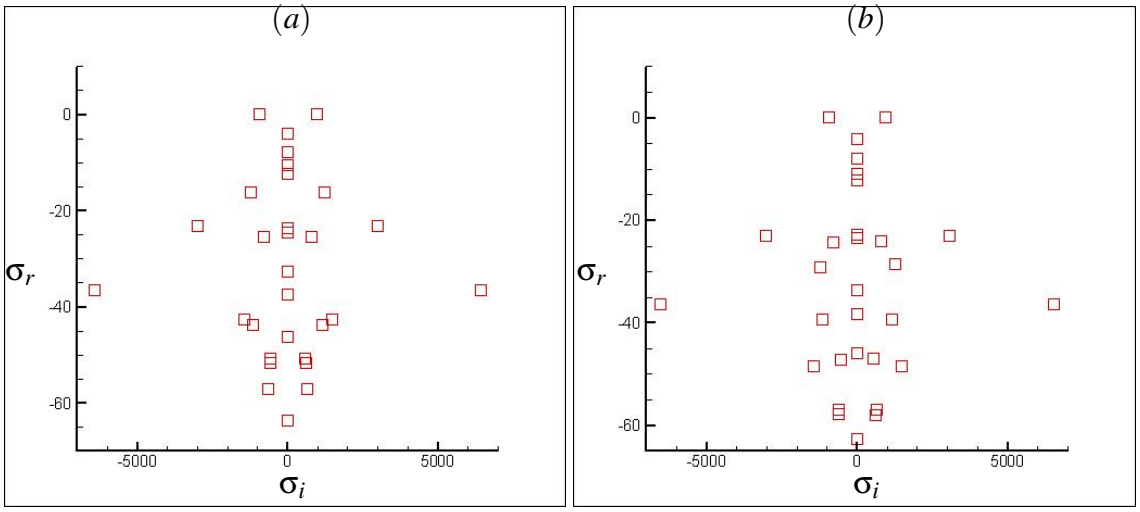


Figure 5.10: *The eigenvalue spectrum of the top 30 modes at the upper bifurcation point on the upper branch for* $\alpha = 1.1$, *M=0.1 for (a) constant flux (b) constant pressure*

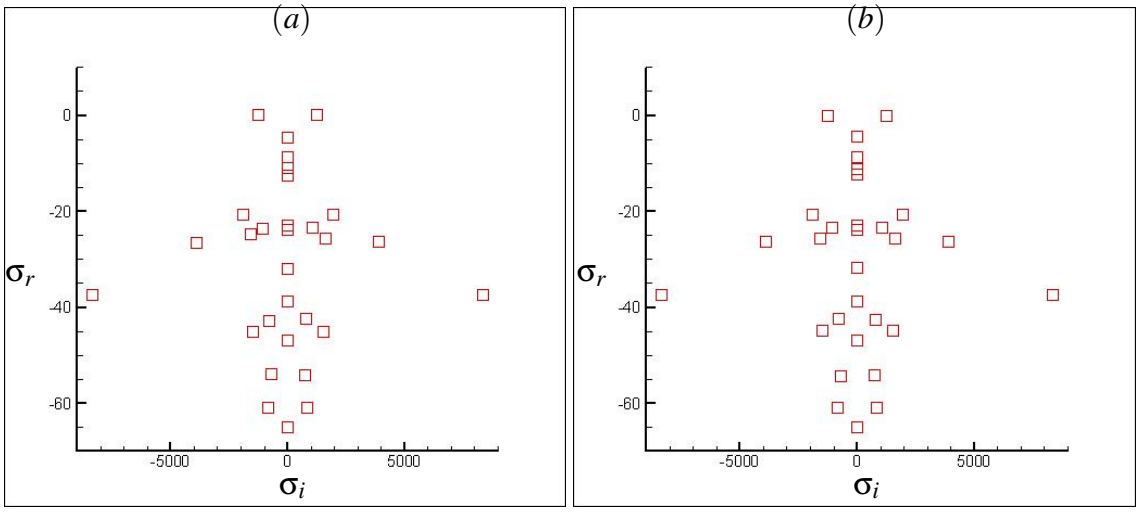


Figure 5.11: *The eigenvalue spectrum of the top 30 modes at the upper bifurcation point on the upper branch for* $\alpha = 1.01$, *M=1.0 for (a) constant flux (b) constant pressure*

### 5.1.3 Three-dimensional secondary instabilities

From experiments [95] turbulence in shear flows is considered a three-dimensional phenomenon especially in the non-linear *Tollmein-Schlichting* wall instability in which vortex tilting and stretching play an important role. The *Tollmein-Schlichting* waves were generated artificially using a vibrating ribbon and three-dimensional secondary disturbances of a fixed spanwise period were applied by means of equally spaced strips of tape. Klebanoff et al. [43] performed a similar more accurate experiment to look at the development of three-dimensional disturbances superimposed on a field of *Tollmein-Schlichting* waves. They observed the three-dimensional perturbations grew rapidly when the *Tollmein-Schlichting* waves reached a threshold value of about 1% of the $U_0$ velocity. The perturbations quickly took the form of $\Lambda$-shaped vortices with the same streamwise periodicity as the fundamental *Tollmein-Schlichting* wave and continued to grow until the boundary layer became fully turbulent. $\Lambda$-shaped vortices with twice the periodicity as the *Tollmein-Schlichting* waves have also been observed in PPF [48]. This produces a staggered "herringbone" structure and is referred to as sub-harmonic.

Guided by experiment Orszag & Patera [71] and Herbert [29] showed that the exponential growth of small three-dimensional disturbances, observed in PPF and other shear-flow experiments such as Blaisus layer flows, can be explained by a three-dimensional linear secondary instability of the non-linear two-dimensional travelling waves. The secondary instability originates from *parametric resonance* of a periodic flow and the different types of parametric resonance can explain the different routes to transition [29]. Parametric resonance differs from normal resonance and super-harmonic resonance because it is an instability phenomenon and arises when a given parameter in the system is varying periodically in time. Orszag & Patera [73] went on to show that positive temporal amplification rates exist below the non-linear critical Reynolds number $Re_c$. They used two-dimensional quasi-equilibrium states in conjunction with a shape assumption. They obtained a threshold Reynolds number of $Re \approx 1000$ in good agreement with experimental data. If the scenario they describe is correct it would fully explain the early stage transition in PPF. There work has not been given the accolades it perhaps deserves due to the heuristic nature of their hypothesis that quasi-equilibrium states have the same form as the exact two-dimensional wave like equilibrium solutions but with a different growth rate $\varepsilon_{shape}$. This result prompted Ehrenstein & Koch [16] to study exact three-dimensional travelling

wave equilibrium solutions that bifurcate from the neutral growth rate points of the phase locked secondary instability modes.

## 5.2 Three-dimensional results

### 5.2.1 PPF

In this section three-dimensional super-harmonic secondary disturbances are applied on to the two-dimensional PPF secondary equilibrium solutions at $Re = 5000$, $\alpha = 1.1$ on the lower and upper branches for both the constant pressure and constant flux condition. Figures 5.12 - 5.15 shows the temporal amplification rate $\sigma_r$ as a function of the span-wise wavenumber $\beta$. Fig 5.12 shows the 6 unstable modes on the lower branch although there appear to be only four modes as the bottom two curves trace one another as they are complex conjugate pairs with similar real and imaginary parts of the eigenvalues. Fig 5.13 again shows the lower branch but this time the phase locked modes are represented by solid lines and the most unstable non-phase locked mode is depicted by the dashed line. The phase locked secondary instability modes are in phase with the two-dimensional travelling wave solutions and consequently have $\sigma_i = 0$ and represent limit cycles in the moving frame, the non-phase locked modes correspond to quasi-periodic solutions. From the graph it is clear that the two phase locked modes are the most dangerous, the phase locked modes always appear in pairs due to the symmetric profile and the fact the calculations are carry out across the full channel and therefore both the symmetric and antisymmetric solutions are included although they do not interact with one another, the symmetric mode is always the most unstable of the two. The neutral growth rate points of the phase locked modes ($(\sigma_r = 0)$, points A1 and B1, are of greatest interest as it is from these points the three-dimensional secondary equilibrium solutions bifurcate from. Only the top non-phase locked mode is shown as they are hard to study and their physical importance is not fully understood. As expected on the lower branch the constant pressure and constant flux conditions have similar results as they are essentially the same.

Fig 5.14 depicts the top 40 eigenvalues on the upper branch for $\beta = 0 - 15$. From the graph it is clear to see that all 40 of the modes are unstable for varying ranges of $\beta$, as expected their are far more unstable modes than when only N=1 or N=2 Fourier modes

are considered [16]. In fact there are 46 unstable modes for the constant pressure condition and 68 for the constant flux. This is a far greater number than on the lower branch, the growth rate of $\sigma_{r1}$ is also about three times greater than its equivalent on the lower branch due to the higher amplitude of the disturbances on the upper branch. This is quite different from the two-dimensional secondary stability case, where at $Re = 5000$, $\alpha = 1.1$ in both the constant flux and constant pressure case this point would be stable. The large number of unstable modes complicates the picture and makes it difficult to distinguish between the individual modes as they are ordered by the real part of the eigenvalues whose order is constantly changing with $\beta$, many are complex conjugate pairs which trace one another and it is impossible to tell which are phase locked and which are not. In order to simplify this Fig 5.15 shows the three unstable phase locked pairs of modes and the most unstable non-phase locked mode. Again the neutral growth rate point of the phase locked modes are of greatest interest because as was the case on the lower branch this is where the three-dimensional secondary equilibrium solutions bifurcate from. The non-phase locked solution is a complex conjugate pair and becomes the most dangerous mode at higher $\beta$ values lending credence to Orszag & Patera quasi-equilibrium state theory [73]. As expected the constant flux condition is the more unstable of the two and has a higher number of unstable modes because the two-dimensional travelling wave solution has a higher $L_2 - norm$ value and is therefore more non-linear. The calculations were performed at the same truncation level as the two-dimensional secondary equilibrium solutions with n=5 Fourier modes and k=39 Chebyshev modes as are all the secondary as are all the secondary instability results.

### 5.2.2 PPMF

In this section the three-dimensional secondary perturbations are imposed on to the PPMF secondary equilibrium solutions in a similar manner to the PPF case. Fig 5.16 shows the unstable modes on the lower branch at Re=5000, $\alpha = 1.1$, M=1.0, for the constant pressure condition there are 22 unstable modes and constant flux condition has 16 positive eigenvalues. The reason the constant pressure and constant flux graphs differ is because $Re = 5000$ is close to the limit point of the constant pressure curve which has a higher $L_2 - norm$ value on the lower branch and consequently the two curves have started to diverge, see Fig 4.11. This also explains why their are far more unstable modes than in

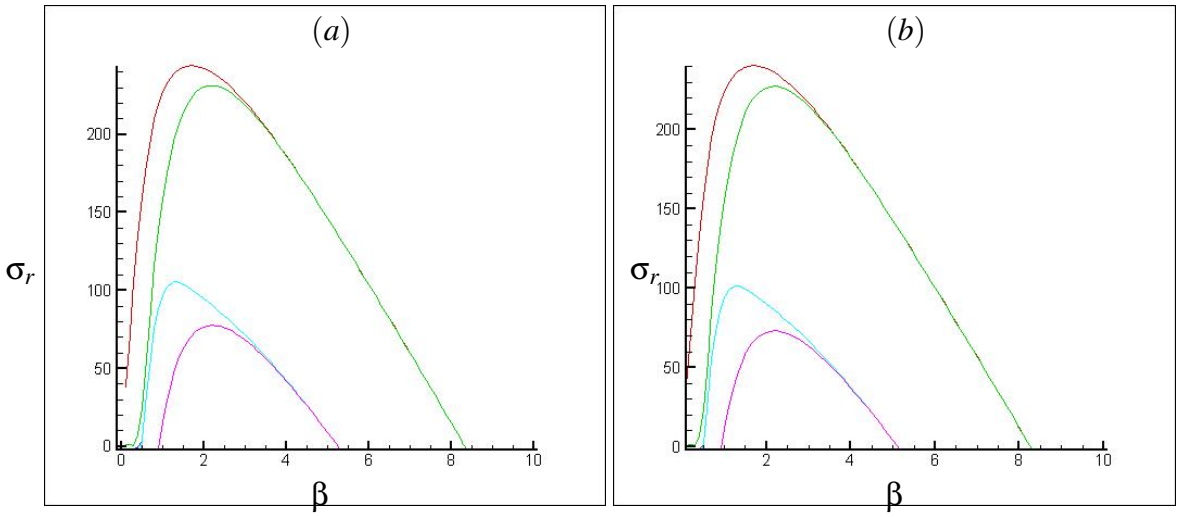


Figure 5.12: *The temporal amplification rate* $\sigma_r$ *vs the spanwise wavenumber* $\beta$ *for all the unstable modes on the lower branch at* $\alpha = 1.1$, *Re=5000 for (a) constant pressure, (b) constant flux*

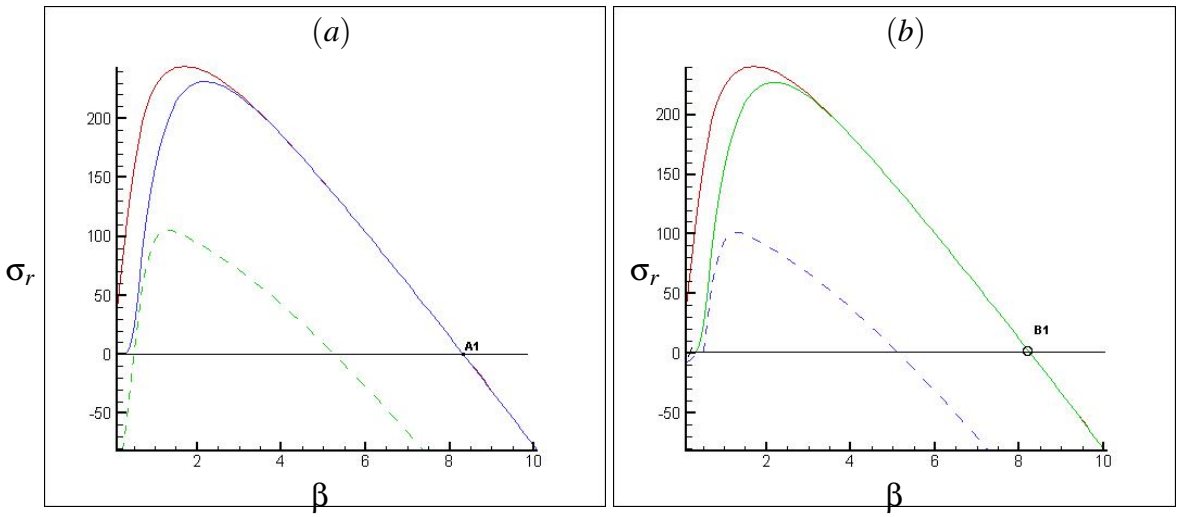


Figure 5.13: *The temporal amplification rate* $\sigma_r$ *vs the spanwise wavenumber* $\beta$ *for the lower branch at* $\alpha = 1.1$, *Re=5000 for (a) constant pressure, (b) constant flux*

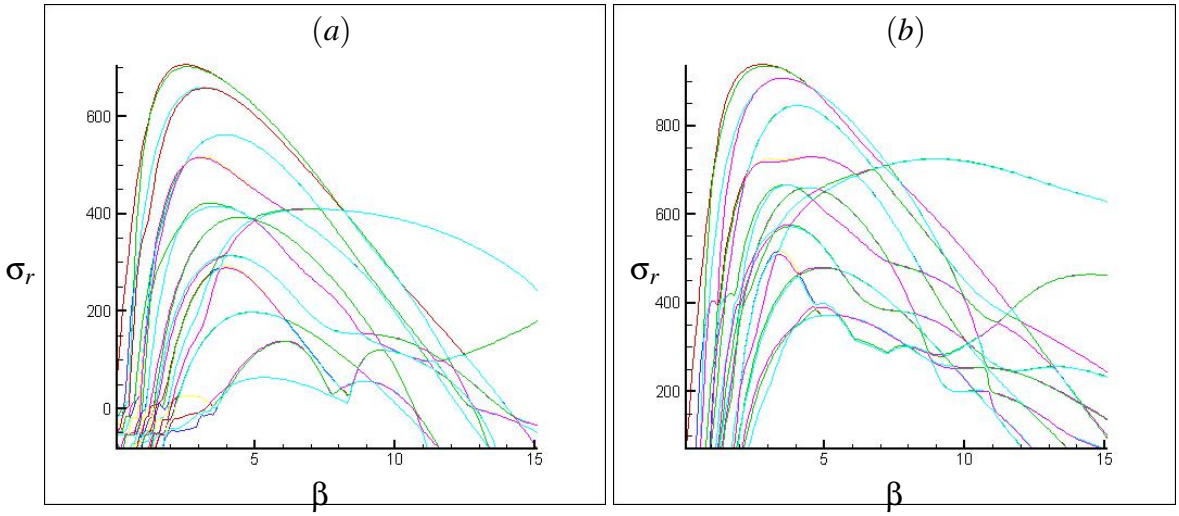


Figure 5.14: *The temporal amplification rate* $\sigma_r$ *vs the spanwise wavenumber* $\beta$ *for the top 40 eigenvalues on the upper branch at* $\alpha = 1.1$, *Re=5000 for (a) constant pressure, (b) constant flux*

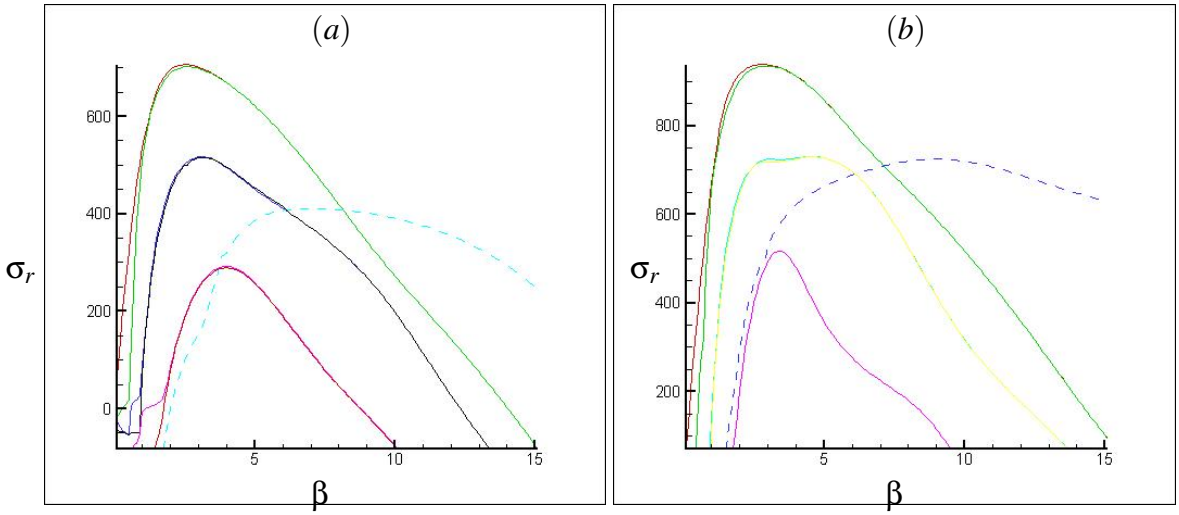


Figure 5.15: *The temporal amplification rate* $\sigma_r$ *vs the spanwise wavenumber* $\beta$ *for the top 6 phase locked modes and the most dangerous non-phase locked mode on the upper branch at* $\alpha = 1.1$, *Re=5000 for (a) constant pressure, (b) constant flux*

the PPF case. Straight away it can be seen that there is a far richer pattern with three discernible peaks along with a far higher number of unstable modes than was the case for the lower branch of PPF. Fig 5.17 illustrates the three unstable phase locked modes and the two most unstable non-phase locked modes. The first peak is that of a single phase locked mode which dies away quickly, the second peak is made up of two non-phase locked modes with the third consisting of a phase locked pair. This is qualitatively different from the PPF case but the most interesting thing is the existence of a single phase locked mode with suggests a symmetry breaking has taken place. The non-phase locked modes are not a complex conjugate pair but two separate distinct modes. In the constant pressure case the three peaks are in descending order but all of comparable magnitude whereas when the constant flux condition is applied the non-phase locked modes are the most dangerous. The third peak is far lower meaning the $\beta$ value range in which it is unstable is greatly reduced as well as reducing the overall number of unstable modes. The three peak pattern implies that different modes dominate at different $\beta$ value ranges and the fact they overlap creates a more complex situation with the different modes competing for dominance. The phase locked modes do not overlap, if they did this would be and ideal place to look for a bifurcation point, it is not clear how if at all the phase and non-phase locked modes interact when they intersect. Again as with the PPF case the neutral growth rate point of the phase locked secondary instability modes are where the three-dimensional secondary equilibrium solutions bifurcate from.

Fig 5.18 shows 18 unstable modes on the upper branch for the constant pressure condition and 36 unstable modes for the constant flux condition. The discrepancy between the number of unstable modes is again due to the fact that $Re = 5000$ is very close to the turning point on the constant pressure equilibrium solution curve so this point corresponds to a $L_2 - norm$ value on the lower branch of the constant flux curve. This explains why it appears to be a cross between the constant pressure and constant flux condition on the lower branch diagram. The constant flux graph has a different structure it still has the three peaks except there is a fourth peak / plateau between the second and third. This time the last peak is the most dangerous with the whole system being nearly twice as unstable as on the lower branch. Fig 5.19 simplifies the diagram and shows three phase locked modes and two non-phase locked complex conjugate pairs. It is possible to make out the three peak pattern as before except there is a fourth phase locked plateau curve which bridges

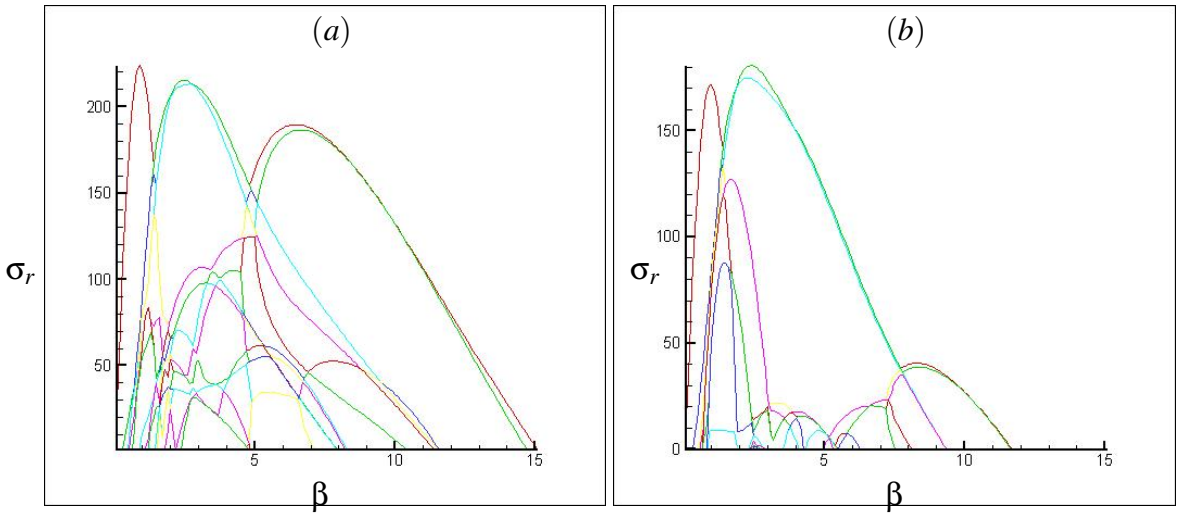


Figure 5.16: *The temporal amplification rate* $\sigma_r$ *vs the spanwise wavenumber* $\beta$ *for the top 20 eigenvalues on the lower branch at* $\alpha = 1.1$*, Re=5000, M=1.0 for (a) constant pressure, (b) constant flux*

the second and third peaks. This proves to be an intriguing result as it intersects both the first and third peaks which are also locked peaks which make these areas ideal candidates for bifurcation points as you would expect the modes to interact with one another. This has not been shown to be the case yet but is be an obvious area for future work.

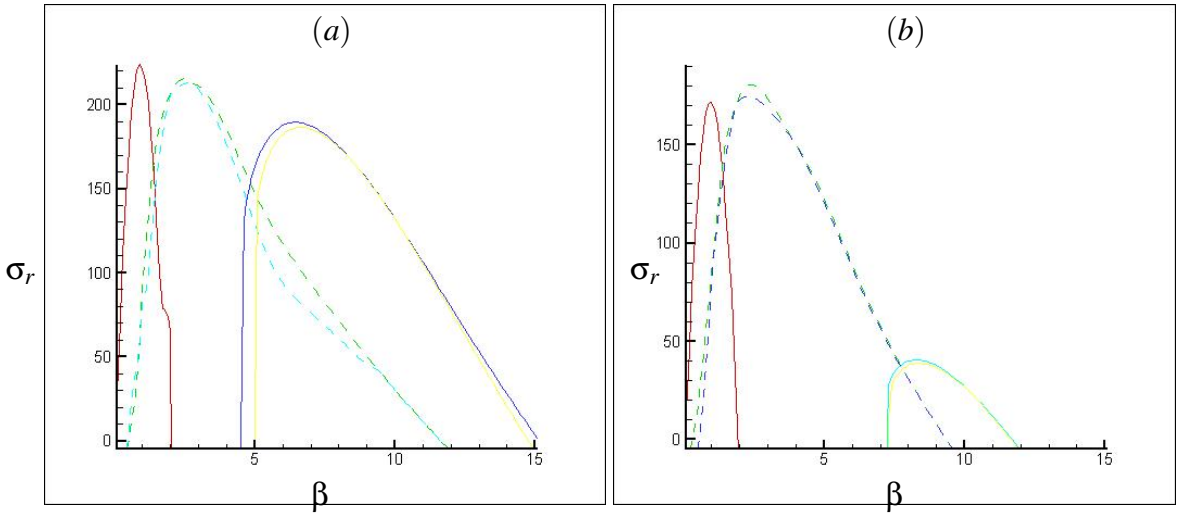


Figure 5.17: *The temporal amplification rate* $\sigma_r$ *vs the spanwise wavenumber* $\beta$ *for the top 3 phase locked modes and the top 2 non-phase locked modes on the lower branch at* $\alpha = 1.1$, *Re=5000, M=1.0 for (a) constant pressure, (b) constant flux*

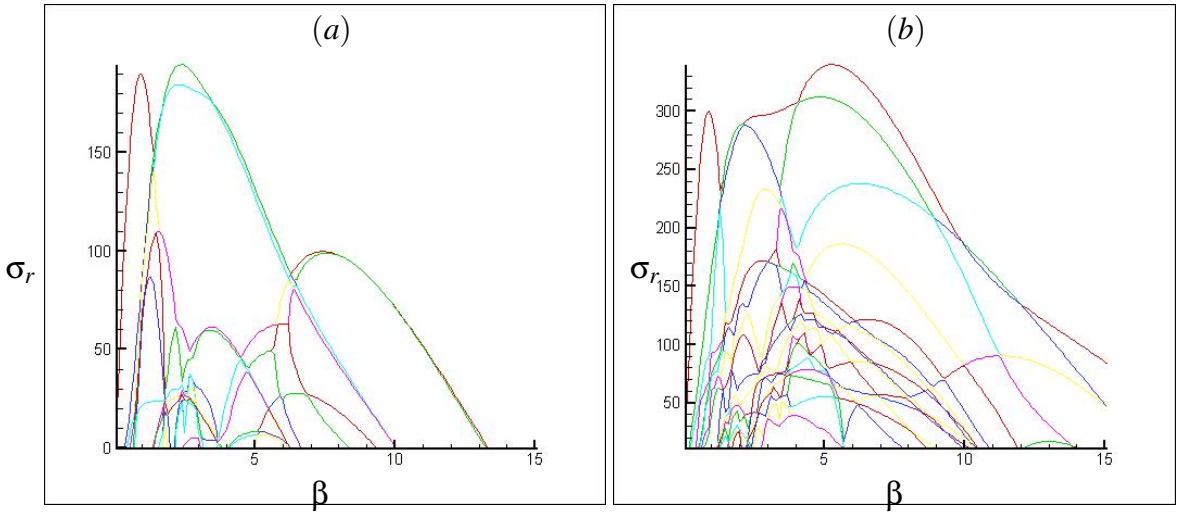


Figure 5.18: *The temporal amplification rate* $\sigma_r$ *vs the spanwise wavenumber* $\beta$ *for the unstable modes on the upper branch at* $\alpha = 1.1$, *Re=5000, M=1.0 for (a) constant pressure, (b) constant flux*

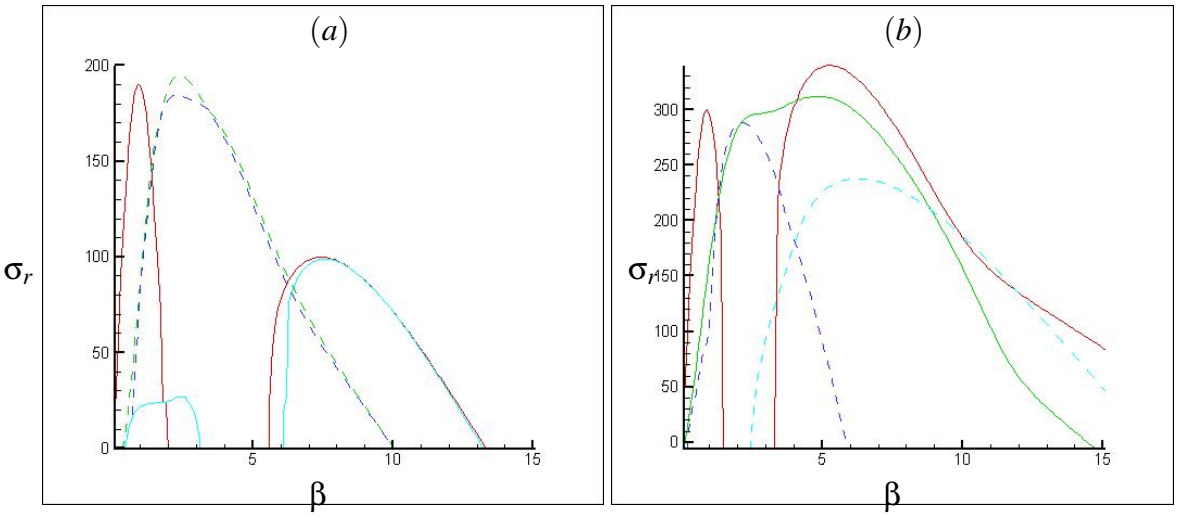


Figure 5.19: *The temporal amplification rate* $\sigma_r$ *vs the spanwise wavenumber* $\beta$ *for the top few phase and non-phase locked modes on the upper branch at* $\alpha = 1.1$, *Re=5000, M=1.0 for (a) constant pressure, (b) constant flux*

# 6 Conclusion

The aim of this study was to conduct a stability analysis of pressure driven flows in a channel with and without an externally applied transverse homogeneous magnetic field. This was done in three essential stages, Linear stability analysis, the calculation of two-dimensional secondary non-linear equilibrium solutions and finally a two and three dimensional secondary stability analysis of the two-dimensional secondary equilibrium solutions. In the linear case Squires theorem is applicable to both PPF and PPMF so only the two-dimensional disturbances were considered as the spanwise disturbances have a powerful stabilizing effect in both cases. The linear analysis in the $(Re, \alpha)$ plane for Hartmann numbers M=0-4 showed that the neutral curve corresponds to a Hopf bifurcation known as the Tollmein-Schlichting instability, where one wall mode becomes unstable and goes on to produce a streamwise time periodic motion. From the curves of marginal stability it can be seen that the critical Reynolds number $Re_c$ rises rapidly with Hartmann number M. By excluding the Lorentz force term from the PPMF Orr-Sommerfeld equation but retaining the PPMF velocity profile it was possible to conclude that the vast majority of the stabilising effect is caused by the flattening of the basic velocity profile which in turn compresses the boundary layer rather than the Lorentz force term.

The non-linear two-dimensional equilibrium states were obtained numerically using a Galerkin method which utilizes harmonic expansions. Two classes of solutions were differentiated both of which bifurcate sub-critically, one set that bifurcated from the linear neutral curve and were exemplified by $\alpha = 1.02$ and a second set that bifurcated from infinity which were exemplified by $\alpha = 1.1$. It should also be noted that supercritical bifurcations do occur from points $\alpha < \alpha_c$ on the linear curve but have been largely ignored in this thesis as they do not lower the critical Reynolds number. Two types of non-linear equilibrium solution constant flux and constant pressure were also calculated. It was found the constant flux case always had the lower limit point of the two, on the lower branch the two cases are identical until they start to diverge. On the upper branch it was shown if the disturbances had the same amplitude or $L_2 - norm$ value they were also identical even though the states existed at different $Re$ values. This indicated they are not strictly separate cases but differ by the base PPF and a scaling factor $U_Q/U_P$. At any point in the sub-critical bifurcation region on the $(Re, \alpha)$ plane their are two disturbances acting with different amplitudes which effectively changes the nature of the disturbance and puts them directly into the turbulent region. Qualitatively the PPMF non-linear equilibrium so-

lutions are similar to those of PPF in the $M = 0 - 1$ range, which is to be expected as the two have the same non-linear terms. It is also shown that again $Re_c$ increases with $M$ but not to the same extent as in the linear case as the equilibrium states are not as sub-critical in the PPMF case, so the non-linear effect are comparatively less stabilising for PPMF than PPF.

Finally the stability of the secondary flow was analysed by applying the Floquet theory. Both two and three dimensional linear secondary disturbances were superimposed onto the secondary equilibrium states for Hartmann numbers M=0-1. In the two-dimensional PPF case, where $M = 0.0$, it was found that their was one unstable phase-locked mode on the lower branch. This mode became stable as it passed through the limit point on the constant flux curve, but this did not happen until the upper branch on the constant pressure curve. This is because the key parameter as far as transitions are concerned is the amplitude of the disturbance or $L_2 - norm$ value, which occur when both are the same. The solutions on the upper branch remain stable up to a given point, after which another bifurcation takes place and a complex conjugate pair become positive. Although this bifurcation takes place at different $Re$ values on the constant flux and constant pressure curves, the $L_2 - norm$ values are again identical. It should be noted that a stationary neutral mode was always present throughout all these transitions. This suggests that the tertiary flow is phase locked with the secondary flow. These results show that as the vortices propagate down stream with the same speed as the frame of reference the initial instability arises at the lead point of the eddies. This is where the particles are forced backwards along the boundaries due to the direction of rotation of the vortices. The neutrally stable stationary eigenvalue corresponds to the back point of the vortices where the pressure gradient becomes negative.

For the PPMF case it was found rather than have a single unstable stationary eigenvalue and an ever present stationary neutral mode, rather there was an unstable complex conjugate pair on the lower branch with no sign of the stationary neutral mode so the tertiary flow will not be phase locked. The complex conjugate pair become more unstable and move more slowly as they travel down the lower branch towards the limit point. This implies that some of the energy from the particles velocity is being diverted to cause the instability. Once the limit point is reached the complex conjugate pair start to become more stable and speed up again until a certain point on the upper branch where they be-

come stable. One again the stability transition occurs at different Re values on the two curves but at corresponding $L_2 - norm$ values. The upper branch remains stable until a certain point where another complex conjugate pair becomes unstable and once again the bifurcation takes place when the $L_2 - norm$ values are the same. These results suggest that the instabilities arise at the side of the vortices because the magnetic field keeps the system stable despite the adverse pressure gradient the most surprising result is that there is not a neutrally stable point at the back of the eddie implying the vortices have been squashed and where as with PPF they are more oval in shape with the sharp ends at front and back they are more circular now.

Despite all this the two-dimensional secondary stability results are slightly academic as in real life the system will be subject to disturbances in all directions although they do provide valuable insight. The PPF three-dimensional secondary stability result agree well with the literature and are highly unstable for the whole of the $(Re, \alpha)$ plane. Although not shown in this thesis the results show the three-dimensional travelling wave solutions bifurcate from the neutral growth rate points A1, B1 as expected. In the PPMF case it is again found that the system is highly unstable in the entire $(Re, \alpha, M)$ volume. The most interesting PPMF results come from the upper branch of the constant flux condition at $Re = 5000$, $M = 1.0$results. It is found that phase-locked modes intersect, which are obvious points to look for vortical state bifurcations as the modes will probably interact as they have the same phase velocity. From this it can be concluded that even weak magnetic fields totally alter the both two and three dimensional secondary stability characteristics of the flow. The majority of the alteration is caused by the basic magnetic velocity profile as with the linear case. If the intersection point do lead to bifurcations with lower state then it may be possible to use a homopothy method to find lower two and three dimensional PPF states. To overcome the type two Chebechev convergence issues scalar potentials could be used instead. All this is ideal for future work.

# Bibliography


[1] D. J. Acheson. *Elementary Fluid Dynamics*. Oxford University Press, 1990.

[2] F. Alavyoon, D. S. Henningdon, and P. H. Alfredsson. Turbulent spots in plane poiseuille flow - flow visualisation. *Phys. Fluids*, 29:1328–1331, 1986.

[3] G. K. Batchelor. On steady laminar flow with closed streamlines at large reynolds numbers. *J. Fluid Mech.*, 1:177–190, 1956.

[4] J. A. Baylis and J. C. R. Hunt. Mhd flow in an annular channel: theory and experiment. *J. Fluid Mech.*, 48(3):423–428, 1971.

[5] B. J. Bayly, S. A. Orszag, and T. Herbert. Instability mechanism in shear-flow transition. *Ann. Rev. Fluid Mec.*, 20:359–391, 1988.

[6] H. Blasius. Grenzschichten in flussigkeiten mit kleiner reibung. *Z. Math. Phys.*, 56:1–37, 1908.

[7] E. Boltz. *Grenzchichten an rotationskorpern.* PhD thesis, Gottingen, 1908.

[8] G. G. Branover. Resistance of magnetohydrodynamic channels. *Magnetohydrodynamics*, 3:1–11, 1967.

[9] D. Carlson, S. E. Widnall, and M. F. Peeters. A flow visualisation study of transition in plane poiseuille flow. *J. Fluid Mech.*, 121:487–505, 1982.

[10] S. Chandrasekhar. *Hydrodynamic and hydomagnetic stability*. Dover publications, 1961.

[11] T. S. Chen and D. D. Joseph. Subcritical bifurcations of plane poiseuille flow. *J. Fluid Mech.*, 58:337–351, 1973.

[12] A. D. D. Craik. Nonlinear resonant instability in boundary layers. *J. Fluid Mech.*, 50:393–413, 1971.

[13] S. J. Davies and C. M. White. An experimental study of the flow of water in pipes of rectangular section. *Proc. Roy. Soc.*, 119:92, 1928.

[14] P. G. Drazin and W. H Reid. *Hydrodynamic stability second edition*. Cambridge university press, 1980.

[15] U. Ehrenstein. *Nonlinear bifurcation study of plane Poiseuille flow*. PhD thesis, Institut fur Theoretische Stronmungsmechanik Gottingen, 1989.

[16] U. Ehrenstein and W. Koch. Three-dimensional wavelike equilibrium states in plane poiseuille flow. *J. Fluid Mech.*, 228:111–148, 1991.

[17] M. Feigenbaum. The transition to aperiodic behaviour in turbulent systems. *Comm. Math. Phys*, 77:65, 1980.

[18] S. C. Generalis and T. Itano. Characterization of the hairpin vortex solution in plane couette flow. *Physical Review E*, 82:1–7, 2010.

[19] S. C. Generalis and M. Nagata. Transition in homogeneously heated inclined plane parallel shear flows. *Journal of Heat transfer*, 125:795–803, 2003.

[20] G. H. Gollub and C. F. Van Loan. *Matrix Computations.* John Hopkins, 1983.

[21] D. Grohne. Die stabilitat der ebenen kanalstromung gegenuber dreidimensionalen storungen von endlicher amplitude. *AVA Gottingen Rep.*, 69:A 30, 1969.

[22] L. H. Gustavsson. Resonant growth of three-dimensional disturbances in plane poiseuille flow. *J. Fluid Mech.*, 112:252–264, 1981.

[23] L. H. Gustavsson. Excitation of direct resonancein plane poiseuille flow. *Studies in Appl. Math.*, 75:227–248, 1986.

[24] J. Hartmann. Theory of the laminar flow of an electrically conducting liquid in a homogeneous magnetic field. *K. Dan. Vidensk. Selsk. Mat. Fys. Medd.*, 15(6):1–28, 1937.

[25] J. Hartmann and F. Lazarus. Experimental investigations on the flow of mercury in a homogeneous magnetic field. *Math. fys. Medd*, 15:6–7, 1937.

[26] W. Heisenberg. Uber stabilitat und turbulentz von flussigkeitsstromen. *Annln Phys., Lpz.*, 74:577–627, 1924.

[27] T. Herbert. Periodic secondary motion in a plane channel. In *Proc. 5th Intl Conf. on Numerical Methods in Fluid Dynamics*, 1976.

[28] T. Herbert. *Die Neutralflache der ebenen Poiseuillestromung*. PhD thesis, Universitat Karlsruhe, 1977.

[29] T. Herbert. A secondary instabilitymechanism in plane poiseuille flow. *Bull. Am. Phys. Soc.*, 26:1257, 1981.

[30] T. Herbert. Secondary instability of boundary layers. *Ann. Rev. Fluid Mech.*, 20:487–526, 1988.

[31] K. Hiemenz. Die grenzschicht an einem in den gleichformigen flussigkeitsstron eingetauchten ger-aden kreiszylinder. *Dinglers J.*, 326:321–24, 1911.

[32] R. C. Hilborn. *Chaos and nonlinear dynamics, second edition*. Oxford University Press, 2000.

[33] K. Hocking, L. M. Stewartson. On the nonlinear response of a marginally unstable plane parallel flow to a two-dimensional disturbance. *Proc. R. Soc. Lond.*, A 326:289–313, 1972.

[34] J. C. R. Hunt and K. Stewartson. Magnetohydrodynamic flow in rectangular ducts 2. *J. Fluid Mech.*, 23(3):563–581, 1965.

[35] J. Jimenez. Coherent structures and dynamical systems. *Proc. 1987 Summer Program of the NASA Stanford Centerfor Turbulence Res.*, CTR-S87:323–324, 1987.

[36] J. Jimenez. Transition to turbulence in two-dimensional poiseulle flow. *J. Fliud Mech.*, 218:265–297, 1989.

[37] T. Kakutani. The hydromagnetic stability of the modified plane couette flow in the presence of a transverse magnetic field. *J. Phys. Soc. Japan*, 19:1041, 1964.

[38] T. W. Kao and C. Park. Experimental investigation of the stability of channel flow. part 1. flow of a single liquid in a rectangular channel. *J. Fluid Mech.*, 43:145, 1970.

[39] M. A. Karnitz, M. C. Potter, and M. C. Smith. An experimental investigation of a plane poiseuille flow. *J. Fluids Engng*, 96:384, 1974.

[40] Lord Kelvin. Hydrokinetic solutions and observations. *Mathmatical and Physical papers*, 4:69–85, 1871.

[41] J. Kim. On the structure of wall bounded turbulent flows. *Phys. Fluids*, 26:2088–2097, 1983.

[42] J. Kim, P. Moin, and R. Moser. Turbulent statistics in fully developed channel flowat low reynolds number. *J. Fluid Mech.*, 177:133–166, 1987.

[43] P. S. Klebanoff, K. D. Tidstrom, and L. M. Sargent. The three-dimensional nature of boundary-layer instability. *J. Fluid Mech.*, 12:1–34, 1962.

[44] L. Kleiser. Spectral simulations in laminar-turbulent transition in plane poiseuille flow and comparisons with experiments. In *In Proc. 8th Intl Conf. on Numerical Methods in Fluid Dynamics Aachen (ed. E. Krause). Lecture Notes in Physics, vol. 170, p.280. Springer*, 1982.

[45] L. Kleiser and A. Zang, T. Numerical simulations of transition in wall-bounded shear flows. *Annu. Rev. Fluid Mech.*, 23:495–537, 1991.

[46] W. Koch. *Nonlinear limit-cycle solutions - arational method for transition prediction in shear flow*. Springer, 1988.

[47] V. V. Kozlov and M. P. Ramazanov. Experimental investigation of the growth process of disturbances in plane poiseuille flow. *Inst. Theor. Appl. Mech., AN SSSR SO, Novosibirsk*, Preprint 21, 1980.

[48] V. V. Kozlov and M. P. Ramazanov. Development of finite-amplitude disturbances in poiseuille flow. *J. Fluid Mech.*, 147:149–157, 1984.

[49] C. C. Lin. Some mathematical problems in the theory of the stability of parallel flows. *J. Fluid Mech.*, 10:430–438, 1961.

[50] C.C. Lin. On the stability of two-dimensional parallel flows. *Appl. Maths*, 3:117–142, 1945.

[51] R. C. Lock. The stability of the flow of an electrically conducting fluid between parallel planes under a transverse magnetic field. Technical report, Aerodynamics Division National Physics Laboratory, 1955.

[52] S. Lundquist. An energy principle for hydromagnetic stability problems. *Ark. Fys.*, 5:338 (ch. VII), 1952.

[53] P. S. Lykoudis. Transition from laminar to turbulent flow in magneto-fluid mechanic channels. *Rev. Mod. Phys.*, 32:796–798, 1960.

[54] L. M. Mack. A numerical study of the temporal eigenvalue spectrum of the blasius boundary layer. *J. Fluid. Mech.*, 73:497–520, 1976.

[55] P. Mannneville and Y. Pomeau. Different ways to turbulence in dissipative dynamic systems. *Physica*, D1:219, 1980.

[56] J. E. Marsden and M. McCracken. *The Hopf Bifurcation and its Applications.* Springer, 1976.

[57] D. Meksyn and J. T. Stuart. Stability of viscous motion between parallel planes for finite disturbances. *Proc. Roy. Soc*, A208:517–526, 1951.

[58] F. A. Milinazzo and P. G. Saffmann. Finite-amplitude steady waves in plane viscous shear flows. *J. Fluid Mech.*, 160:281–295, 1985.

[59] W. Murgatroyd. Experiments on magneto-hydrodynamic channel flow. *Phil. Mag.*, 44:1348–1354, 1953.

[60] M. Nagata. Nonlinear solutions of modified plane couette flow in the presence of a transvers magnetic field. *J. Fluid Mech*, 307:231–243, 1996.

[61] M. Nagata. Nonlinear analysis on the neutral convection between vertical plates in the presence of a horizontal magnetic field. *Eur. J. Mech. B/Fluids*, 17:33–50, 1998.

[62] M. Nagata and S. Generalis. Transition in convective flows heated internally. *J. Heat Transfer*, 124:635–642, 2002.

[63] M. A. B. Narayanan and T. Narayana. Some studies on transitions from laminar to turbulent flow in a two-dimensional channel. *Math. Phys.*, 18:642, 1967.

[64] C. L. Navier. Memoire sur les lois du mouvement des fluides. *Mem. Acad. R. Sci. Paris*, 6:389–416, 1823.

[65] M. Nishioka and M. Asai. Some observations of the subcritical transition in plane poiseuille flow. *J. Fluid Mech.*, 150:441–450, 1985.

[66] M. Nishioka, S. Iida, and J. Ichikawa. An experimental investigation on the stability of plane poiseuille flow. *J. Fluid Mech*, 72:731–751, 1975.

[67] F. Noether. Das turbulenzproblem. *Z. Angew. Math. Mech.*, 1:125–138 218–219, 1921.

[68] W. McF. Orr. The stability of the steady motion of a perfect liquid and of a viscous liquid. *Proc. Irish Acad*, A 27:9–68, 69–138, 1907.

[69] S. A. Orszag. Accurate solutions of the orr-sommerfeld equation. *J. Fluid Mech.*, 50:731–751, 1971.

[70] S. A. Orszag and L. C. Kells. Transition to turbulence in plane poiseuille and plane couette flow. *J. Fluid Mech.*, 96:159–206, 1980.

[71] S. A. Orszag and A. T. Patera. Subcritical transition to turbulence in plane channel flow. *Phys. Rev. Lett.*, 45:989–993, 1980.

[72] S. A. Orszag and A. T. Patera. Subcitical transition to turbulent in planar shear flows. In *Transition and Turbulence*, 1981.

[73] S.A Orszag and A.T. Patera. Secondary instability of wall-bounded shear flows. *J. Fluid Mech.*, 128:347–385, 1983.

[74] V. C. Patel and M. R. Head. Some observations in skin friction and velocity profiles in fully developed pipe and channel flows. *J. Fluid Mech.*, 38:181–201, 1969.

[75] C. L. Pekeris and B. Shkoller. The neutral curves for periodic perturbations of finite amplitude of plane poiseuille flow. *J. Fluid Mech.*, 39:629–639, 1969.

[76] O. M. Phillips. Nonlinear dispersive waves. *Ann. Rev. Fluid Mech.*, 6:93–110, 1974.

[77] S. D. Poisson. Memoire sur lequilibre et le mouvement des corps elastiques. *J. Ec. Polytech. Paris*, 1:139–166, 1831.

[78] M. C. Potter and J. A. Kutchey. Stability of plane hartmann flow subject to a transverse magnetic field. *Phys. Fluids*, 16:1848, 1973.

[79] L. Prandlt. Ulber fliiissigkeitsbewegung bei sehr kleiner reibung. *Verh. Int. Math. Kongr. 3rd. Heidelelburg.*, pages 484–491, 1905.

[80] M. R. E. Proctor and A. D. Gilbert. *Lectures on solar and planetary dynamos.* Cambridge University Press, 1994.

[81] J. D. Pugh. *Finite amplitude waves in plane Poiseuille flow.* PhD thesis, California Institute of Technology, 1987.

[82] J. D. Pugh and P. G. Saffman. Two-dimensional superharonic stability of finite amplitude waves in plane poiseuille flow. *J. Fluid Mech.*, 194:295–307, 1988.

[83] Lord Rayleigh. On the stability or instability , of certain fluid motions. *Proc. London Math. Soc.*, 11:57–70, 1880.

[84] Lord Rayleigh. On the instability of jets. *Proc. London Math. Soc.*, 10:4–13, 1979.

[85] C. B. Reed and B. F. Picologlou. Sidewall flow instabilities in liquid metal mhd flow under blanket relevant conditions. *Fusion Technol.*, 15:705–715, 1989.

[86] O. Reynolds. An experimental investigation of the circumstances which determine whether the motion of water shall be direct or sinuous, and of the law of resistance in parallel channels. *Phil. Trans. Roy. Soc. London*, 174:935–982, 1883.

[87] W. C. Reynolds and M. C. Potter. Finite amplitude instability of parallel shear flows. *J. Fluid Mech.*, 27:465–492, 1967.

[88] P. H. Roberts. *An introduction to magnetohydrodynamics*. Longmans, 1967.

[89] S. K. Robinson. Coherent motions in the turbulent boundary layer. *Annu. Rev. Fluid Mech.*, 23:601, 1991.

[90] B. L. Rozhdestvensky and I. N. Simakin. Secondary flows in a plane channel: their relationship and comparison with turbulent flows. *J. Fluid Mech.*, 147:261–289, 1984.

[91] D. Ruelle and F. Takens. On the nature of turbulence. *Comm. Math. Phys.*, 20:167–192, 1971.

[92] P. G. Saffman. Vortices, stability and turbulence. *Annals of the New York Academy of Science*, 404:12–24, 1983.

[93] B. Saint-Venant. *Acad. Sci. Paris Ser. A*, 17:1240–1242, 1843.

[94] H. Schlichting. Berechnug der anfachung kleiner storungen bei der plattenstromung. *Z. Angew. Math. Mech.*, 13:171–174, 1933.

[95] G. B. Schubauer and H. K. Skramstard. Laminar boundary-layer oscillations and transition on a flat plate. *J. Res. Nat. Bur. Stand.*, 38:251–292, 1943.

[96] A. M. O. Smith and N. Gamberoni. Transition, pressure gradient and stability theory. Technical report, Douglas Aircraft Co., 1956.

[97] A. Sommerfeld. Ein beitrag zur hydrodynamischen erklarung der turbulenten flussigkeitsbewegung. *4th International Congress of Mathematicians*, 3:116–124, 1908.

[98] H. B. Squire. On the stability of three-dimensional disturbances of viscous flow between parallel walls. *Proc. Roy. Soc.*, A142:621–628, 1933.

[99] K. Stewartson and J. T. Stuart. A nonlinear instability theory for a wave system in plane poiseuille flow. *J. Fluid Mech.*, 48:529–545, 1971.

[100] G. G. Stokes. *Trans. Cambridge Philos. Soc.*, 9:8–106, 1951.

[101] G.G. Stokes. *Trans. Cambridge Philos. Soc.*, 8:287–305, 1845.

[102] J. T. Stuart. On the stability of a viscous flow between parallel planes in the presence of a co-planar magnetic field. *Proc. Roy. Soc. A,*, 221:189, 1954.

[103] J. T. Stuart. On the nonlinear mechanics of wave disturbances in stable and unstable parallel flows. part 1. the basic behaviour in plane poiseille flow. *J. Fluid Mech.*, 9:353–370, 1960.

[104] J. T. Stuart. *Hydrodynamic stability. In laminar boundary layers, ed.* Oxford: Clarendon Press, 1963.

[105] M. Takashima. The stability of natural convection in a vertical layer of electrically conducting fluid in the presence of a transverse magnetic field. *Fluid Dyn. Res.*, 14:121, 1994.

[106] M. Takashima. The stability of modified plane poiseuille flow in the presence of a transverse magnetic field. *Fluid Dynamics Research*, 17:293–310, 1995.

[107] I. Tani. History of boundary layer theory. *Ann. Rev. Fluid Mec.*, 9:87–111, 1977.

[108] G. I. Taylor. Stability of a viscous liquid contained between two rotating cylinders. *Phil. Trans. Roy. Soc.*, A223:289–343, 1923.

[109] T. Theodorsen. Mechanism of turbulence. *Proceedings of the Second Midwesttern Conference on Fluid Mechanics (unpublished)*, pages 1–19, 1952.

[110] L. H. Thomas. The stability of plane poiseuille flow. *Phys. Rev.*, 91:780–783, 1953.

[111] W. Tollmien. Uber die ensttehung der turbulenz. *Nachr. Ges. Wiss. Gottingen Math.-phys*, K1:21–44, 1929.

[112] H. von Helmholtz. Uber discontinuirliche flussigkeitsbewegungen. *Monats. Konigl. Preuss. Akad. Wiss. Berlin*, 23:215–228, 1868.

[113] J. Waleffe. Exact coherent structures in channel flow. *J. Fluid Mech.*, 435:93–102, 2001.

[114] J. Watson. On the nonlinear mechanics of wave disturbances in stable and unstable parallel flows. part 2. the development of a solution for plane poiseuille flow and for plane couette flow. *J. Fluid Mech*, 9:371–389, 1960.

[115] J. P. Zahn, J. Toomre, E. A. Spiegel, and D. O. Gough. Nonlinear cellular motions in poiseuille chennel flow. *J. Fluid Mech.*, 64:319–345, 1974.

# A Appendix 1

$$\nabla^2 h = -\partial_z \psi \tag{A.1}$$

$$h = \sum_{m,n}(z) expi(m\alpha x + n\beta y) \tag{A.2}$$

$$\psi = \sum_{l=1}^{\infty}\sum_{m=-\infty}^{\infty}\sum_{n=-\infty}^{\infty} b_{l,m,n} expi(m\alpha x + n\beta y) T_n(1-z^2) \tag{A.3}$$

$$\begin{aligned}(\partial_z^2 - ((m\alpha)^2 + (n\beta)^2)) \sum_{m,n} expi(m\alpha x + n\beta y) & \\ = \sum_{l}\sum_{m,n} b_{lmn} expi(m\alpha x + n\beta y) & \\ (T_n'(z) - z^2 \cdot T_n'(z) - 2z \cdot T_n(z)) & \end{aligned} \tag{A.4}$$

$T_n'(z) = nU_{n-1}$ where $U_n$= type 2 Chebychev n=1,2,3...

$$\Rightarrow [\partial_z^2 - ((m\alpha)^2 + (n\beta)^2]_{q,m,n} = \sum_{l} b_{l,m,n}(nU_{n-1}(z) - z^2 \cdot nU_{n-1}(z) - 2z \cdot T_n(z)) \tag{A.5}$$

# B Appendix 2

Fourier's theorem states a periodic function with period T satisfies $f(t+T) = f(t)$ for all t. Therefore any periodic function with period T can be written as:

$$f(t) = \frac{a_0}{2} + \sum_{n=1}^{\infty} a_n cos(n\omega_0 t) + \sum_{n=1}^{\infty} b_n sin(n\omega_0 t) \tag{B.1}$$

A periodic function can be expressed as a sum of a constant term and a series of cosine and sine terms, where the frequencies associated with the sines and cosines are integer multiples(harmonics) of the fundamental frequency. To find the Fourier amplitudes or coefficients $a_n$ and $b_n$ we have:

$$a_n = \frac{2}{T} \int_0^T dt f(t) cos(m\omega_0 t) \tag{B.2}$$

$$b_n = \frac{2}{T} \int_0^T dt f(t) sin(m\omega_0 t) \tag{B.3}$$

A Fourier series can be simplified by rewriting the sine and cosine in terms of complex exponential functions using Euler formula:

$$\begin{aligned} f(t) &= \frac{a_0}{2} + a_1 cos(\omega_0 t) + b_1 cos(\omega_0 t) + \dots \\ &= \frac{a_0}{2} + \frac{a_1}{2}\left[exp(i\omega_0 t + exp(-i\omega_0 t\right] + \frac{b_1}{2i}\left[exp(i\omega_0 t) - exp(-i\omega_0 t)\right] + \dots \\ &= \frac{a_0}{2} + exp(i\omega_0 t)\left[\frac{a_1}{2} - \frac{ib_1}{2}\right] + exp(-i\omega_0 t)\left[\frac{a_1}{2} + \frac{ib_1}{2}\right] + \dots \end{aligned} \tag{B.4}$$

Thus we can write $f(t)$ as a sum of complex exponentials:

$$f(t) = \sum_{n=-\infty}^{\infty} c_n exp(in\omega_0 t) \tag{B.5}$$

with $c_n = 1/2(a_n - ib_n) and c_{-n} = 1/2(a_n + ib_n)$.

# C Appendix 3

$\phi - \phi$ Terms

$$(\partial_x\partial_z\phi)(\partial_x^5\phi + \partial_x\partial y^4\phi + 2\partial_x^3\partial_y^2\phi + \partial_x^3\partial_z^2\phi + \partial_x\partial_y^2\partial_z^2\phi) + (\partial_y\partial_z\phi)(\partial_y^5\phi + \partial_x^4\partial_y\phi + 2\partial_x^2\partial_y^3\phi + \partial_y^3\partial_z^2\phi + \partial_x^2\partial_y\partial_z^2\phi) - (\partial_x^3\phi)(\partial_x^3\partial_z\phi + \partial_x\partial_z^3 + \partial_x\partial_y^2\partial_z\phi) - (\partial_x\partial_y^2\phi)(\partial_x^3\partial_z\phi + \partial_x\partial_z^3\phi + \partial_x\partial_y^2\partial_z\phi) - (\partial_x^2\partial_y\phi)(\partial_y^3\partial_z + \partial_y\partial_z^3\phi + \partial_x^2\partial_y\partial_z\phi) - (\partial_y^3\phi)(\partial_y^3\partial_z\phi + \partial_y\partial_z^3\phi + \partial_x^2\partial_y\partial z\phi) - (\partial_x^2\phi)(\partial_x^4\partial_z\phi + \partial_y^4\partial_z\phi + 2\partial_x^2\partial_z^3\phi + \partial_y^2\partial_z^3\phi + \partial_x^2\partial_y^2\partial_z\phi) - (\partial_y^2)(\partial_x^4\partial_z\phi + \partial_y^4\partial_z\phi + \partial_x^2\partial_z^3\phi + \partial_y^2\partial_z^3\phi + 2\partial_x^2\partial_y^2\partial_z\phi) - (\partial_x^2\partial_z\phi)(2\partial_x^4\phi + 2\partial_y^4\phi + \partial_x^2\partial_z^{2\phi} + 2\partial_y^2\partial_z^2\phi) + 4(\partial_x\partial_y\partial_z)(\partial_x^3\partial_y\phi + \partial_x\partial_y^3\phi + \partial_x\partial_y\partial_z^2\phi)$$

$\phi - \psi$ Terms

$$(\partial_x^3\phi)(\partial_y\partial_z^2\psi) + 2(\partial_x\partial_y^2\phi)(\partial_y\partial_z^2\psi) + 2(\partial_x\partial_y\partial_z\phi)(\partial_x^2\partial_z\psi) - 2(\partial_x^2\partial_z\phi - \partial_y^2\partial_z\phi)(\partial_x\partial_y\partial_z\psi) - 2(\partial_x\partial_y\partial_z\phi)(\partial_y^2\partial$$
$$(\partial_x^2\partial_y\phi)(\partial_x\partial_z^2\psi) - (\partial_y^3\phi)(\partial_x\partial_z^2\psi) + (\partial_x^4\partial_y\phi + \partial_y^5\phi + 2\partial_x^2\partial_y^3\phi + \partial_x^2\partial_y\partial_z^2\phi + \partial_y^3\partial_z^2\phi)(\partial_x\psi) - (\partial_x^5\phi + \partial_x\partial_y^4\phi + 2\partial_x^3\partial_y^2\phi + \partial_x^3\partial_z^2\phi + \partial_x\partial_y^2\partial_z^2\phi)(\partial_y\psi) - (\partial_x^3\phi + \partial_x\partial_y^2\phi)(\partial_x^2\partial_y\psi) - (\partial_x^3\phi + \partial_x\partial_y^2\phi)(\partial_y^3\psi) + (\partial_x^2\partial_y\phi + \partial_y^3\phi)(\partial_x^3\psi) + (\partial_x^2\partial_y\phi + \partial_y^3\phi)(\partial_x\partial_y^2\psi) + 2(\partial_x^3\partial_y\phi + \partial_x\partial_y^3\phi + \partial_x\partial_y\partial_z^2\phi)(\partial_x^2\psi) - 2(\partial_x^4\phi - \partial_y^4\phi + \partial_x^2\partial_z^2\phi - \partial_y^2 + \partial_z^2\phi)(\partial_x\partial_y\psi) - 2(\partial_x^3\partial_y\phi + \partial_x\partial_y^3\phi + \partial_x\partial_y\partial_z^2\phi)(\partial_y^2\psi)$$

$\psi - \psi$ Terms

$$4(\partial_x\partial_y\partial_z\psi)(\partial_x\partial_y\psi) - 2(\partial_x^2\psi)(\partial_y^2\partial_z\psi) - 2(\partial_y^2\psi)(\partial_x^2\partial_z\psi)$$